OPTIMIZATION OF CEMENT PRODUCTION AND HYDRATION FOR IMPROVED PERFORMANCE, ENERGY CONSERVATION, AND COST

By

CHENGCHENG TAO

A DISSERTATION PRESENTED TO THE GRADUATE SCHOOL
OF THE UNIVERSITY OF FLORIDA IN PARTIAL FULFILLMENT
OF THE REQUIREMENTS FOR THE DEGREE OF
DOCTOR OF PHILOSOPHY

UNIVERSITY OF FLORIDA

2017

To my family

ACKNOWLEDGMENTS

I would like to express my deepest gratitude and sincere appreciation to my advisor Prof. Forrest Masters for accepting me into Ph.D. program and providing me academic guidance for the last three years study at University of Florida. Without his support, this dissertation and research would not come to realization. His expert knowledge and attitude on research and work are great inspiration to be. It is a great privilege to work with him.

I also sincerely appreciate the help I received from Dr. Christopher Ferraro and his Ph.D. student Mr. Benjamin Watts. My Ph.D. research is a collaborative project with them. Dr. Ferraro and Ben have always been very supportive for the last three years in regards of our research and experiment. Without their support, these achievements would not be possible.

I am grateful to my committee members: Prof. Kurtis Gurley from the Department of Civil and Coastal Engineering, and Dr. Luisa Amelia Dempere from the Department of Materials Science and Engineering. I would like to thank Prof. Anthony Straatman and Mr. Christopher M. Csernyei from University of Western Ontario for their help on the development of cement kiln model.

I also want to acknowledge the support of this research by the Florida Department of Transportation (FDOT).

I could not have asked for better labmates than Mr. Pedro Fernández Cabán and Mr. Ryan Catarelli. I want to thank them for many interesting conversations on research and life. It has been a great pleasure working with them in the same lab and office.

In addition, I want to give my special thanks to my parents. They have been always supportive for my whole life. I would not be here today without their patience, encouragement and love.

TABLE OF CONTENTS

page

LIST OF TABLES

LIST OF FIGURES

LIST OF ABBREVIATIONS

A_{cgb}	Convection area internal gas to bulk bed (m)
A_{cgw}	Convection area internal gas to internal wall (m)
A_{cwb}	Conduction area internal wall to bed (m)
A_{rgb}	Radiation area internal freeboard gas to bulk bed (m)
A_{rgw}	Radiation area internal freeboard gas to internal wall (m)
A_{rwb}	Radiation area internal wall to bulk bed (m)
A_s	Area of bed segment (m)
A_{sh}	Area of steel shell (m)
A_i	Initial mass fraction of Al_2O_3 at inlet of the kiln
A_j	Pre-exponential factor for j^{th} reaction (1/s)
AR	Alumina ratio
Cp_b	Specific heat of bulk bed (J/kg.K)
C_{Tmax}	Maximum coating thickness (m)
D_e	Hydraulic diameter of kiln (m)
D	Diameter of kiln (m)
d_n	Normalized Pareto front distance
E_j	Activation energy for j^{th} reaction (J/mol)
E_0	Minimum allowable modulus
F_i	Initial mass fraction of Fe_2O_3 at inlet of kiln
f_i	Objective function
h_{cgb}	Convection heat transfer coefficient freeboard gas to bed ($W/m^2.K$)
h_{cgw}	Convection heat transfer coefficient gas to internal wall ($W/m^2.K$)
h_{cwb}	Conduction heat transfer coefficient from wall to bed ($W/m^2.K$)

h_{csh}	Convective heat transfer coefficient from shell to air ($W/m^2.K$)
k_a	Thermal conductivity of air (W/m.K)
k_b	Thermal conductivity of bulk bed (W/m.K)
k_g	Thermal conductivity of fluid (W/m.K)
k_1	Reaction rate $CaCO_3$ (1/s)
k_2	Reaction rate C_2S (1/s)
k_3	Reaction rate C_3S (1/s)
k_4	Reaction rate C_3A (1/s)
k_5	Reaction rate C_4AF (1/s)
LSF	Lime saturation factor
P_c	Probability of non-exceedance
Q_{cgb}	Convection heat transfer freeboard gas to bulk bed (W/m)
Q_{cgw}	Convection heat transfer freeboard gas to internal wall (W/m)
Q_{cwb}	Conduction heat transfer internal wall to bulk bed (W/m)
Q_{rgb}	Radiation heat transfer freeboard gas to bulk bed (W/m)
Q_{rgw}	Radiation heat transfer freeboard gas to internal wall (W/m)
Q_{rwb}	Radiation heat transfer internal wall to bulk bed (W/m)
Q'	Heat gained by bulk bed due to heat transfer (W/m)
q_c	Heat generated by chemical reactions (W/m^3)
R_g	Universal gas constant (J/mol.K)
R	Internal radium of kiln (m)
S_{comb}	Combining score
S_i	Initial mass fraction of SiO_2 at inlet of the kiln

SR	Silica ratio
T_g	Freeboard gas temperature (K)
T_b	Bulk bed temperature (K)
T_w	Internal wall temperature (K)
T_o	Temperature of atmosphere (K)
T_{sh}	Temperature of steel shell (K)
V_i^{k+1}	Velocity of i^{th} particle at k^{th} generation
v_s	Velocity of bulk bed (m/s)
x_i^{k+1}	Position of i^{th} particle at k^{th} generation
Y_n	Mass fraction of n^{th} species
α_b	Bulk bed thermal diffusivity (m^2/s)
α_g	Absorptivity of freeboard gas
β	Angle of repose (rad)
ε_b	Emissivity of bulk bed
ε_g	Emissivity of freeboard gas
ε_{sh}	Emissivity of steel shell
ε_w	Emissivity of internal wall
Γ	Angle of fill of the kiln (rad)
μ_g	Dynamic viscosity of freeboard gas (s/m^2)
η	Degree of solid fill
ω	Rotational speed of kiln (rad/s)
ρ_g	Density of freeboard gas (kg/m^3)
ρ_s	Density of solids (kg/m^3)

σ	Stefan-Boltzmann constant
v_g	Kinematic viscosity of freeboard gas (m^2/s)
ΔH_{CaCO3}	Heat of reaction $CaCO_3$ (J/kg)
ΔH_{C2S}	Heat of reaction C_2S (J/kg)
ΔH_{C3S}	Heat of reaction C_3S (J/kg)
ΔH_{C3A}	Heat of reaction C_3A (J/kg)
ΔH_{C4AF}	Heat of reaction C_4AF (J/kg)

Abstract of Dissertation Presented to the Graduate School
of the University of Florida in Partial Fulfillment of the
Requirements for the Degree of Doctor of Philosophy

OPTIMIZATION OF CEMENT PRODUCTION AND HYDRATION FOR IMPROVED PERFORMANCE, ENERGY CONSERVATION, AND COST

By

Chengcheng Tao

August 2017

Chair: Forrest J. Masters
Cochair: Christopher C. Ferraro
Major: Civil Engineering

This dissertation presents a new computational framework to optimize the chemistry of cements and thermal energy of cement rotary kiln to achieve user-defined performance criteria for strength, materials cost, energy consumption, durability, and sustainability. Pareto optimization reveals the inherent tradeoff between modulus of elasticity, time of set, and kiln temperature and is applied to objectively rate cements in these contexts. A scalable approach built on particle swarm optimization of the NIST Virtual Cement and Concrete Testing Laboratory (VCCTL) is successfully demonstrated for ~150,000 combinations of cement phase distributions and water-cement ratios, using ~10% of the VCCTL runs required to fully enumerate the discretized solution space.

VCCTL was also coupled with a virtual cement plant (VCP) to study the cement production lifestyle from the raw feed to the finished product. Clinker production process consumes most of the energy and all of the fuel used in cement industry, and the rotary kiln wastes the most heat in the plant. A one-dimensional physical-chemical model incorporating clinker chemistry and thermodynamics within a rotary cement kiln was developed to characterize the temperature profiles of freeboard gas, bulk bed, internal wall and shell of the cement kiln and

clinker mass fractions under given kiln inlet conditions. Predictions are verified by comparing them with published experimental data. The clinker mass fractions at the kiln outlet are then imported into the VCCTL to simulate hydration and predict mechanical performance for hardened mortar and concrete.

Metaheuristic optimization algorithms were paired with the kiln-cement virtual model on the HiPerGator High Performance Computer (HPC) at the University of Florida. Insofar as VCCTL/VCP accurately models cement hydration and the resultant mechanical and thermal properties, the proposed approach opens a new pathway to optimally proportion and blend raw materials (and eventually, waste byproducts) to reduce production costs, extend the life of a quarry, or reduce a plant's carbon footprint.

CHAPTER 1
INTRODUCTION

The computational framework presented in this dissertation applies multi-objective metaheuristic optimization to virtual cement and virtual cement plant modeling. It is unique to connect metaheuristic algorithms with models of cement production and cement hydration. The optimization algorithms guide the search for optimal cements based on their performance, which would save more computational expense than blind search. It serves as a quantitative optimization tool to study energy efficiency measures within cement plants that conserve energy, increase cement productivity, and decrease greenhouse gas emissions. It also provides guidance on the design of raw material distribution and cement phases to optimize material cost and ensure competitive performance of the materials.

1.1 Background

Portland cement concrete is widely used in the global construction industry (Aïtcin, 2000; Mindess & Young, 1981) because of its flexibility in civil engineering applications and the widespread availability of its constituent materials; however, there is a growing need to reduce the energy costs and environmental impact associated with cement production (Romeo, Catalina, Lisbona, Lara, & Martínez, 2011; Worrell, Kermeli, & Galitsky, 2013; Zhang et al., 2011). From an operational perspective, the goal is to increase energy efficiency without sacrificing productivity.

Plants have incorporated efficiency measures during raw meal preparation, clinker production, and finish grinding, among other areas (Worrell et al., 2013). For example, process knowledge based systems (KBS) have been applied to the energy management and process control during clinker production, e.g., the predictive control system described in Caddet (2000a). Also, switching from coal to natural gas as the fuel for the cement kiln has been shown

to provide higher flame temperature, higher levels of clinker production (5-10%), lower fuel consumption, lower build-ups and dust losses (Akhtar, Ervin, Raza, & Abbas, 2013).

Due to the complexity of the reactions of cement hydration and scale of cement plant, full scale experimental testing for cement properties and energy cost within the production are costly and impractical. Therefore, there is an increasing need for the development of computational modeling for cement and cement plant (Bićanić, De Borst, Mang, & Meschke, 2003; Bullard, Ferraris, Garboczi, Martys, & Stutzman, 2004; Garboczi, Bullard, & Bentz, 2004; Hain & Wriggers, 2008; Vallgårda & Redström, 2007). The current study applies the Virtual Cement and Concrete Testing Laboratory (VCCTL), which is available for commercial use from The National Institute of Standards and Technology (NIST) (Bullard, 2014).

VCCTL incorporates microstructural modeling of Portland cement hydration and supports the prediction of different properties of hydrated products. For computational modeling both in cement and cement plant, the number of control parameters is sufficiently large, making it impossible to analyze all combinatorial cases. Thus, the problem of identifying optimal mixtures is not possible without introducing techniques that require a smaller sample space. Some statistical methods have been used to conduct the optimization for high performance concrete and cement (Ahmad & Alghamdi, 2014; Lagergren, Snyder, & Simon, 1997; MJ Simon, 2003; M Simon, Snyder, & Frohnsdorff, 1999); however, these methods have some difficulties in solving large discrete problems with multi-objective optimization problems due to computational limitations.

Cement plant models have also been investigated to simulate heat and chemistry in cement production (Barr, 1986; C. Csernyei & Straatman, 2016; Darabi, 2007; S. Q. Li, Ma, Wan, & Yao, 2005; Martins, Oliveira, & Franca, 2002; Mastorakos et al., 1999; K. Mujumdar &

Ranade, 2006; Sadighi, Shirvani, & Ahmad, 2011; Spang, 1972). These models predicted the behavior cement plant with respect to heat transfer and clinker formation inside the cement rotary kiln considering given kiln conditions and raw material inputs.

During the last two decades, metaheuristics techniques have been extensively applied to complicated optimization problems in different fields (Collins, Eglese, & Golden, 1988; Jaumard, OW, & Simeone, 1988; Nissen, 1993; Osman, 1995; Pirlot, 1992; Rayward-Smith, Osman, Reeves, & Smith, 1996; Sharda, 1994; Stewart, Liaw, & White, 1994; Voß, Martello, Osman, & Roucairol, 2012). The algorithms employ strategies that guide a subordinate heuristic method to find the near-optimal solution efficiency by intelligently searching space with different strategies (Osman & Laporte, 1996). Among these metaheuristic methods, two important and widely used computational methods that deal with the engineering optimization problems are the particle swarm optimization (PSO) (Hu, Eberhart, & Shi, 2003; L. Li, Huang, & Liu, 2009; L. Li, Huang, Liu, & Wu, 2007; Shi, 2001) and the genetic algorithm (GA) (Goldberg & Samtani, 1986; Rajeev & Krishnamoorthy, 1992; Wu & Chow, 1995). They are both pattern search techniques, which do not need to calculate the gradients of objective functions to optimize using methods such as quasi-Newton or gradient descent (Bonnans, Gilbert, Lemaréchal, & Sagastizábal, 2006; Press, Teukolsky, Vetterling, & Flannery, 2007). This dissertation will show how metaheuristic algorithms are applied for discrete problems matching the discrete input data required by VCCTL.

1.2 Organization of Dissertation

Chapter 2 provides a brief summary of the background of the Portland cement composition and hydration mechanics inside VCCTL and optimization methods applied on cement and concrete. This chapter also reviews the literature relevant to the development of computational models for rotary cement kiln.

Chapter 3 discusses the metaheuristic optimization algorithms applied to Portland cement and evaluation of optimal solutions. Single objective and multi-objective optimization cases with Pareto analysis are demonstrated on Portland cements. Convergence is discussed to assist users replicating this approach. Finally, we demonstrate that tri-objective optimization is a flexible and objective tool to rate cements and offer remarks on the potential of this approach to solve much larger combinatorial problems arising from the introduction of other variables such as cement fineness and aggregate proportions.

Chapter 4 discusses the virtual cement plant (VCP) with a one-dimensional physical-chemical model including clinker chemistry and heat transfer within a rotary cement kiln. Formulations from previously developed computational fluid dynamics (CFD) modeling of temperature profiles and calcination of raw meal into cement clinkers that happened in solid bed of cement kilns are integrated to form the model. Predictions of the model are verified by comparing them with published experiment data and Bogue calculation in Portland cement clinker (Bogue, 1929).

Chapter 5 discusses the coupling of VCP and VCCTL model by importing the output of the cement kiln model into VCCTL and running the integrated VCP-VCCTL model on HiPerGator High Performance Computer (HPC) at the University of Florida. Metaheuristic algorithms are applied on the integrated model to optimize energy consumption, cement strength, CO_2 emissions, and production cost. Pareto fronts are plotted to show the trade-off solutions between energy, price and greenhouse gas emissions.

Chapter 6 summarizes all the research reported in this dissertation on optimization of virtual cement and virtual cement plant and provides recommendations for blending raw materials to reduce production cost, increase sustainability and extend life of a quarry.

Challenges and limitations are also present for future studies to continue the advancement of the proposed methods.

CHAPTER 2
BACKGROUND

2.1 Introduction

This Chapter describes cement production modeling, cement hydration modeling and current optimization techniques in cement modeling.

2.2 Cement Production

Portland cement is the most common type of cement used in construction worldwide because of its affordability and the widespread availability of its constituent materials (e.g., limestone and shale). (Mindess & Young, 1981; Watts, 2013). It is produced from the grinding of clinker, which is produced by the calcination of limestone and other raw minerals in a cement rotary kiln. Combining Portland cement with water causes a set of exothermic hydraulic chemical reactions that result in hardening and ultimately the curing of placed concrete.

According to United States Geological Survey (USGS), U.S. cement and clinker production in 2015 was 82.8 million tons and 75.8 million tons, respectively. U.S. ready mixed concrete production is 325 million tons (Worrell et al., 2013). The production of cement and concrete consumes a significant amount of energy. The associated energy assumption accounts for 20-40% of the total cost (Chatziaras, Psomopoulos, & Themelis, 2016; Worrell et al., 2013).

In 2008, the U.S. cement industry spent $1.7 billion on energy alone, with electricity and fuel costing $0.75 billion and $0.9 billion, respectively. Cement production contributes 4% of the global industrial carbon dioxide (CO_2) emissions. Among the emissions, 40% CO_2 comes from the consumption of fossil fuels, 50% comes from calcination/decomposition of limestone inside the cement kiln, and 10% comes from transportation of raw meal and electricity consumption (Benhelal, Zahedi, Shamsaei, & Bahadori, 2013). During the cement and concrete production, clinker production process inside the cement rotary kiln consumes more than 90% of the total

energy use and all of the fuel use. For the modern cement plant, coal and coke have become principal fuel, which took the place of natural gas in 1970s (Worrell et al., 2013).

Currently, industry is seeking different energy efficiency technologies to reduce these energy costs. The challenge lies in reducing production costs and energy consumption without negatively affecting product quality. (Worrell et al., 2013) measured the energy efficiency through multiple technologies including finer raw meal grinding, multiple preheater stages, combustion improvement, lower lime saturation factor, cement kiln shell heat loss reduction, location optimization of cement factory for transportation cost reduction and high efficient facility such roller mills, fans and motors, which means there is ample room for energy efficiency improvement. Among all of the energy-efficient technologies in cement production, fuel combustion improvement is most important because it costs most energy (>50%) and produces most emissions (>40%). There are two types of rotary cement kilns: wet and dry. Wet kilns are typically longer (200 m) than dry kilns (50-100 m) in order to consider evaporation of water (C. M. Csernyei, 2016). Dry-type rotary kilns are more thermally efficient and common in industry (Worrell et al., 2013). There are four regions in a kiln: Preheating/Drying, Calcining/Decomposition, Burning/Clinkerizing, and Cooling (Peray & Waddell, 1986). Precalciners are typically utilized to dry kilns to improve thermal efficiency, which allows for shorter kilns. In this dissertation, dry-type rotary kilns are modeled.

Prior research has produced mathematical models to simulate thermal energy within the cement kiln and clinker formation to characterize the operation parameters, temperature profiles, clinker formation and energy consumption in the design.(Akhtar et al., 2013; Atmaca & Yumrutaş, 2014; C. Csernyei & Straatman, 2016; C. M. Csernyei, 2016; K. S. Mujumdar,

Ganesh, Kulkarni, & Ranade, 2007; Nørskov, 2012; Sadighi et al., 2011; Saidur, Hossain, Islam, Fayaz, & Mohammed, 2011; Spang, 1972; Stadler, Poland, & Gallestey, 2011).

Due to the complexities of rotary kiln modeling, there is no single, universal model developed in research or commercial use. The oldest cement kiln model developed by (Spang, 1972) , is a dynamic model that predicts the temperature file of freeboard gas, bulk bed and internal wall and the species compositions of each clinker product as they progress along the kiln. Different from other models, Spang's model does not give steady-state solution inside the kiln. The formulations of wall temperature profiles and species mass fractions are function of time. Partial differential equations are built to calculate temperature and species mass fraction at different stage.

For models applying a steady-state solution, there exists two types of one-dimensional models (K. Mujumdar & Ranade, 2006). The first type is a two-point boundary value problem, where the inlet temperature profiles of freeboard gas and bulk bed are given (C. Csernyei & Straatman, 2016; S. Q. Li et al., 2005; Martins et al., 2002; K. Mujumdar & Ranade, 2006; Sadighi et al., 2011; Spang, 1972). From the solution of a series of ordinary differential equations, the temperature profiles and species mass fraction along the kiln are solved numerically. The second type incorporates coupled the three-dimensional CFD models of burner for freeboard gas profile and clinker chemistry due to the complexity of three-dimensional nature of flow generated from a burner (Barr, 1986; Darabi, 2007; Mastorakos et al., 1999; K. S. Mujumdar, Arora, & Ranade, 2006).

In this study, a steady-state one-dimensional kiln model is applied because of its flexibility of parameters and computational availability for solvers in MATLAB paired with high performance cluster. Mathematical formulations are built based on Sadighi, Mujumdar and

Csernyei's work, which are covered in Section 2.3. This one-dimensional physical-chemical kiln model is developed to simulate the behavior of virtual cement plant (VCP). VCP was then coupled with VCCTL and metaheuristic optimization tool for an integrated optimized computational model that predicts measures of performance and sustainability.

2.3 Formulation of 1D Physical-chemical Model of a Rotary Cement Kiln

A Rotary cement kiln is a large piece of equipment converting raw meal to cement clinkers. Figure 2-1 shows the schematic of rotary cement kiln (C. M. Csernyei, 2016). Raw meal enters at the higher end with a certain solid flow rate. Fuel (coal, natural gas or petroleum coke) enters at the lower end.

There are four main processes in the rotary kiln: Drying, calcining, burning and cooling (Peray & Waddell, 1986). First, the raw materials are preheated and dried to reduce moisture of the mixture for calcination. Then the limestone ($CaCO_3$) is calcined into calcium oxide (also known as free lime) and carbon dioxide (CO_2). After the calcination, a series of solid-solid and solid-liquid chemical reactions happens to form clinker. During this burning process, the temperature inside the kiln reaches its highest point. Alite (C_3S) and belite (C_2S) are formed from free lime. Coating also happens in this stage because of the presence of liquid. After burning process, the hot clinkers are transported into a cooler for fast cooling. After that, the clinkers are grinded with cement mill and added some additives (such as gypsum and limestone) based on the requirement of users to get final cement. Table 2-1 shows the name and chemical formula of raw meal and clinkers.

In Portland cement production, rotary kilns are considered as the core for cement manufacturing plants. At the entry of the kiln, grinded and homogenized raw material—comprised of limestone ($CaCO_3$), alumina (Al_2O_3), iron (Fe_2O_3), silica (SiO_2) and small amount of other minerals—pass through a preheater for initial calcination. Inside the kiln, the formation

of cement clinker occurs from a series of chemical reactions including limestone calcination/ decomposition and clinker formation. Clinker is then cooled at the exit of the kiln and grinded to fine powder for package. During the entire cement production process, the production of clinker inside cement kiln consumes most thermal energy, which is about 90% of the total energy (Atmaca & Yumrutaş, 2014). 50 – 60% of the energy consumption is attributed to the combustion of fuel (Kabir, Abubakar, & El-Nafaty, 2010).

Multiple 2D and 3D physical chemical models exist in the literature, e.g., (Barr, 1986; Darabi, 2007; Mastorakos et al., 1999; K. S. Mujumdar et al., 2006). More recent research has focused on creating a simplified 1D model, which is more computationally efficient (C. Csernyei & Straatman, 2016; S. Q. Li et al., 2005; Martins et al., 2002; K. Mujumdar & Ranade, 2006; Sadighi et al., 2011; Spang, 1972). The current study applies the 1D kiln model described in (C. M. Csernyei, 2016; K. Mujumdar & Ranade, 2006) from University of Western Ontario. It couples the heat-balance equation and clinker chemical reaction rate equations to calculate the temperature of the different components of the kiln and the mass fraction for each phase of clinker production at steady state.

2.3.1 Heat Transfer Equations

For the kiln model, three types of heat transfer: radiation, convection and conduction happen inside and outside the kiln simultaneously. The interactive heat transfer happens between the gas phase and the solid phase, the gas phase between the wall, the solid and the wall, which is shown as cross-section of the kiln in Figure 2-2.

A group of heat equations including conduction from internal wall to solid bed, convection from freeboard gas to solid bed, convection from freeboard gas to internal wall, radiation from freeboard gas to solid bed, radiation from freeboard gas to internal wall and radiation from wall to solid have been developed to investigate the heat transfer. Figure 2-3

shows the heat transfer between internal wall, freeboard gas and solid bed inside the cement rotary kiln.

First, Equation (2-1) describes general energy balance of a steady-state, steady-flow model.

$$Q_{net,in} - \dot{W}_{net,out} = \Sigma \dot{m}_{out} h_{out} - \Sigma \dot{m}_{in} h_{in} \quad (2\text{-}1)$$

Equations (2-2) to (2-9) show the formulation describing each heat transfer variables inside the kiln based on the previous heat transfer knowledge and numerical models for rotary kiln (Hottel & Sarofim, 1965; S. Q. Li et al., 2005; Martins et al., 2002; K. Mujumdar & Ranade, 2006; K. S. Mujumdar et al., 2006; Tscheng & Watkinson, 1979)

The conduction heat transfer happens when two objects are in contact. Inside the kiln, conduction happens between the solid and the internal wall from direct contact. Q_{cwb} is expressed as the conduction heat transfer between the internal wall and the solid bed.

$$Q_{cwb} = h_{cwb} A_{cwb} (T_W - T_B) \quad (2\text{-}2)$$

$$h_{cwb} = 11.6 \left(\frac{k_b}{A_{cwb}}\right) \left(\frac{\omega R^2 \Gamma}{\alpha_B}\right)^{0.3} \quad (2\text{-}3)$$

Where, A_{cwb} is the conduction area between the internal wall and the solid bed, which is the product of solid bed arc length and kiln length. Convection and radiation areas are calculated in similar ways. k_b is the thermal conductivity of the solid bed. ω is the rotational speed of the kiln, R is the radius of the of the kiln. All of the parameters are listed at the beginning of this dissertation as List of Abbreviations.

The radiative heat transfer happens by the emissions of the electromagnetic radiation from the high-temperature object. Inside the cement rotary kiln, both gas and the internal wall

emit the radiation. Q_{rwb} is expressed as the radiative heat transfer from the internal wall to solid bed

$$Q_{rwb} = \sigma A_{rwb} \varepsilon_B \varepsilon_W \Omega (T_W^4 - T_B^4) \quad (2\text{-}4)$$

$$\Omega = \frac{L_{gcl}}{(2\pi - \beta)R} \quad (2\text{-}5)$$

Q_{rgb} is the radiative heat transfer from the freeboard gas to solid bed. Q_{rgw} is the radiative heat transfer from the freeboard gas to internal wall

$$Q_{rgb} = \sigma A_{rgb} (\varepsilon_b + 1)(\frac{\varepsilon_G T_G^4 - \alpha_G T_B^4}{2}) \quad (2\text{-}6)$$

$$Q_{rgw} = \sigma A_{rgw} (\varepsilon_w + 1)(\frac{\varepsilon_G T_G^4 - \alpha_G T_W^4}{2}) \quad (2\text{-}7)$$

The convection heat transfer happens between the object and its environment which happens between the freeboard gas phase and the wall, and between the gas phase and the solid. Q_{cgb} is the convective heat transfer from the freeboard gas to solid bed. Q_{cgw} is the convective heat transfer from the freeboard gas to internal wall. Calculation for h_{cgb} and h_{cgw} are discussed in Csernyei's work (C. M. Csernyei, 2016).

$$Q_{cgb} = h_{cgb} A_{cgb} (T_G - T_B) \quad (2\text{-}8)$$

$$Q_{cgw} = h_{cgw} A_{cgw} (T_G - T_W) \quad (2\text{-}9)$$

From Equations (2-2) to (2-9), the total heat flux received by solid bed from internal heat transfer is calculated as Equation 2-10 (K. Mujumdar & Ranade, 2006)

$$Q' = \frac{Q_{cwb}}{A_{cwb}} + \frac{Q_{rwb}}{A_{rwb}} + \frac{Q_{rgb}}{A_{rgb}} + \frac{Q_{cgb}}{A_{cgb}} \quad (2\text{-}10)$$

From the above equations, the heat transfer between different components is related to each other. The temperature of the wall, the gas phase and the solid phase could not be solved directly from the above equations.

2.3.2 Clinker Formation

Cement clinker formation is a complex chemical process that numerous chemical reactions happen simultaneously. Each reaction requires a separate thermodynamic condition (Babushkin, Matveev, & Mchedlov-Petrosiẫn, 1985). Typically, a series of five reactions has been applied to represent the complex chemical reactions inside cement kiln (Bogue, 1929):

$$CaCO_3 \rightarrow CaO + CO_2 \quad (2\text{-}11)$$

$$2CaO + SiO_2 \rightarrow C_2S \quad (2\text{-}12)$$

$$C_2S + CaO \rightarrow C_3S \quad (2\text{-}13)$$

$$3CaO + Al_2O_3 \rightarrow C_3A \quad (2\text{-}14)$$

$$4CaO + Al_2O_3 + Fe_2O_4 \rightarrow C_4AF \quad (2\text{-}15)$$

where the primary mineral constituents consist of tricalcium silicate C_3S (Alite), dicalcium silicate C_2S (Belite), Tricalcium aluminate C_3A and tetracalcium aluminoferrite C_4AF. The main mineral in all of these compounds is calcium oxide CaO, which is acquired from the calcination and decomposition of limestone $CaCO_3$.

Inside the kiln, the solid material flows to the burner end of the kiln through the 2-5 degree of inclination (shown in Figure 2-1). Heated freeboard gas flows from the burner end to the entry on the top of solid bed material. From the heat transfer between the hot freeboard gas, solid bed material and internal wall of the kiln (shown in Figure 2-2 and Figure 2-3), a series of complex exothermic and endothermic chemical reactions happens inside the kiln for clinker formation. To simplify the process and make it convenient to analyze, only the major clinker formation chemical reactions (shown in Equation (2-11) to (2-15)) are considered.

Table 2-2, taken from (Darabi, 2007) shows the five major chemical reactions occurring inside the cement kiln, which are used for clinker formation analysis in current model. Different reactions happen at different temperature ranges, which are used to set starting and ending point for each reaction in the model.

In Table 2-2, positive sign indicates the reaction is endothermic and negative sign indicates the reaction is exothermic. Equation (2-16) from (C. M. Csernyei, 2016; Spang, 1972) gives the heat transfer from chemistry including heat absorbed from 1st and 3rd reactions and heat generated from 2nd, 4th and 5th reactions.

$$q_c = \frac{\rho_s}{1+A_i+F_i+S_i}[-\Delta H_{CaCO_3} k_1 Y_{CaCO_3} - \Delta H_{C_2S} k_2 Y_{SiO_2} Y_{CaO}^2 - \Delta H_{C_2S} k_3 Y_{CaO} Y_{c_2s} - \Delta H_{C_3A} k_4 Y_{CaO}^3 Y_{Al_2O_3} - \Delta H_{C_4AF} k_5 Y_{CaO}^4 Y_{Al_2O_3} Y_{Fe_2O_3}] \quad (2\text{-}16)$$

Where, A_i, F_i and S_i are the input mass fraction for Al_2O_3, Fe_2O_3 and SiO_2. ΔH is the heat of reaction. k is the reaction rate for j^{th} reaction. Y is the mass fraction for the reactant or product participating in j^{th} reaction. Based on Arrhenius is equation (Arrhenius, 1889), reaction constants for the five chemical reactions inside the kiln are calculated from Equation (2-17).

$$k_j = A_j \exp(-\frac{E_j}{R_g T_b}) \quad (2\text{-}17)$$

Where A_j is the pre-exponential factor for j^{th} reaction (1/s), E_j is the activation energy for j^{th} reaction (J/mol). R_g is the universal gas constant, which is 8.314 (J/g.mol.K).

Table 2-3 list the calculation of reaction rates and values for Aj and Ej, which are taken from (Darabi, 2007; Spang, 1972). Once reaction rates are calculated, the production rate of each component could be calculated based on the reactions the component participates in. For example, CaO is the product of 1st reaction and reactant of 2nd -5th reaction. Therefore,

production rate for CaO is $r_1 - r_2 - r_3 - r_4 - r_5$. Table 2-4 lists the reaction rate for all components in the five chemical reactions.

Mass fraction of each species could be calculated from material balance equation (2-18), which is from plug flow reactor with constant axial velocity at steady-state (Darabi, 2007).

$$v_s \frac{dY_n}{dx} = R_n \tag{2-18}$$

where R_n is the production rate for species n, v_s is the solid velocity (m/s) in the kiln.

The production rates for the 10 components listed in Table 2-4 are substituted into Equation (2-18) and normalized with mass of CaO, shown as Equation (2-19) - (2-27)

$$v_s \frac{dY_{CaCO_3}}{dx} = -\frac{M_{CaCO_3}}{M_{CaO}} k_1 Y_{CaCO_3} \tag{2-19}$$

$$v_s \frac{dY_{CaO}}{dx} = k_1 Y_{CaCO_3} - k_2 Y_{SiO_2} Y_{CaO}^2 - k_3 Y_{CaO} Y_{c_2s} - k_4 Y_{CaO}^3 Y_{Al_2O_3} - k_5 Y_{CaO}^4 Y_{Al_2O_3} Y_{Fe_2O_3} \tag{2-20}$$

$$v_s \frac{dY_{SiO_2}}{dx} = -\frac{M_{SiO_2}}{2M_{CaO}} k_2 Y_{SiO_2} Y_{CaO}^2 \tag{2-21}$$

$$v_s \frac{dY_{Al_2O_3}}{dx} = -\frac{M_{Al_2O_3}}{3M_{CaO}} k_4 Y_{CaO}^3 Y_{Al_2O_3} - \frac{M_{Al_2O_3}}{4M_{CaO}} k_5 Y_{CaO}^4 Y_{Al_2O_3} Y_{Fe_2O_3} \tag{2-22}$$

$$v_s \frac{dY_{Fe_2O_3}}{dx} = -\frac{M_{Fe_2O_3}}{4M_{CaO}} k_5 Y_{CaO}^4 Y_{Al_2O_3} Y_{Fe_2O_3} \tag{2-23}$$

$$v_s \frac{dY_{C_2S}}{dx} = \frac{M_{C_2S}}{2M_{CaO}} k_2 Y_{SiO_2} Y_{CaO}^2 - \frac{M_{c_2s}}{M_{CaO}} k_3 Y_{CaO} Y_{C_2S} \tag{2-24}$$

$$v_s \frac{dY_{C_3S}}{dx} = \frac{M_{C_3S}}{M_{CaO}} k_3 Y_{CaO} Y_{C_2S} \tag{2-25}$$

$$v_s \frac{dY_{C_3A}}{dx} = \frac{M_{C_3A}}{3M_{CaO}} k_4 Y_{CaO}^3 Y_{Al_2O_3} \tag{2-26}$$

$$v_s \frac{dY_{C_4AF}}{dx} = \frac{M_{C_4AF}}{4M_{CaO}} k_5 Y_{CaO}^4 Y_{Al_2O_3} Y_{Fe_2O_3} \tag{2-27}$$

After the equations for mass fraction of each component is done, the temperature of solid bed could be calculated based on the mass fractions and the total heat received by solid bed Q', which is expressed as Equation (2-28)

$$v_s Cp_b A_s \frac{d(\rho_b T_b)}{dx} = Q' L_{gcl} + A_s q_c - S_{CO_2} \quad (2\text{-}28)$$

The meanings of each variables are given in the List of Abbreviations.

The production rate for mass fraction of each component in the reactions is related to the temperature of solid bed (Equation (2-16) – (2-27)). And heat received by solid bed is calculated from heat transfer (Equations (2-1) – (2-10)). The heat transfer items and clinker chemistry items are coupled by Equation (2-28).

By solving the ordinary differential equations (2-1) to (2-28), the temperature and the mass fractions of each species inside the kiln could be calculated simultaneously. More importantly, the above equations could be integrated with the metaheuristic method to optimize the factor as the user requests.

2.3.3 Heat Balance

Equation (2-29) from (C. M. Csernyei, 2016)) shows the heat balance relation among shell, refractory and coating satisfied for a kiln at steady state. The calculation for shell temperature is shown in Csernyei's dissertation (C. M. Csernyei, 2016), which will not be explained in detail in this section.

$$Q_{rgw} + Q_{cgw} - Q_{rwb} - Q_{cwb} = \sigma A_{sh} \varepsilon_{sh} (T_{sh}^4 - T_0^4) + h_{csh} A_{sh} (T_{sh} - T_0) \quad (2\text{-}29)$$

The heat balance equation is applied to check the accuracy temperature profiles using the Newton Raphson Method, which will be discussed in Chapter 4.

2.4 Cement Hydration Modeling

The concrete research community has long sought to reduce its reliance on physical testing of Portland cements (Bićanić et al., 2003; Bullard et al., 2004; Garboczi et al., 2004; Hain & Wriggers, 2008; Vallgårda & Redström, 2007), however advancements in computational modeling (Bentz, 1997; C. Haecker, Bentz, Feng, & Stutzman, 2003; Thomas et al., 2011) have yet to produce a widely accepted, purely numerical approach that performs as reliably and accurately as experimental methods (ASTM C109, ASTM C1702, ASTM C191).

One of the longest standing efforts to create a numerical framework is the software known as the Virtual Cement and Concrete Testing Laboratory (VCCTL), which has been available for commercial use from the National Institute of Standards and Technology (NIST) for several years. The study model predicts the thermal, electrical, diffusional, and mechanical properties of cements and mortars from user-specified phase distribution, particle size distribution, water/cement ratio (w/c), among other parameters (Bullard et al., 2004). Figure 2-4 and Figure 2-5 illustrates VCCTL model, which is a three-stage process:

1. Volume and surface area fractions of the four major cement phases (alite, belite, aluminate and ferrite) are obtained from X-ray powder diffraction, scanning electron microscopy, and multispectral image analysis to create a 3D microstructure of unreacted paste Figure 2-4 that is comprised of Portland cement, fly ash, slag, limestone and other cementitious materials
2. Kinetics and thermodynamics of Portland cement hydration are simulated under specified curing conditions including adiabatic and isothermal heating, producing virtual models of the material that can be analyzed for multiple properties, including linear elastic modulus, compressive strength, and relative diffusion coefficient (Bentz, 1997). The rate of hydration and resulting products are governed largely by the relative concentrations of the four major constituents of Portland cement: alite (C_3S), belite (C_2S), aluminate (C_3A), and ferrite

(C_4AF). The most reactive compounds are C_3A and C_3S. For strength development, although the calcium silicates provide most of the strength in the first 3 to 4 weeks, both C_3A and C_2S contribute equally to ultimate strength. C_2S hydrates in a similar way with C_3S; however, C_2S hydrates much slower since it is a less reactive compound. Consequently, the amount of heat liberated by the hydration of C_2S is also lower than the amount of heat C_3S liberates (Mamlouk & Zaniewski, 1999). Gypsum is introduced into the raw meal to slow the early rate of hydration of C_3A.

3. Finite element analysis of the resultant virtual microstructure gives the elastic modulus (E) (Watts, 2013)

In order to validate VCCTL model, researchers have analyzed the sensitivity to various inputs for the model, checked errors related with the digital image approximation method (Garboczi & Bentz, 2001), and compared simulated results to plastic and hardened properties of CCRL reference cements (Bentz, Feng, & Stutzman, 2000; Bullard & Stutzman, 2006). Those validation results show VCCTL could simulate hydration and predict strength and other properties quite well.

2.5 Optimization Techniques in Cement and Concrete

As discussed in previous sections, cement compounds play critical roles in the hydration process. Changing the proportion of each constituent compound, adjusting other factors such as particle size or fineness can vastly change the mechanical and thermal properties of the hydration process, and ultimately the final product. Due to the various factors in cement production and hydration, it is necessary and efficient to develop optimal computational models reflecting the effect of each factor and giving directions based on specific performance requirements instead of conducting large amounts of physical testing.

As the awareness of potential of cement and concrete to achieve higher performance grows, the problem of designing cement and concrete to exploit the possibilities has become more complex. In the past few years, statistical design of experiments, such as the response surface approach (Ahmad & Alghamdi, 2014; Ghezal & Khayat, 2002; Lagergren et al., 1997; Muthukumar & Mohan, 2004; Patel, Hossain, Shehata, Bouzoubaa, & Lachemi, 2004; MJ Simon, 2003; M Simon et al., 1999; Sonebi & Bassuoni, 2013; Soudki, El-Salakawy, & Elkum, 2001; Tan, Zaimoglu, Hinislioglu, & Altun, 2005; Xiaoyong & Wendi, 2011), were developed to optimize cement and concrete mixtures to meet a set of performance criteria at the same time with lease computational cost. Those performance criteria within cement and concrete properties include time of set, modulus of elasticity, viscosity, creep and shrinkage, heat of hydration and durability. Considering that cement and concrete mixtures consist of several components, the optimization should be able to take into account several attributes at a time. However, statistical methods become inefficient due to the excessive number of trial batches for each simulation to find optimal solutions.

Here we apply a metaheuristic optimization method, which is an iterative searching process that guides a subordinate heuristic by exploring and exploiting the search space intelligently with different learning strategies. Optimal solutions are found efficiently with this technique. Those methods have had widespread success and become influential methods in solving difficult combinational problems during the last several decades in engineering, mathematics, economics and social science (Collins et al., 1988; Jaumard et al., 1988; Nissen, 1993; Osman, 1995; Osman & Laporte, 1996; Pirlot, 1992; Rayward-Smith et al., 1996; Stewart et al., 1994). Some of the most popular metaheuristic algorithms include genetic algorithms,

particle swarm optimization, neutral networks, harmony search, simulated annealing, tabu search, *etc* (Osman & Laporte, 1996).

Particle Swarm Optimization is a population-based metaheuristic originally proposed by Kennedy and Eberhart in 1995 (Eberhart & Kennedy, 1995). This metaheuristic algorithm mimics swarm behavior in nature, e.g., the synchronized movement of flocking birds or schooling fish. It is straightforward to implement and is suitable for a non-differentiable and discreditable solution domain (Bonnans et al., 2006; Press et al., 2007). A PSO algorithm guides a swarm of particles as it moves through a search space from a random location to an objective location based on given objective functions.

Another important search method is the genetic algorithm (GA), which is developed from principles of genetics and natural selection (Bremermann, 1958; Fraser, 1957). This method was developed by John Holland at the University of Michigan for machine learning in 1975 (Holland, 1975). GA encodes the decision variables of a searching problem with series of strings. The strings contain information of genes in chromosomes (Burke & Kendall, 2005). GA analyzes coding information of the parameters. A key factor for this method is working with a population of designs that can mate and create offspring population designs. For this method to work, fitness is used to select the parent populations based on their objective function value, and the offspring population designs are created by crossing over the strings of the parent populations. Selection and crossover form an exploitation mechanism for seeking optimal designs. Furthermore, the mutations are added to the string as an element of exploration.

A multi-objective optimization problem (MOOP) considers a set of objective functions. For most practical decision-making problems, multiple objectives are considered at the same time to make decisions. A series of trade-off optimal solutions instead of a single optimum, is

obtained in such problems (Burke & Kendall, 2005). Those trade-off optimal solutions are also called Pareto-optimal solutions.

For the current cement and concrete modeling, multi-objective optimizations are applied because several performance criteria of cement and concrete need to be considered at the same time. As introduced above, VCCTL requires a number of input variables to execute a complete virtual hydrated cement model for analyzing mechanical and material properties. There are a large number of potential combinations for inputs ($\sim 10^6$). It takes one hour to run each combination on VCCTL with high performance computing cluster. Therefore, a blind search for specified performance criteria is not practical. Metaheuristic techniques, however, provide a reasonable direction for searching through a large feasible domain, which is efficient and suitable for the inputs and outputs from VCCTL. Both PSO and GA solve MOOPs to give a Pareto frontier, which consists of optimal solutions. Elitism strategy (Burke & Kendall, 2005) is applied to keep the best individual from the parents and offspring population. Also, the idea of non-dominated sorting procedure can be applied to the PSO to solve the MOOP and increase the efficiency of optimization. In this dissertation, metaheuristic algorithms are applied based on VCCLT to solve MOOP in virtual cement.

Table 2-1. Raw meal components and clinker phases

Type	Name	Chemical Formula
Raw meal	Calcium carbonate	$CaCO_3$
	Silicon dioxide (Silica)	SiO_2
	Aluminium oxide (Shale)	Al_2O_3
	Ferrate oxide	Fe_2O_3
Clinker phases	Tricalcium silicate (Alite)	C_3S ($3CaO.SiO_2$)
	Dicalcium silicate (Belite)	C_2S ($2CaO.SiO_2$)
	Tricalcium aluminate	C_3A ($3CaO.Al_2O_3$)
	Tetracalcium aluminoferrite	C_4AF ($4CaO.Al_2O_3.Fe_2O_3$)

Table 2-2. Thermal information for clinker reaction (Darabi, 2007)

No.	Reaction	Temperature Range (K)	Enthalpy of Reaction (J/kg)
1	$CaCO_3 \rightarrow CaO + CO_2$	823-1233	+1.782e6
2	$2CaO + SiO_2 \rightarrow C_2S$	873-1573	-1.124e6
3	$C_2S + CaO \rightarrow C_3S$	1473-1553	+8.01e4
4	$3CaO + Al_2O_3 \rightarrow C_3A$	1473-1553	-4.34e4
5	$4CaO + Al_2O_3 + Fe_2O_4 \rightarrow C_4AF$	1473-1553	-2.278e5
6	$Clinker_{solid} \rightarrow Clinker_{liquid}$	>1553	+6.00e5

Table 2-3. Reaction rate, pre-exponential factors and activation energies for clinker reactions

No.	Reaction Constant	Reaction Rate	Pre-exponential Factor (A_j) (1/s)	Activation Energy (E_j) (J/mol)
1	k_1	$r_1 = k_1 Y_{CaCO_3}$	4.55e31	7.81e5
2	k_2	$r_2 = k_2 Y_{SiO_2} Y_{CaO}^2$	4.11e5	1.93e5
3	k_3	$r_3 = k_3 Y_{CaO} Y_{c_2s}$	1.33e5	2.56e5
4	k_4	$r_4 = k_4 Y_{CaO}^3 Y_{Al_2O_3}$	8.33e6	1.94e5
5	k_5	$r_5 = k_5 Y_{CaO}^4 Y_{Al_2O_3} Y_{Fe_2O_3}$	8.33e8	1.85e5

Table 2-4. Production rates for each component of reactions

Component of Reactions	Production Rate
$CaCO_3$	$R_1 = -r_1$
CaO	$R_2 = r_1 - r_2 - r_3 - r_4 - r_5$
SiO_2	$R_3 = -r_2$
C_2S	$R_4 = r_2 - r_3$
C_3S	$R_5 = r_3$
Al_2O_3	$R_6 = -r_4 - r_5$
C_3A	$R_7 = r_4$
Fe_2O_3	$R_8 = -r_5$
C_4AF	$R_9 = r_5$
CO_2	$R_{10} = r_1$

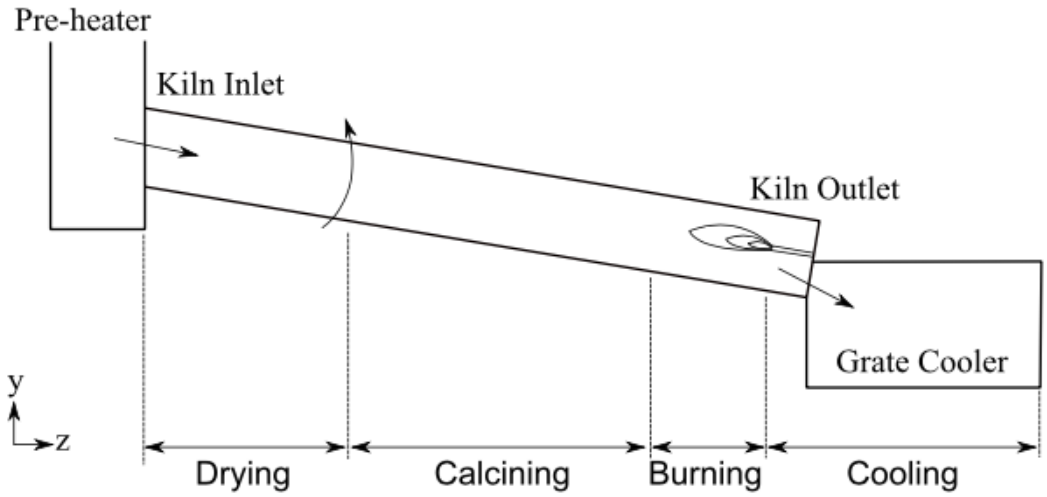

Figure 2-1. Schematic of rotary cement kiln with four regions (C. M. Csernyei, 2016).

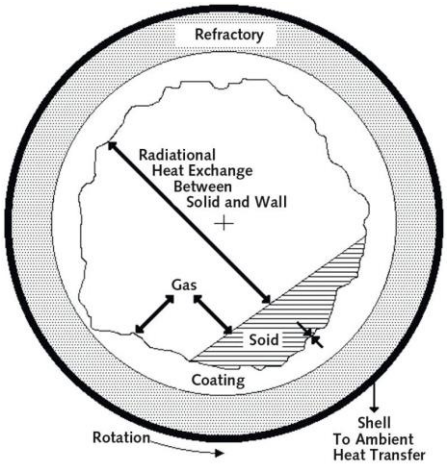

Figure 2-2. Cross-section of rotary cement kiln (Noshirvani, Shirvani, Askari-Mamani, & Nourzadeh, 2013).

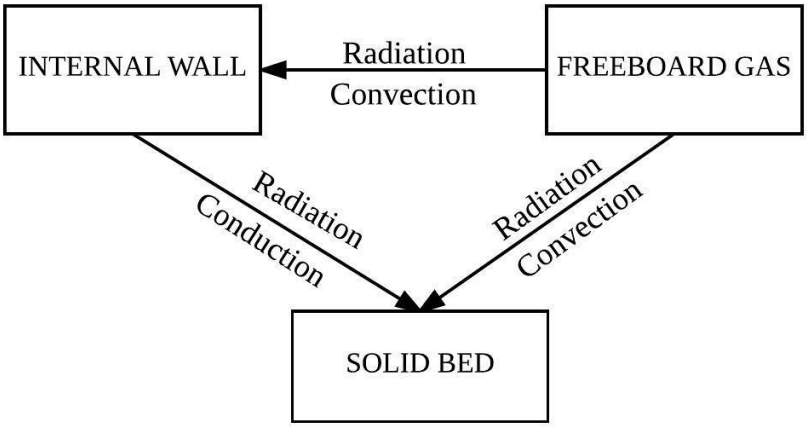

Figure 2-3. Heat transfer (radiation, convection, conduction) among internal wall, freeboard gas and solid bed

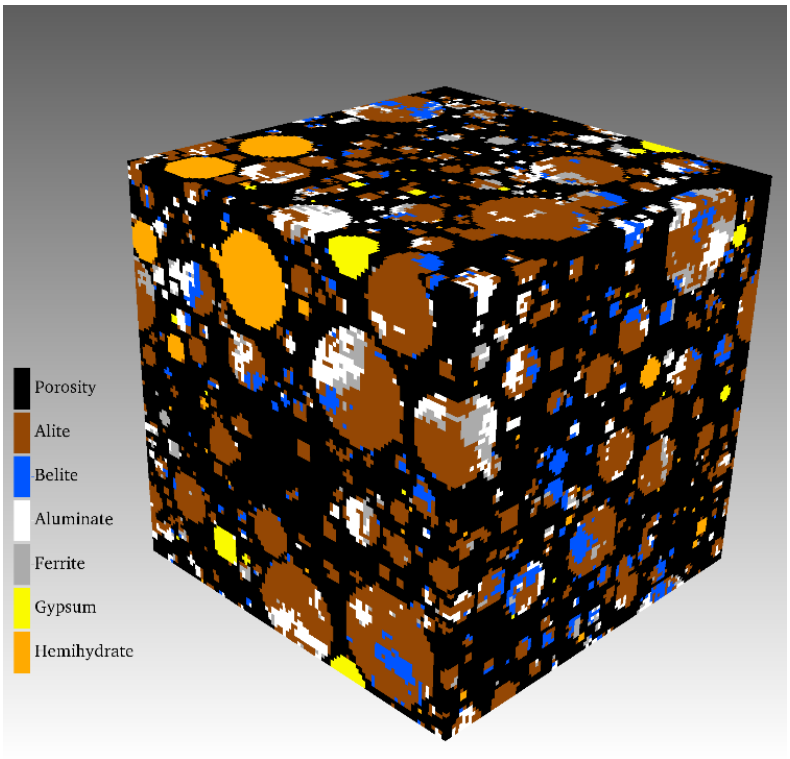

Figure 2-4. 3D initial microstructure from VCCTL

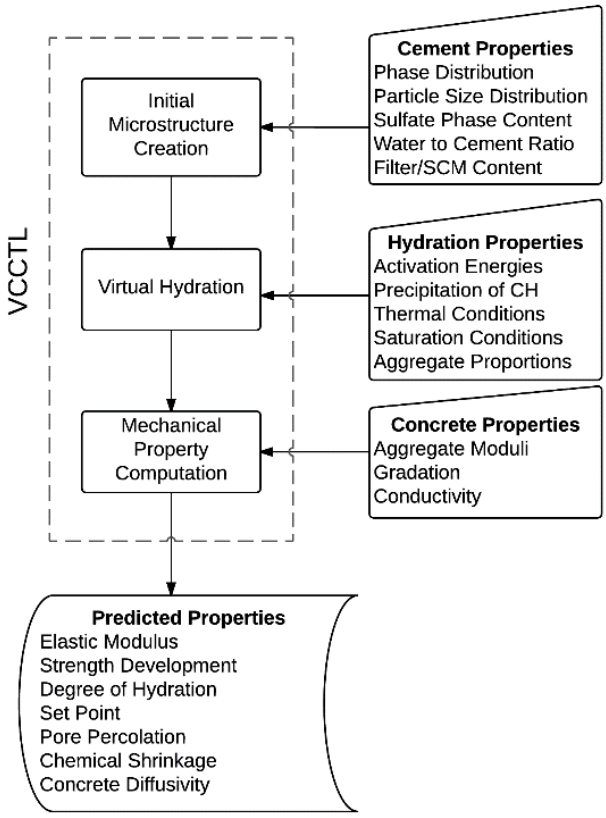

Figure 2-5. Algorithm of VCCTL

CHAPTER 3
METAHEURISTIC ALGORITHMS APPLIED TO VIRTUAL CEMENT MODELING

3.1 Overview

This chapter presents the application of metaheuristic algorithms on VCCTL to optimize chemistry and water-cement ratio of cement and mortar. This study adopts a forward-looking view that this goal will be reached, turning to how its full investigative power can be applied to characterize a broad range of cements and hydration conditions. It successfully demonstrates that a multi-objective metaheuristic optimization technique can generate the Pareto surface for the modulus of elasticity, time of set and kiln temperature for approximately 150,000 unique cements that encompass the clear majority of North American cement compositions in ASTM C150 (Cement). Insofar as the hydration model is accurate, the benefit of applying large-scale simulations to characterize the strength, durability and sustainability of an individual cement relative to a broad range of cement compositions is shown.

This section describes the hydration study model in VCCTL, the metaheuristic algorithm, and different case studies that demonstrate the utility of metaheuristic algorithms to find optimal solutions and Pareto analysis on Portland cements. Convergence is discussed to assist users replicating this approach. Finally, the study demonstrates that tri-objective Pareto analysis is a flexible and objective tool to rate cements and offer remarks on the potential of this approach to solve much large combinatorial problems arising from the introduction of other variables such as cement fineness and aggregate proportions.

3.2 Methodology

The VCCTL algorithm was ported to the University of Florida HiPerGator High Performance Computer (HPC), operating up to 500 cores for nearly one month to complete 149,572 unique simulations based on the input bounds shown in Table 3-1. Cement phases and

w/c were discretized into ten and 15 equally spaced intervals, respectively, with the constraint that the mass fractions for all phases must sum to unity. These data were archived and reused during algorithm development (thus preventing the need to rerun VCCTL) and for the case studies in Section 3.3 that compare the Pareto Front technique to the fully enumerated solution space.

Once a completed VCCTL simulation is done, a set of outputs for hydrated cement paste models is created from the hydration, transport and mechanical properties. Model data applied in this study were the (a) output seven-day elastic modulus, (b) output time of set of the hydrated paste, and (c) a proxy for kiln temperature, the ratio of inputs alite (C_3S) and belite (C_2S).

A brief introduction for the three outputs is as follows:

(a) Seven-day elastic modulus is calculated directly from the 3D image using a finite element method (Garboczi & Berryman, 2001). The elastic modulus of the cement paste is directly related to the stiffness of a concrete made with that paste and provides an indication of the relative stiffness for different cement compositions and water cement ratios. The elastic modulus can also be used to calculate the compressive strength of concrete, which is considered as an important design parameter in many applications; (b) Time of set is the final setting time of the concrete (Mamlouk & Zaniewski, 1999). Setting refers to the stage changing from a plastic to a solid state, also known as cement paste stiffening. It is usually described in two levels: initial set and final set. Initial set happens when the cement paste starts to stiffen noticeably. Final set happens when the cement has hardened enough for load. To determine the setting time, measurements are taken through a penetration test; (c) A proxy for kiln temperature, alite : belite was chosen based on the assumption that they form at higher and lower kiln temperatures, which represent the embodied energy in cement production process due to the direct relationship

between embodied energy and carbon content (Reddy & Jagadish, 2003; Reddy, Leuzinger, & Sreeram, 2014). A kiln model developed by (C. M. Csernyei, 2016) was combined with VCCTL to simulate virtual cement plant. Input including gas temperature, raw meal composition was given to VCP to get clinker composition. Figure 3-1 shows the position relation between kiln gas temperature and alite to belite ratio. Thus alite:belite was chosen to represent kiln temperatures. Figure 3-2 plots values for each cement, with marker color corresponding to the w/c (shown on the right).

Seen as a whole, the results compare well with expected behavior. The range of E, time of set, and C_3S/C_2S are [11.1, 32.0] GPa, [3.2,17.4] hrs, and [1.2,3.9], respectively, which are acceptable ranges based on the bounds shown in Table 3-1. The model captures the effect of paste densifying as w/c decreases, which causes the modulus to increase (Neville, 1995). Further, the observed relationship between E and w/c matches the experimental measurements described by (C.-J. Haecker et al., 2005). The modulus is also observed to increase proportionally with increasing C_3S/C_2S, which is consistent with past research (e.g., (Taylor, 1997)) that has shown alite is the primary silicate phase contributing to early strength development in Portland cement. The model also captures the decrease in time of set associated with a lower w/c, which increases the rate of hydration (Odler, 1998). The setting of paste occurs as the growth of hydration solids bridges the spaces between suspended cement particles (Chen & Odler, 1992). Higher water to cement ratios result in larger spaces between particles, generally increasing the time required for setting to occur (Garboczi & Bentz, 1995), as well as the sensitivity of setting time to differences in cement composition. Table 3-2 lists the structure of VCCTL database for virtual cement. The database consisting of inputs and outputs of VCCTL for 149,572 different Portland cement compositions is sample data for metaheuristic optimization, introduced in the following sections.

3.3 Cement Optimization based on Metaheuristic Algorithms

3.3.1 Overview

Multiple objectives drive cement production (e.g., minimize kiln temperature while maximizing the modulus), thus a set of trade-off optimal solutions must be obtained instead of a single optimum (Burke & Kendall, 2005). The solution is the so-called Pareto front, which is an envelope curve on the plane for two objectives and a surface in space for three objectives. The optimal solution set on a Pareto front are the set of solutions not dominated by any member of the entire search space (Burke & Kendall, 2005). This is generally not the case for cements, however. For example, one composition may have a larger E than a second composition with a lower heat proxy than the first. All else being equal, neither cement dominates another in terms of quality without additional user input to differentiate the relative importance of each variable. Therefore, non-dominated solutions were selected by simultaneously comparing three objectives (described in Section 3.3.2) to evaluate the fitness (optimality) of each cement.

Another consideration in the analysis was the combinatorial explosion arising from studying larger variable sets. While the Pareto front can be calculated directly from enveloping VCCTL results for every unique combination of cement phase and w/c, it would generally be impractical for a problem larger than what this paper presents. Consider Figure 3-3, which depicts the number of computer simulations as a function of the variable count.

The current study (8 variables) required hundreds of cores on a HPC running nearly one month to complete. Adding one new variable (e.g., concrete fineness) would increase the run time by a factor of ten. Adding a second new variable would render the simulation impractical in most HPC infrastructures.

The realization that computational expense would ultimately be a significant barrier to implementation motivated the application of the multi-objective metaheuristic search algorithm

described in the next section. The study will show that it is possible to study the Pareto front of Portland cement with a vastly reduced number of simulations than what is required to build a data-driven Pareto front, thus hopefully creating extensibility to larger combinatorial problems that will follow this work.

Cement and concrete optimization primarily applies statistical methods, (Ahmad & Alghamdi, 2014; Ghezal & Khayat, 2002; Lagergren et al., 1997; Muthukumar & Mohan, 2004; Patel et al., 2004; MJ Simon, 2003; M Simon et al., 1999; Sonebi & Bassuoni, 2013; Soudki et al., 2001; Tan et al., 2005; Xiaoyong & Wendi, 2011). In contrast, this study applies metaheuristic optimization, which has shown widespread success in solving difficult combinational problems in other fields (Collins et al., 1988; Jaumard et al., 1988; Nissen, 1993; Osman, 1995; Osman & Laporte, 1996; Pirlot, 1992; Rayward-Smith et al., 1996; Stewart et al., 1994; Voß et al., 2012). Common methods include particle swarm optimization (PSO) (Eberhart & Kennedy, 1995; Hu et al., 2003; L. Li et al., 2009; L. Li et al., 2007; Shi, 2001), genetic algorithms (Goldberg & Samtani, 1986; Rajeev & Krishnamoorthy, 1992; Wu & Chow, 1995), harmony search (Geem, Kim, & Loganathan, 2001), simulated annealing (Aarts & Korst, 1988; Kirkpatrick, 1984), and TABU search (Glover & Laguna, 2013).

This research applies the PSO and Genetic Algorithm because they are straightforward to implement and suitable for a non-differentiable and discretizable solution domain (Bonnans et al., 2006; Press et al., 2007). Both methods are population-based metaheuristic approaches, which maintain and improve multiple candidate solutions by using population characteristics to guide the search.

To conduct a metaheuristic search, good solutions need to be distinguished from bad solutions. In the current study, solutions for each individual are evaluated from objectives such

as seven-day modulus, time of set, heat proxy of each virtual cement from simulation result in VCCTL. And the elitism strategy (or elitist selection), known as the process to allow best individuals from current generation to next generation, is used by both search algorithms to guide the evolution of good solutions (Burke & Kendall, 2005). The population size, which is defined by users, plays an important role in algorithms. It affects the performance of the algorithm: if too small, premature convergence will happen to give unacceptable solutions; if too large, a lot of computational cost will be wasted. The basic ideas and procedures of PSO and GA are explained as follows (Burke & Kendall, 2005).

3.3.2 Pareto Front Generation Applying Particle Swarm Optimization

The PSO algorithm developed by (Eberhart & Kennedy, 1995) mimics swarm behavior in nature, e.g., the synchronized movement of flocking birds or schooling fish (Parsopoulos & Vrahatis, 2002). Each particle (here the unique combination of phase chemistry and w/c) in the search space has a fitness value calculated from a user-specified objective function. During each iteration, the particle 'velocities' are updated to cause the swarm to move towards the better solution area in the search space (Grosan, Abraham, & Chis, 2006). The procedure is as follows:

1. Initialize the particle positions $x_i^{k=0}$ from the set:

   $\{w/c, C_3S, C_2S, C_4AF, C_3A, Gypsum, Anhydrite, Hemihydrate\}$

   drawing from the uniform distribution of each design variable within the bounds shown in Table 3-1, where *i* is the particle number and *k* is the generation
2. Copy $x_i^{k=0}$ to P_i^k, which are the best positions of each particle up to the current generation
3. Calculate the corresponding objective functions $f_1^{k=0}(x_i)$, $f_2^{k=0}(x_i)$, $f_3^{k=0}(x_i)$, i.e., E, time of set and C_3S/C_2S from VCCTL

4. Randomly assign one of the non-dominated positions in the swarm to P_g^k. For example, consider the tri-objective case minimizing time of set and C_3S/C_2S and maximizing E. The variable $x_i^{k=0}$ is a non-dominated position if and only if there is no $x_j^{k=0}(j \neq i)$ in the generation with one of the three characteristics below for min f_1 – min f_2 – max f_3 case:

$$f_1(x_j) \leq f_1(x_i) \text{ and } f_2(x_j) \leq f_2(x_i) \text{ and } f_3(x_j) > f_3(x_i)$$
$$f_1(x_j) \leq f_1(x_i) \text{ and } f_2(x_j) < f_2(x_i) \text{ and } f_3(x_j) \geq f_3(x_i) \quad (3\text{-}1)$$
$$f_1(x_j) < f_1(x_i) \text{ and } f_2(x_j) \leq f_2(x_i) \text{ and } f_3(x_j) \geq f_3(x_i)$$

5. If $k = 0$, initialize the velocities to zero, $v_i^{k=0} = 0$
6. If $k > 0$, update the velocities of each particle with

$$V_i^{k+1} = wV_i^k + c_1 r_1(P_i^k - x_i^k) + c_2 r_2(P_g^k - x_i^k) \quad (3\text{-}2)$$

where c_1 and c_2 are the acceleration coefficients associated with cognitive and social swarm effects, respectively; r_1 and r_2 are random values uniformly drawn from [0,1], and w is the inertia weight, which represents the influence of previous velocity (L. Li et al., 2007). Based on trial and error, we selected both c_1 and c_2 to equal 0.8 respectively, and w decrease linearly from 1.2 to 0.1 over 500 generations

7. Update the new position of each particle i:

$$x_i^{k+1} = x_i^k + V_i^{k+1} \quad (3\text{-}3)$$

8. Calculate the three objective functions for each particle of the current generation (Eq. 3-2), and update P_i^k with the non-dominated positions if it is better than P_i^{k-1}
9. Update P_g^k by randomly assigning one of the non-dominated positions in the swarm
10. Store and update non-dominated solution found from the current generation in an external archive (known as elitist selection)
11. Repeat steps 6-10 until the algorithm converges (Section 3.5 gives more detail)

3.3.3 Pareto Front Generation Applying Genetic Algorithm

Based on principles of genetics in evolution and natural selection, Holland came up with Genetic Algorithm in 1975 (Holland, 1992). In this algorithm, strings containing the information of the design variables are created, which imitates DNA containing gene information in nature. Once the optimization problem for virtual cement is encoded in a chromosomal manner and objectives are calculated to evaluate the fitness of the solutions, GA starts to evolve a solution using the following steps:

1. Similar with PSO, initialize the population set

   $\{w/c, C_3S, C_2S, C_4AF, C_3A, Gypsum, Anhydrite, Hemihydrate\}$

   by randomly generating from the uniform distributed searching space of design variable with bounds shown in Table 3-1
2. Evaluate the fitness of each candidate solution by calculating and comparing the objectives with Equation 3-1
3. Select solutions with better fitness based on Step 2 to assign more good solutions for next generation. Tournament selection, is used in current study (Burke & Kendall, 2005)
4. Conduct crossover by combining parts of the parent population to create offspring population
5. Randomly modify one or two points at the parent chromosomes during the crossover, which mimics the gene mutation to give more randomness in the nearing space to candidate solution
6. After steps 3-5, replace parent population by offspring population. Replacement: The offspring population created by selection, crossover and mutation replaces the original parental population. One of the most popular replacement techniques, Elitism (Deb, Pratap, Agarwal, & Meyarivan, 2002) is applied for replacement in current study
7. Repeat steps 2 to 6 until algorithm converges

3.4 Case Studies

3.4.1 Example 1: Single Objective Optimum for Modulus

To verify whether the optimization method is appropriate to solve optimization problems based on VCCTL, a single-objective optimization is conducted as the first case study. Since the 7-day elastic modulus (E) factor is directly related to the strength of cement, it is selected as the objective to be optimized to a user-specified value. From the output database of VCCTL, the range of the 7-day elastic modulus is from 11.1 to 32 GPa which is consistent with literature (Odelson, Kerr, & Vichit-Vadakan, 2007). To demonstrate this case, the 7-day elastic modulus is optimized to a target value E_{target} of 15 GPa. Other target values could also be selected based on user's requirement. In this way, the single objective function of this problem is $| E - E_{target} |$, which should be minimized to get the optimal solution.

For this single-objective problem, the PSO algorithm is applied. The procedure was illustrated in Section 3.3.2. For this problem, the particle population size is set to 100, balancing between the number of generation required to converge and computational cost. And the optimization process is considered converged when the objective function is less than 10^{-6}.

Figure 3-4 shows the values of the objective function for 100 iterations. The whole optimization process converges after about 40 iterations, where the 7-day elastic modulus is closest to E_{target}. The exact solution is also calculated and shown in Figure 3-4, which is the same value after PSO method converges. Furthermore, Figure 3-5 shows the distribution of each cement phase at the optimal solution calculated by PSO method. For this case, it takes 3,800 times run in VCCTL to find the target modulus, which is the product of the particle swarm size (100) and the number of generation required for convergence (40) deducting repeated individuals during searching for each generation.

3.4.2 Example 2: Bi-objective Pareto Front for Modulus and Time of Set

Multiple objectives drive cement production, thus a set of trade-off optimal solutions must be obtained instead of a single optimum (Burke & Kendall, 2005). Therefore, the proposed approach is framed as multi-objective optimization problem (MOOP) that calculates the Pareto front, an envelope curve on the plane for a bi-objective case or a surface in space for a tri-objective case that encompasses all optimal solutions. The optimal solution set on Pareto front is defined as a set of solutions that are not dominated by any member of the entire search space (shown in Equation 3-1). The Pareto front is visualized by connecting all the non-dominated solutions.

The second case study calculates the Pareto front (and the inherent trade-off) of E and time of set. Figure 3-6 shows the full simulation outputs, with the Pareto fronts superimposed for four cases: [1] minimize time of set and minimize E (Min-Min); [2] minimize time of set and maximize E (Min-Max); [3] maximize time of set and minimize E (Max-Min); and [4] maximize time of set and maximize E (Max-Max). The Pareto fronts obtained from the PSO were generated using 30% of the simulations required to fully enumerate the sample space. Further, the curves coincide for the majority of the data envelope, varying by less than one hour and 5 GPa on the horizontal and vertical scales, respectively, in the absolute worst case. This example, while simple, demonstrates the potential of the PSO generated Pareto front as a substitute for bulk analysis.

A Genetic Algorithm was also verified to work for the bi-objective optimization problem. The bi-objective optimization results obtained from PSO and GA are compared. From Figure 3-7, the results from both methods have similar Pareto front curves and match very well. This proves that both the PSO and GA methods are appropriate to solve the bi-objective optimization problem of the VCCTL. Also, the converging speed and computational time are also compared

between these two methods with the same population size (1000). The comparison results are shown in Table 3-3. From Table 3-3, PSO and GA require a different number of generations to converge to the optimal solution. It takes about 200 generations to converge for the PSO method, while only about 30 generations for the GA method with a population size of 1000. On the other hand, it takes 80 times longer to execute the GA method than the PSO method. In summary, for this case, GA converges in fewer generations than PSO, but requires more time to execute.

3.4.3 Example 3: Tri-objective Optimization of Modulus, Time of Set and Heat Proxy

After both the optimization algorithms are verified for bi-objective optimization, a more complicated problem is introduced to demonstrate the application of these methods. From the knowledge of cement materials, cement paste with less setting time will develop strength earlier. Thus, time of set of the cement needs to be minimized. As mentioned earlier in Chapter 2, C_3S is the most reactive compound among the cement constituents, whereas C_2S reacts much more slowly. In this way, the compounds are the most abundant within the Portland cement system with C_3S (alite) which requires higher kiln temperatures to form, while the C_2S phase forms at lower kiln temperatures. Thus, C_3S/C_2S should be minimized to ensure less energy is used to create the cement, liberate less heat and less greenhouse gas emissions. The 7-day elastic modulus needs to be maximized to obtain more strength for cement paste.

In the third example, objective functions for C_3S/C_2S, time of set, and 7-day E are optimized simultaneously to identify the Pareto fronts bounded by three cases: [1] minimize C_3S/C_2S, minimize time of set, and maximize E (Min-Min-Max); [2] minimize C_3S/C_2S, minimize time of set, and minimize E (Min-Min-Min); and [3] maximize C_3S/C_2S, maximize time of set, and maximize E (Max-Max-Max).

Figure 3-8 shows the Pareto fronts for different water to cement ratios when minimizing time of set, minimizing kiln temperature proxy, and maximizing 7-day elastic modulus.

Separating the dataset by w/c enables visualization of the variation in the data due to different cement chemistries. The changing slopes of the Pareto surfaces as w/c increases show an increasing sensitivity of modulus and time of set to variations in cement variation. The possible range of moduli at a w/c of 0.53 is larger than that at a w/c of 0.25. C_3S/C_2S is not affected by water-cement ratio because C_3S, C_2S and water-cement ratio are all inputs of cement and independent from one another. The different Pareto fronts provide the non-dominated solutions for different water-cement ratios which could be used as guidance for design. Taking the optimization results with a specified water-cement ratio (0.25) as an example, there are 88 non-dominated solutions found by the PSO algorithm.

Table 3-4 lists the inputs and outputs of the first 30 non-dominated solutions. These solutions provide useful guidance for cement designers. From all trade-off optimal solutions, the selection of inputs for cement design is based on the requirements for cement paste performance.

Figure 3-9 (a) and (b) show the two Pareto fronts (gray meshes) from non-dominated solutions (red markers) for Max-Max-Max and Min-Min-Min. Figure 3-9 (c) shows the two Pareto fronts for all water-cement ratios. The color bar on the left shows the change with water-cement ratio from 0.25 (red) to 0.53 (blue) for cement data and the color bar on the right shows the change with modulus on the Pareto front surfaces.

3.5 Remarks on Convergence

To minimize the computational expense, metaheuristic search algorithms can be terminated once the estimated value is close to the target value. Thus, investigating the convergence properties of the multi-objective evolutionary algorithms is necessary. In the past few years, efficient stopping criteria for MOOP algorithms have been explored (G. Li, Goel, & Stander, 2008; Martí, García, Berlanga, & Molina, 2007; Roudenko & Schoenauer, 2004; Trautmann, Ligges, Mehnen, & Preuss, 2008). Convergence to the global Pareto front is

considered to assess the performance of algorithm (Kaige, Murata, & Ishibuchi, 2003; Zitzler, Thiele, Laumanns, Fonseca, & Da Fonseca, 2003).

In the cases where problems do not have an exact solution, a true Pareto front cannot be established. Therefore, a convergence test is applied based on the self-improvement of the algorithm. Goel and Stander (Goel & Stander, 2010) proposed a metric tracking of the change of the archive based on non-domination criterion to generate the convergence curve for MOOP. As mentioned in Section 3.3, during the process of updating non-dominated solution, an external archive of non-dominated solutions is maintained and updated for each generation. The solutions dominated in the old archive dominated by newly evolved solutions are removed. New solutions which are non-dominated with respect to archive are added. They suggested two terms, the improvement ratio and consolidation ratio. The improvement-ratio is the scaled number of dominated solutions representing the improvement in the solution set while the consolidation-ratio is the scaled number of non-dominated solutions representing the proportion of potentially converged solutions. The algorithm is considered to converge when improvement-ratio is close to zero and consolidation-ratio close to one. This method was applied to the Min-Min-Min case above to test the convergence for the PSO algorithm with different population sizes. Consolidation-ratio and improvement ratio are calculated for each generation to create the convergence table.

Figure 3-10 shows when population size equals 300, the consolidation ratio becomes 1 and improvement ratio becomes 0 at 600^{th} generation, which means the number of convergence generation for the algorithm is 600 when the population size is 300.

The relations between population size with number of PSO simulations, number of convergence generation, number of non-dominated solutions and percentage of PSO search with

blind search are plotted in Figure 3-11. The algorithms will not converge if the population size is less than 10. With increasing population size, the number of generations required for convergence decreases and the number of optimal solutions increases. This trend means a larger population size results in faster convergence. Also, the minimum number of simulations with PSO is about 19,812 out of 149,572 VCCTL simulations, which means the computational cost is reduced by up to 90% by applying PSO compared with the blind search of VCCTL. Thus, the PSO algorithm drastically decreases the computational cost in the process of searching optimal solutions for cement.

3.6 Potential for Objective Rating of Cement Quality

The paper now shifts to how Pareto front analysis can be applied to quantify the performance of a single cement relative to other cements, with user specified constraints such as imposing a minimum allowable modulus or maximum allowable time of set. Currently, a numerical rating system to objectively rate cement quality does not exist in practice. Similar to other civil engineering materials such as timber and steel (Standard), Portland cements are stratified into discrete classes based on physical testing results and intended service applications (Cement). A major limitation of this approach in practice is the assumption that all cements of a given class are equivalent in performance. The integration of PSO with cement hydration modeling allows for performance based scoring on a continuous basis without physical testing, and defines a framework for the practical implementation of performance based specifications that complement existing approaches.

3.6.1 Cement Scoring System

The proposed scoring system is based on the probability of non-exceedance of the data encompassed by the Pareto fronts given a user-specified constraint such as $E \geq E_0$:

$$P_c\,(x, y|\, E \geq E_0) \tag{3-4}$$

where Pc is the joint probability of non-exceedance within time of set (x) and C_3S/C_2S (y), and E0 is the minimum allowable modulus.

In this case, the Min-Min-Min and Max-Max-Max Pareto fronts (Figure 3-9c) give the boundary cases for all modeled cements. These fronts are used as lowest score (0) and highest score (1) for the group of cement. The procedure is shown as follows:

1. Project cements with E $\geqslant$ E0 to the surface E = E0 (E0 = 20 GPa)
2. Unite two Pareto fronts (Min-Min-Min and Max-Max-Max) at E=E0 to create a convex hull
3. Evaluate the marginal probability of non-exceedance $P_c\,(Time\ of\ Set|\ E \geq E_0)$ and $P_c\,(Heat\ Proxy|\ E \geq E_0)$ with regard to for time of set and heat proxy for all cements
4. Since less time of set and less heat proxy get higher scores, the score for each cement is calculated with $S = 1 - P$ with regard to time of set and heat proxy
5. Calculate the joint cumulative probability of time of set and heat proxy, which is considered as score for cement with user-specified constraint

3.6.2 Scoring System Applied to Example 3

Figure 3-13 demonstrates the scoring procedure with an example cement. Figure 3-13 (a) shows the projected convex hull from two Pareto Fronts in the time of set and heat proxy directions. Figure 3-13 (b) and Figure 3-13 (c) illustrate the assignment of probability of non-exceedance score using the cumulative distribution of time of set and heat proxy in Figure 3-13 (a). The probability of non-exceedance of the specific cement (shown in black dot) with regard to time of set and heat proxy are $P_c\,(Time\ of\ Set \leq 7.43hr|\ E \geq E_0) = 0.67$ and $P_c\,(Heat\ Proxy \leq 2.52|\ E \geq E_0) = 0.76$. Thus, the score for that cement $S_c = 1 - P_c\,(Time\ of\ Set \leq 7.43hr|\ E \geq E_0) = 0.33$ and $S_c = 1 - P_c\,(Heat\ Proxy \leq 2.52|\ E \geq E_0) =$

0.24. The two scores shows the marginal non-exceedance probability within time of set and heat proxy.

Figure 3-14 shows the probability of non-exceedance curve with regard to time of set. Cements sharing single chemistry with five different w/c are plotted with five dots in different colors on the curve. Figure 3-15 shows the effect of water cement ratio on cement scores. When the water to cement ratio increases from 0.24 to 0.26 (8.3% increase), score decreases from 0.33 to 0.18 (44.3% decrease). When the water to cement ratio increases from 0.24 to 0.28 (16.7% increase), score decreases from 0.33 to 0.067 (79.5% decrease).

After the scoring system is demonstrated, the full data set of cements is fitted with Hermite (Yang, Gurley, & Prevatt, 2013) and Beta distribution for time of set and heat proxy directions. In order to score the cements with solutions from metaheuristic searching algorithm, the fitting model from the empirical data is demonstrated on randomly picked reduced data. Figure 3-16 shows the distribution fitting for 50% and 10% of the data set compared with empirical data. From Figure 3-16 , Hermite and Beta distribution generated from empirical data fits the reduced data well. 10% of the dataset has the same distribution with empirical data. In this way, cements in space could be scored from the results found by PSO algorithm, which only takes at least 10% of full data set. And the score with fit distribution with existing models will be same as score based on the full dataset.

Figure 3-17 shows the spectrum of joint score $S_c\,(Time\ of\ Set, Heat\ Proxy|\ E \geq E_0)$ for all cement with user-specified constraint. For example, if cements with time of set less than 7.43 hr and heat proxy less than 2.52 is evaluated, joint score for those cements is:

$$S_c = 1 - P_c\,(Time\ of\ Set \leq 7.43hr\ and\ Heat\ Proxy \leq 2.52|\ E \geq E_0) = 0.5092.$$

In the figure colorbar purple represents the lowest score and dark green represents the highest score. This provides a visual map of the ideal cases based on the relative priority of the two scored parameters, where all cases satisfy the constraint E>20 GPa.

3.7 Implication

This chapter presents the successful application of multi-objective optimization of cement modeling, applied to a cement database created from ~150,000 VCCTL simulations. Pareto fronts were explored for constrained bi-objective or non-constrained tri-objective problems. Compared to full enumeration of the VCCTL parameter space, the metaheuristic algorithm search decreases the cost by nearly 90%. This finding suggests that this approach may be promising for evaluating much larger input variable sets.

The Portland cement industry is moving toward the implementation and use of performance specifications (Bickley, Hooton, & Hover, 2006). It is often the case that to ensure durability cement and concrete producers specify concrete mixtures to be stronger than required, even when overdesign is specified, due to perceived uncertainty regarding the ultimate performance of the material. To alleviate this, performance based design must address the needs of the industry, which include the assurance of strength, durability, economy, and sustainability. Pareto front based scoring of virtual testing results allows for the rapid assessment of solutions through constraints on critical parameters, while providing relative performance values for secondary parameters of interest. This enables immediate visualization of possibilities, and rapid selection of ideal cases.

Objective, performance based scoring has the potential to improve the economic performance of ordinary Portland cement (OPC) systems without the requirement of supplementary materials. Modern Type I/II Portland cements are empirically optimized for fast construction and low cost (Shetty, 2005). Current cement compositions require supplementary

materials to improve longevity and increase sustainability (Damtoft, Lukasik, Herfort, Sorrentino, & Gartner, 2008). Quantification of the tradeoffs between rapid strength development, cost of production, and long-term durability for Portland cement could motivate changes to cement chemistry and lead to optimization of the production process.

Table 3-1. Lower and upper bounds of VCCTL inputs

Input	Mass Fraction	
	Lower Bound	**Upper Bound**
Water to Cement Ratio (w/c)	0.20	0.53
Alite (C_3S)	0.50	0.70
Belite (C_2S)	0.15	0.37
Ferrite (C_4AF)	0.05	0.20
Aluminate (C_3A)	0.03	0.10
Gypsum	0.00	0.06
Anhydrite	0.00	0.04
Hemihydrate	0.00	0.04

Table 3-2. Database column identifier.

	Column	Item
Inputs	1	Water to Cement Ratio
	2	Alite Mass Fraction
	3	Belite Mass Fraction
	4	Ferrite Mass Fraction
	5	Aluminate Mass fraction
	6	Gypsum Mass Fraction
	7	Anhydrite Mass Fraction
	8	Hemihydrate Mass Fraction
Outputs	9	7-day Heat (kJ/kg)
	10	Time of Set (hours)
	11	Degree of hydration (%)
	12	7-day Elastic Modulus (GPa)

Table 3-3. Comparison of computational cost

Optimization techniques	Population size	Number of iteration	Time to run (sec)
PSO	1000	200	10.9
GA	1000	30	814.9

Table 3-4. First 30 non-dominated solutions for min-min-max case (w/c=0.25)

Inputs: Mass Fraction							Outputs: Mechanical and Hydration Properties			
Alite	Belite	Ferrite	Aluminate	Gypsum	Anhydrite	Hemihydrate	7-day Heat (kJ/kg)	Time of Set (hours)	Degree of hydration (%)	7-day Elasitc Modulus (GPa)
0.54	0.27	0.07	0.07	0.01	0.03	0.00	264	4.55	0.03	31.1
0.69	0.17	0.06	0.05	0.01	0.01	0.01	288	4.39	0.03	32.0
0.57	0.19	0.07	0.09	0.00	0.04	0.04	275	3.30	0.04	30.7
0.51	0.24	0.08	0.09	0.02	0.04	0.02	257	3.60	0.04	29.8
0.61	0.15	0.06	0.10	0.00	0.04	0.03	285	3.16	0.03	31.4
0.50	0.28	0.07	0.09	0.01	0.03	0.01	248	4.55	0.03	29.9
0.65	0.19	0.05	0.06	0.00	0.03	0.01	275	3.60	0.03	31.1
0.53	0.24	0.07	0.09	0.01	0.03	0.03	262	3.45	0.03	30.4
0.52	0.26	0.07	0.10	0.02	0.03	0.01	269	4.55	0.03	30.7
0.50	0.30	0.10	0.05	0.01	0.03	0.00	242	4.90	0.03	29.8
0.54	0.28	0.05	0.09	0.00	0.03	0.01	271	4.90	0.03	31.0
0.61	0.16	0.11	0.07	0.00	0.03	0.01	280	3.90	0.03	31.8
0.59	0.21	0.11	0.05	0.00	0.02	0.02	267	4.39	0.03	31.3
0.58	0.19	0.11	0.08	0.00	0.03	0.00	277	4.90	0.03	31.8
0.65	0.20	0.07	0.04	0.00	0.02	0.02	274	4.22	0.03	31.7
0.60	0.20	0.12	0.04	0.00	0.03	0.00	268	4.39	0.03	31.4
0.52	0.29	0.07	0.08	0.00	0.03	0.01	259	4.90	0.03	30.8
0.52	0.18	0.14	0.10	0.00	0.03	0.02	273	4.06	0.04	30.9
0.52	0.29	0.10	0.05	0.00	0.03	0.01	249	4.72	0.03	30.5
0.53	0.27	0.09	0.06	0.00	0.03	0.01	252	4.39	0.03	30.7
0.54	0.27	0.07	0.07	0.01	0.03	0.00	264	4.55	0.03	31.1
0.69	0.17	0.06	0.05	0.01	0.01	0.01	288	4.39	0.03	32.0
0.57	0.19	0.07	0.09	0.00	0.04	0.04	275	3.30	0.04	30.7
0.51	0.24	0.08	0.09	0.02	0.04	0.02	257	3.60	0.04	29.8
0.61	0.15	0.06	0.10	0.00	0.04	0.03	285	3.16	0.03	31.4
0.50	0.28	0.07	0.09	0.01	0.03	0.01	248	4.55	0.03	29.9
0.65	0.19	0.05	0.06	0.00	0.03	0.01	275	3.60	0.03	31.1
0.53	0.24	0.07	0.09	0.01	0.03	0.03	262	3.45	0.03	30.4
0.52	0.26	0.07	0.10	0.02	0.03	0.01	269	4.55	0.03	30.7
0.50	0.30	0.10	0.05	0.01	0.03	0.00	242	4.90	0.03	29.8

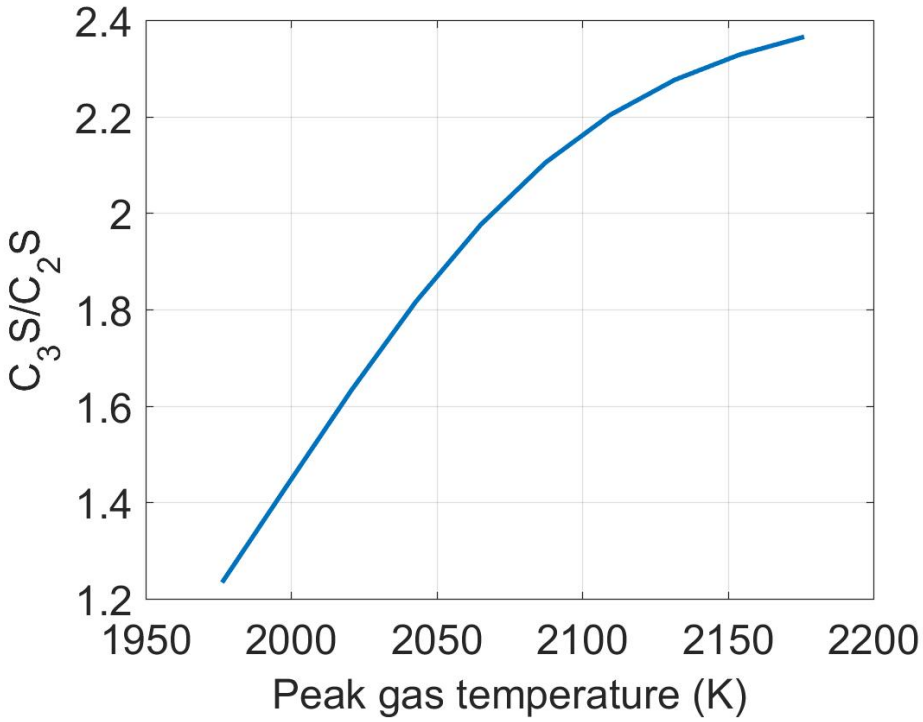

Figure 3-1. Relationship between kiln temperature and C_3S/C_2S

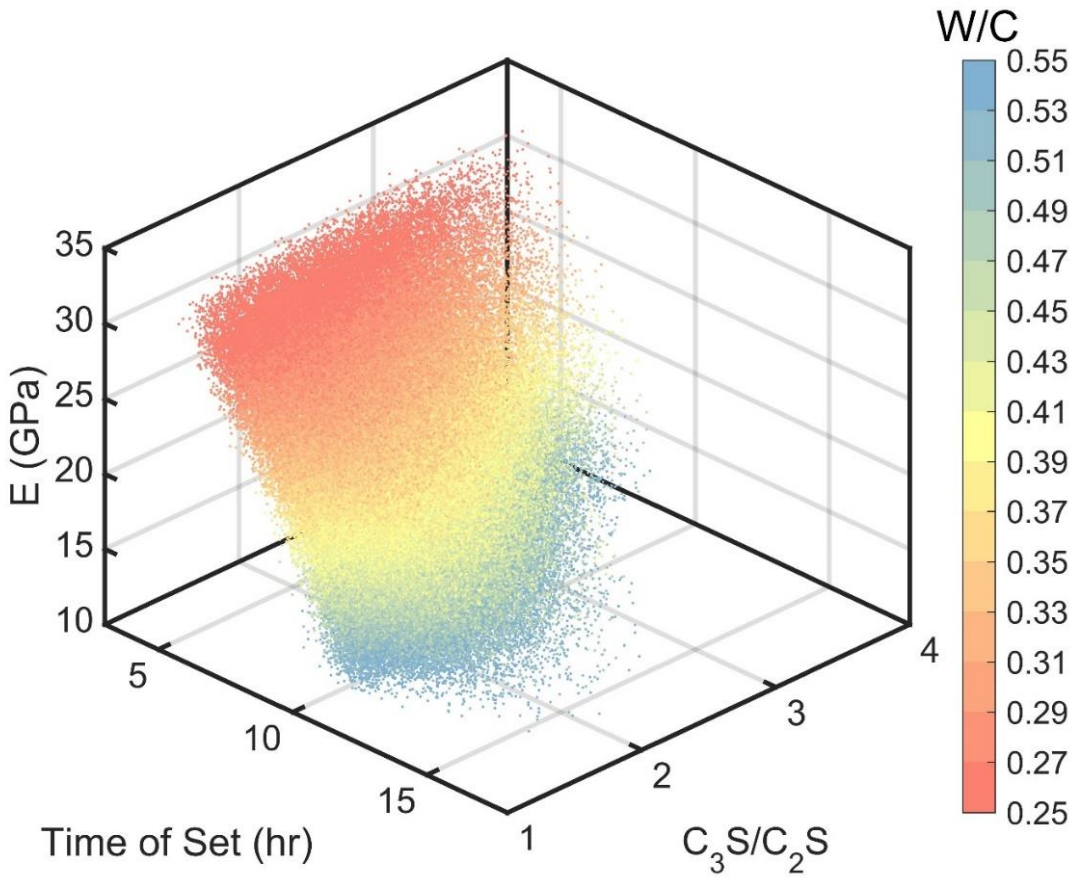

Figure 3-2. Results of VCCTL simulations

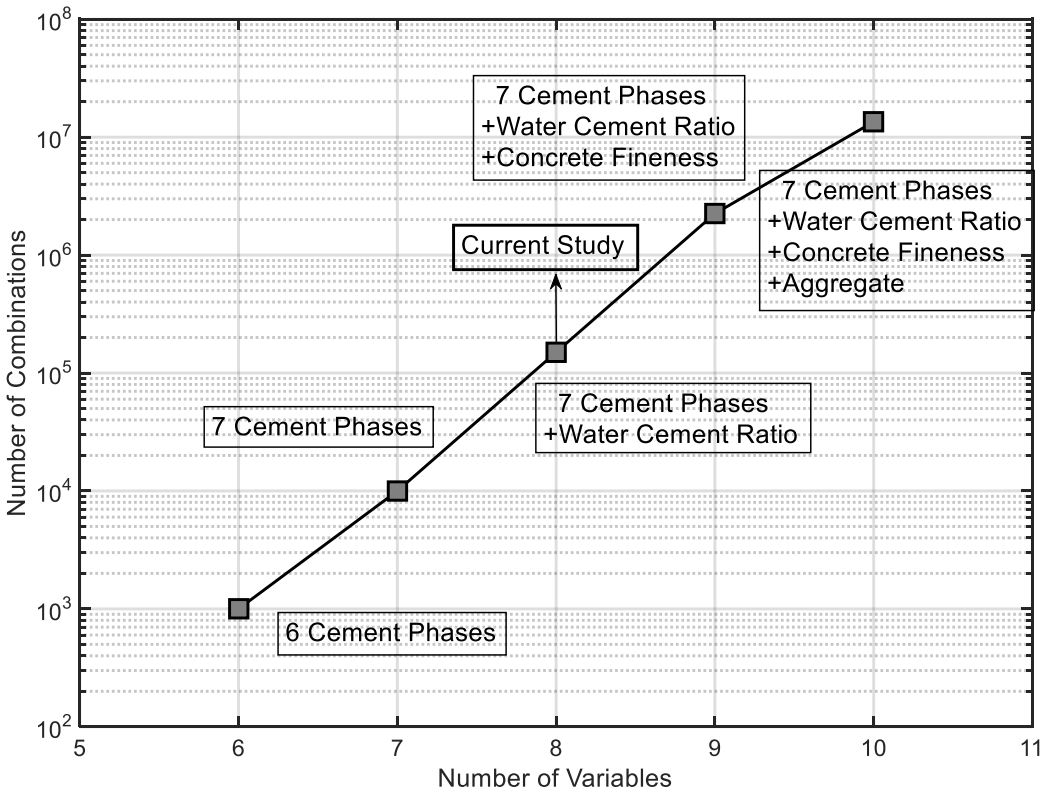

Figure 3-3. Potential discrete combinations of cement and concrete

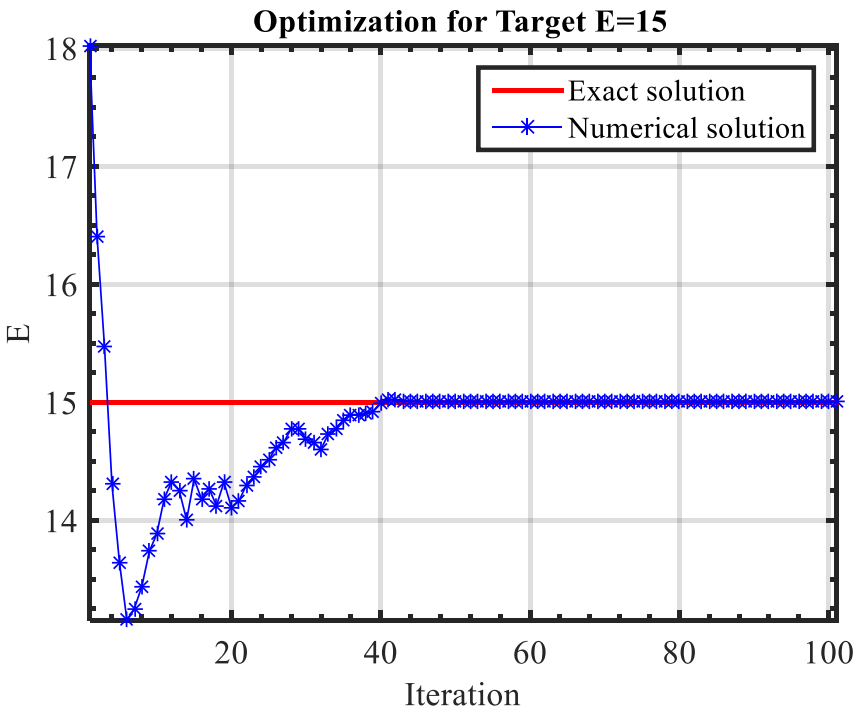

Figure 3-4. Elastic modulus vs. iteration with PSO

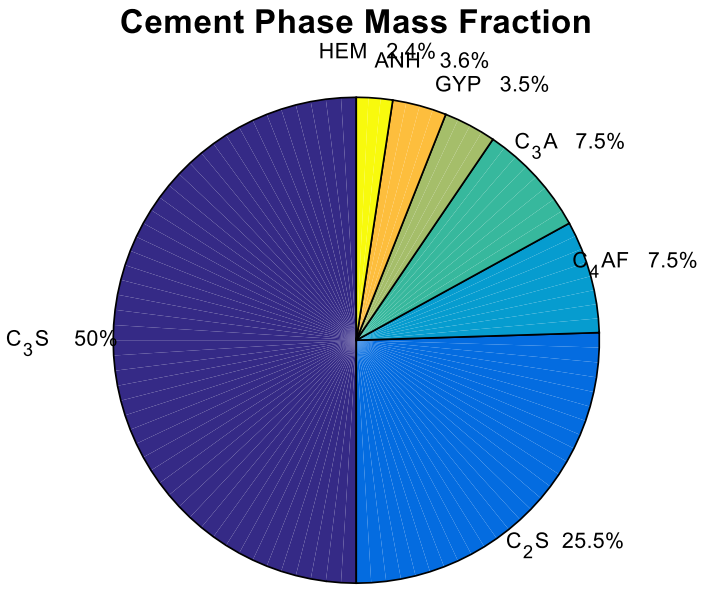

Figure 3-5. Distribution of cement phases for optimum with singe-objective PSO

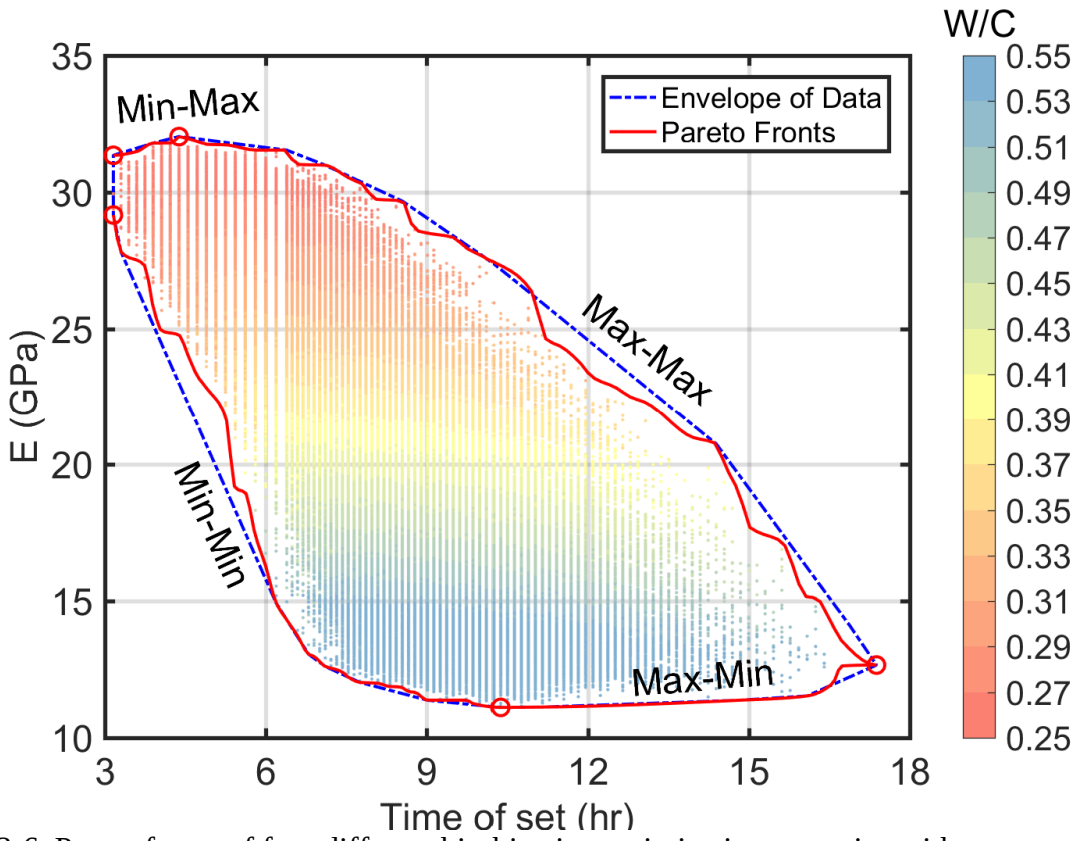

Figure 3-6. Pareto fronts of four different bi-objective optimization scenarios without constraints compared with the data envelope. Exploring the Pareto fronts with the PSO decreases the computational cost by more than 70%

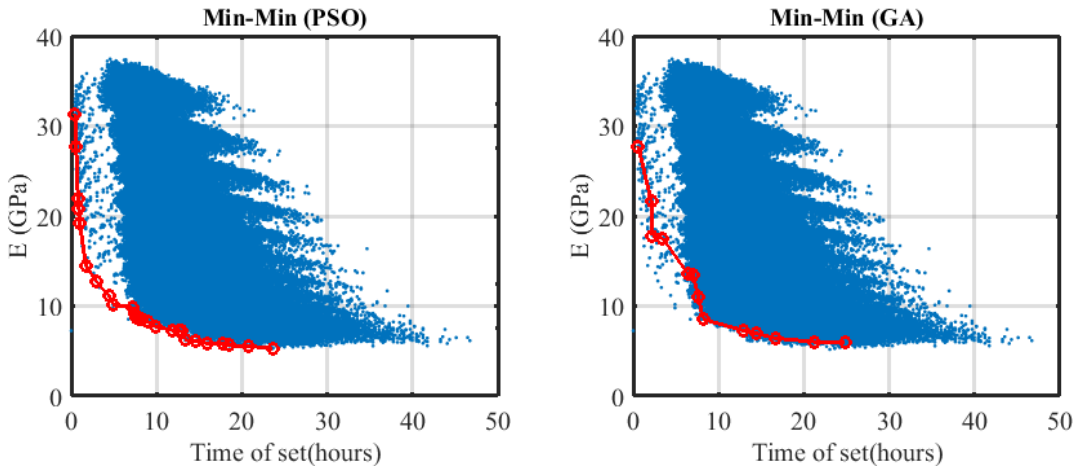

Figure 3-7. Comparison of PSO and GA of bi-objective optimization

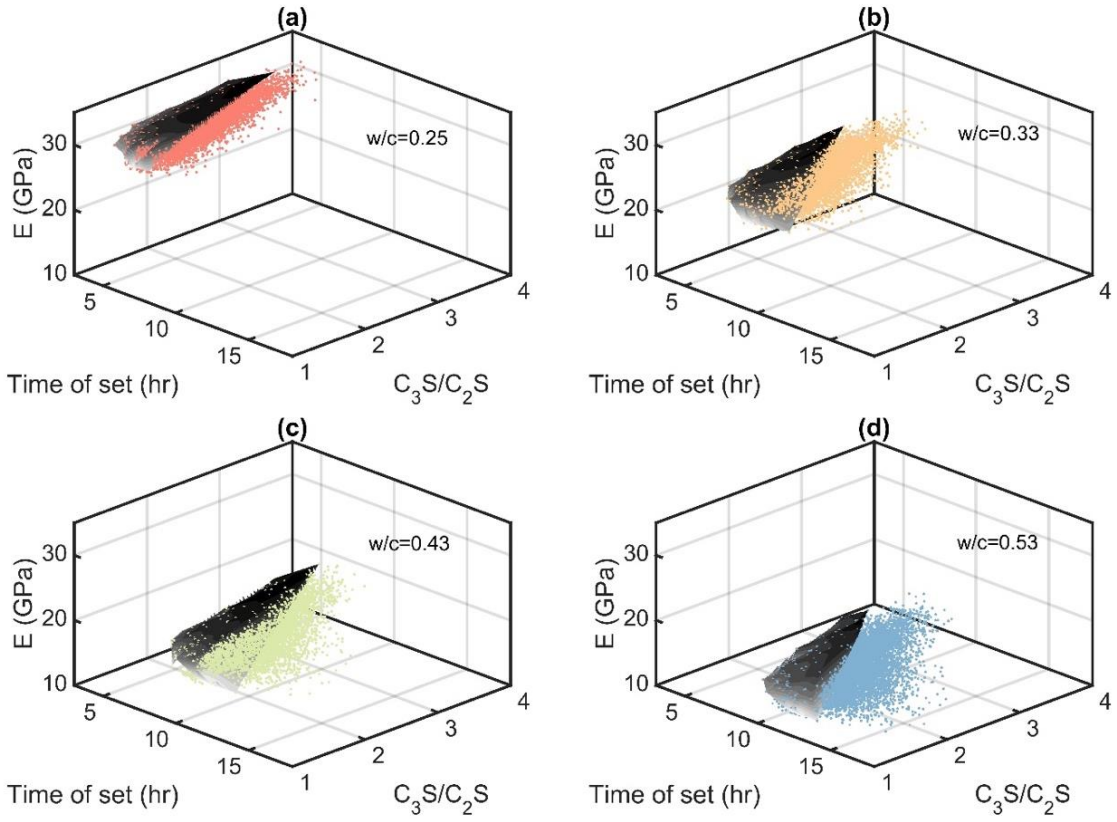

Figure 3-8. 3D surface mesh of Pareto front from non-dominated solution (red dots) for the Min (Time of set) – Min (C_3S/C_2S) – Max (E) case with different water-cement ratios. (a) w/c=0.25; (b) w/c=0.33; (c) w/c=0.43; (d) w/c=0.53

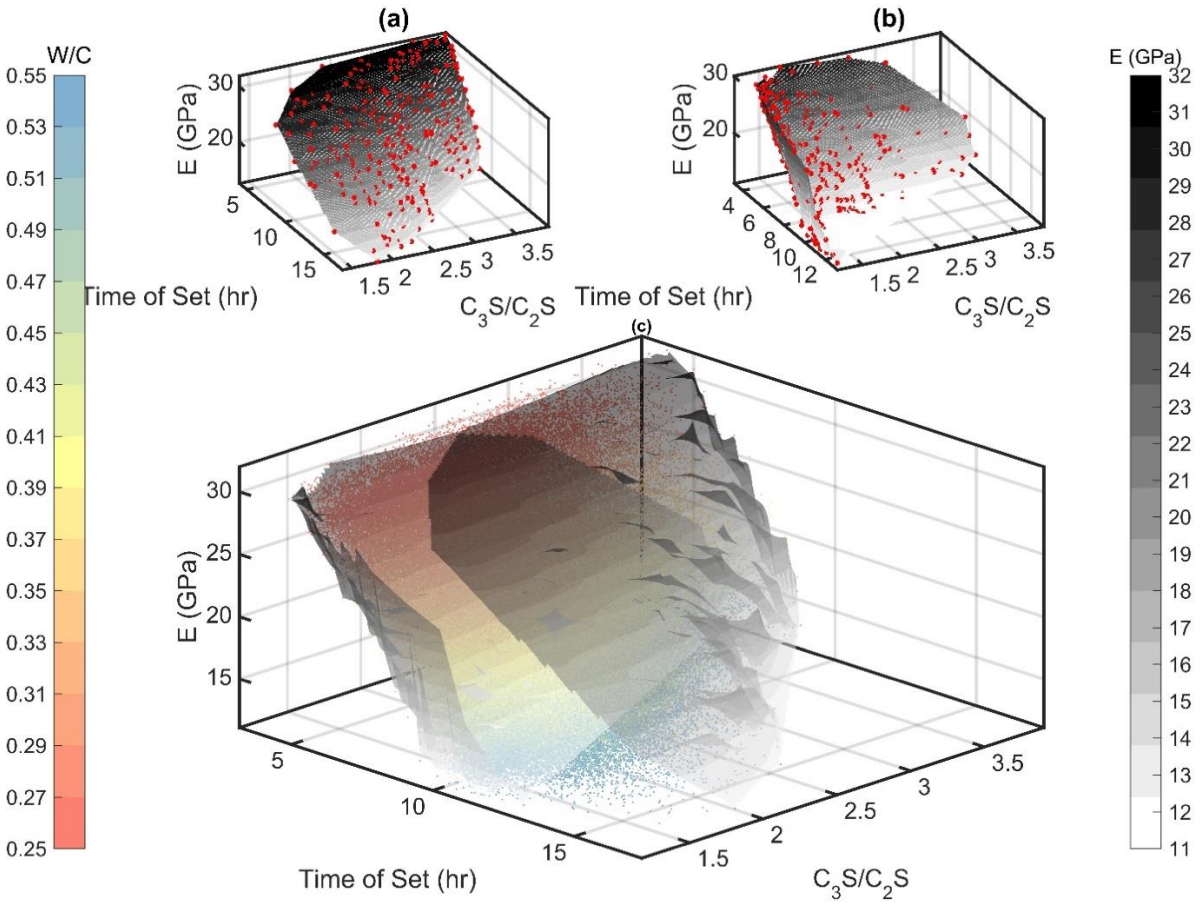

Figure 3-9. (a) 3D surface mesh of Pareto front from non-dominated solution (red dots) for the Max-Max-Max case (b) 3D surface mesh of Pareto front from non-dominated solution (red dots) for the Min-Min-Min case, and (c) 3D surface of Pareto fronts for the combined cases

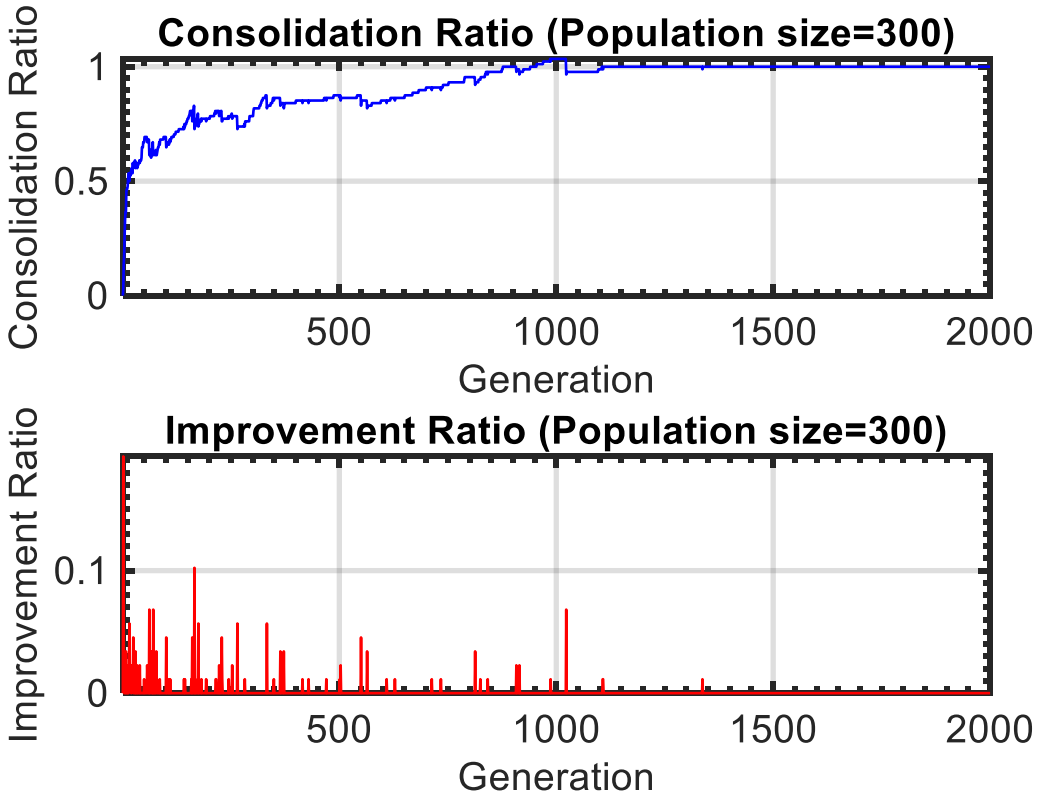

Figure 3-10. Consolidation ratio and Improvement ratio for population size = 300

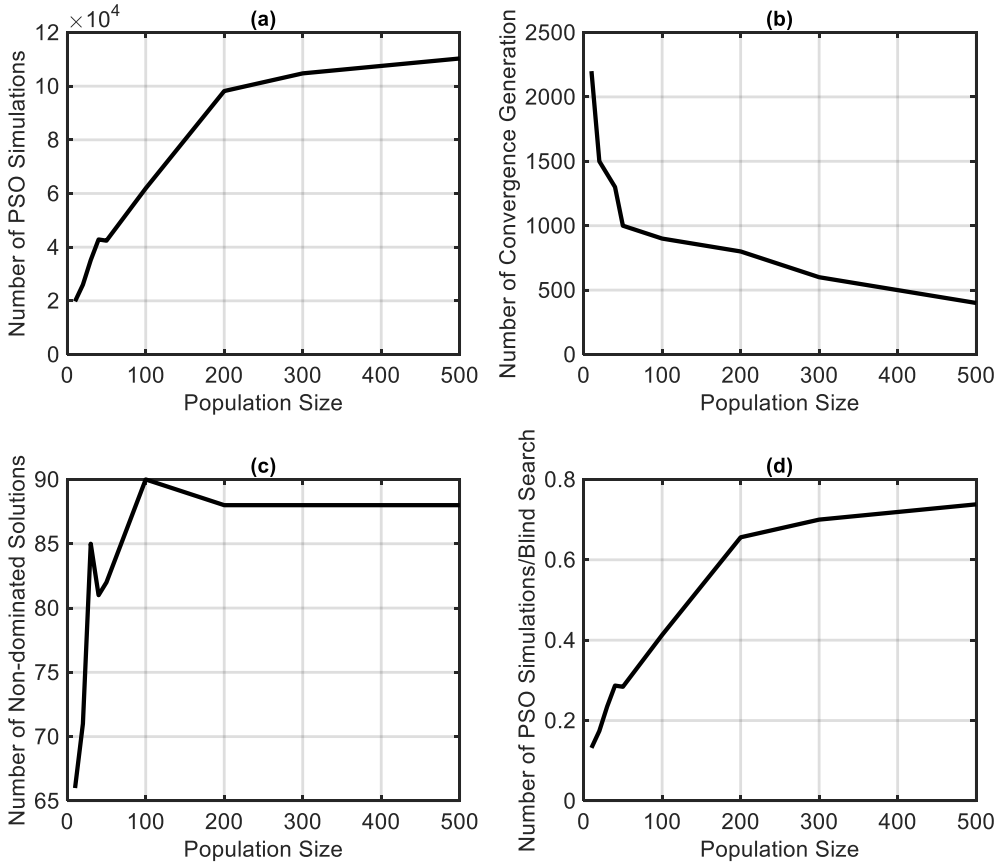

Figure 3-11. Convergence generation, number of simulations, number of optimal solutions vs. population size

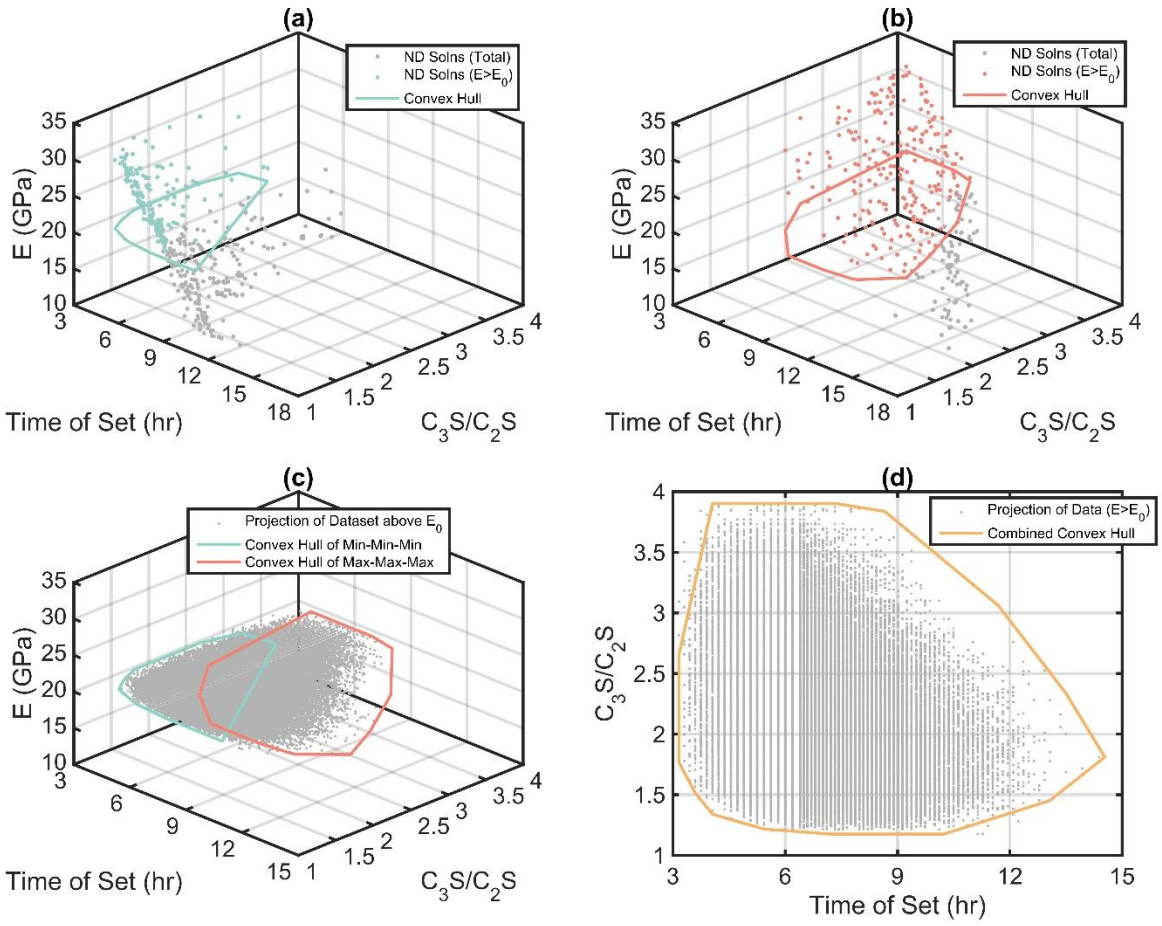

Figure 3-12. Process of deciding convex hull for evaluation cement data. (a) Finding convex hull for Min (Time of set) – Min (C_3S/C_2S) – Min (E) case; (b) Finding convex hull for Max (Time of set) – Max (C_3S/C_2S) – Max (E) case; (c)(d) Combined convex hull. For cement data points close to Min (Time of set) – Min (C_3S/C_2S) – Min (E) Pareto Front have higher score and those close to Max (Time of set) – Max (C_3S/C_2S) – Max (E) Pareto Front have lower score

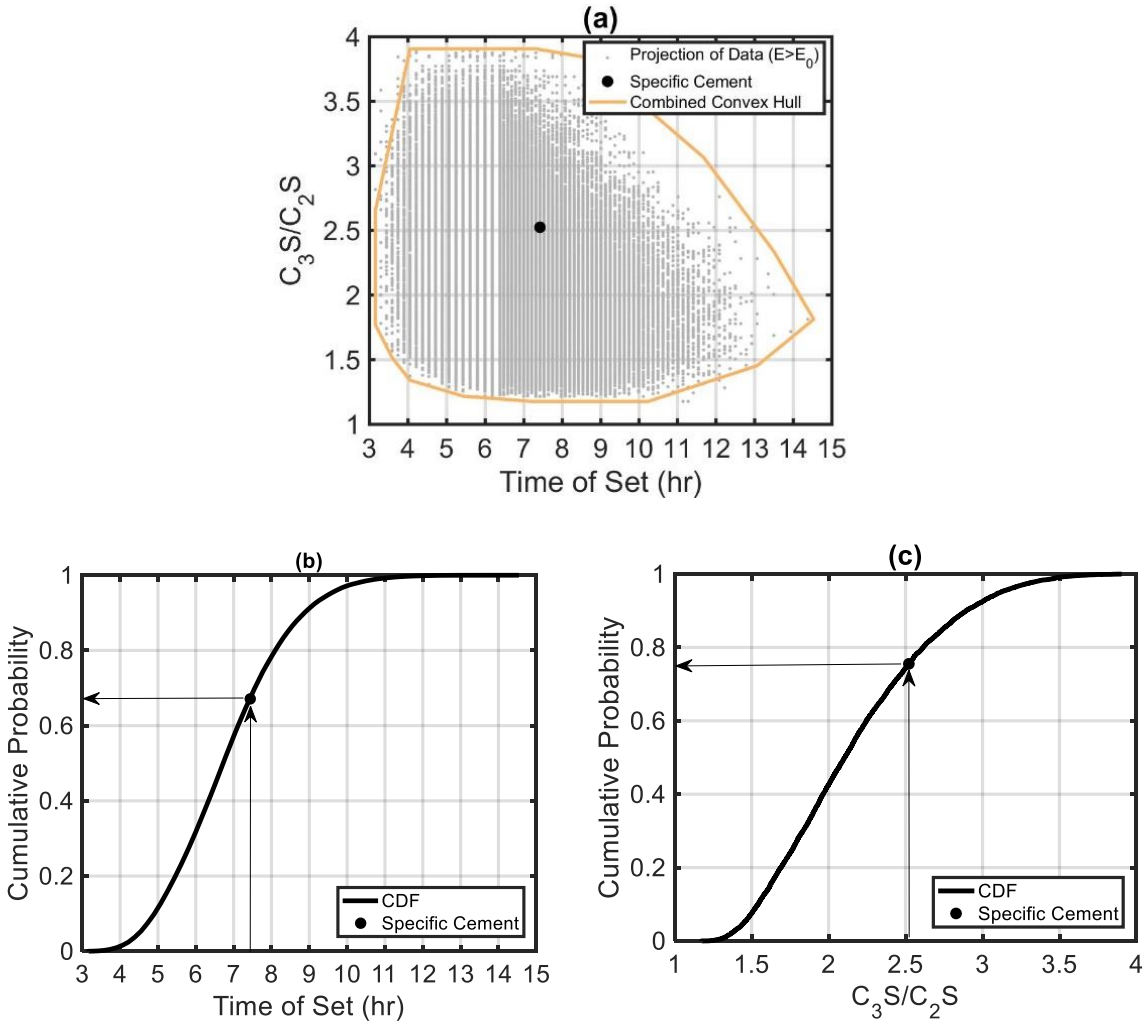

Figure 3-13. Marginal probability of non-exceedance with regard to time of set and heat proxy for E $\geqslant$ 20 GPa cements. The score is defined as the 1-probability of non-exceedance for the specified cement relative to all cement that meet the user specified constraints (here the modulus). Scores of zero and unity represent the worst and best possible outcomes

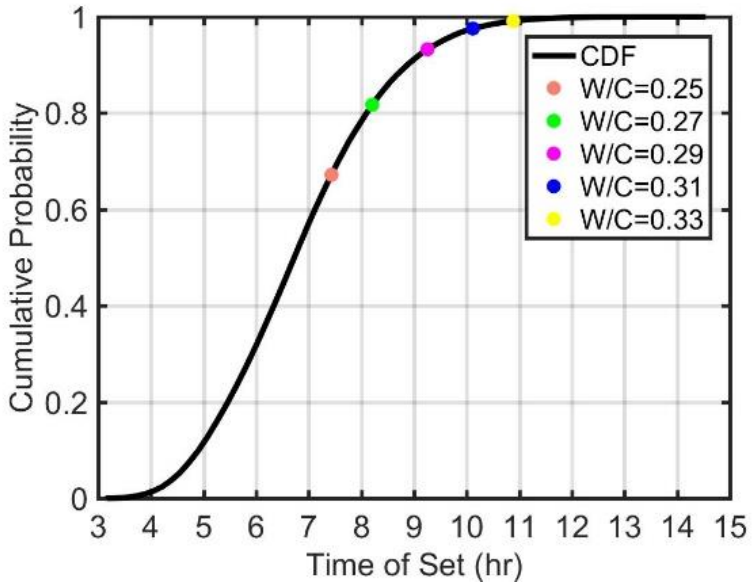

Figure 3-14. Different w/c with single cement chemistry on the marginal probability of non-exceedance curve

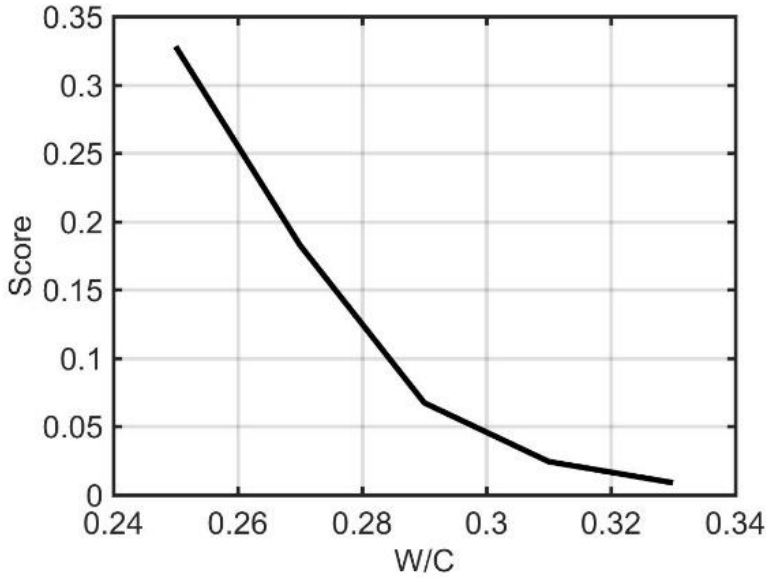

Figure 3-15. Effect of w/c on scores with regard to time of set under single chemistry

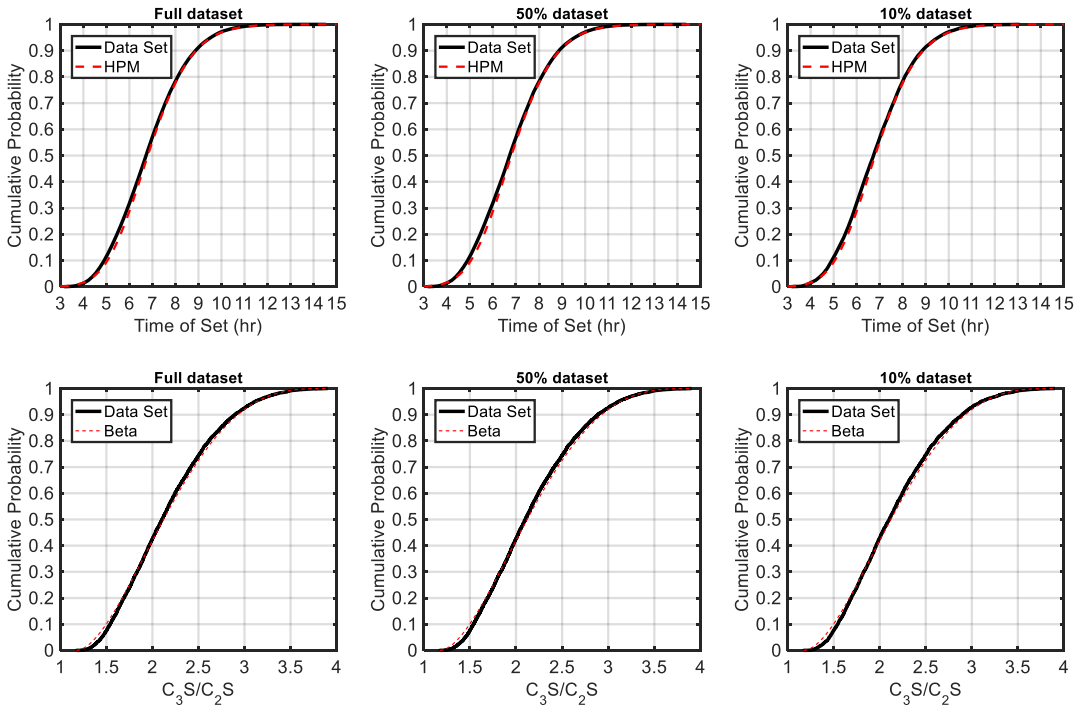

Figure 3-16. Hermite and Beta distribution fitting for reduced data

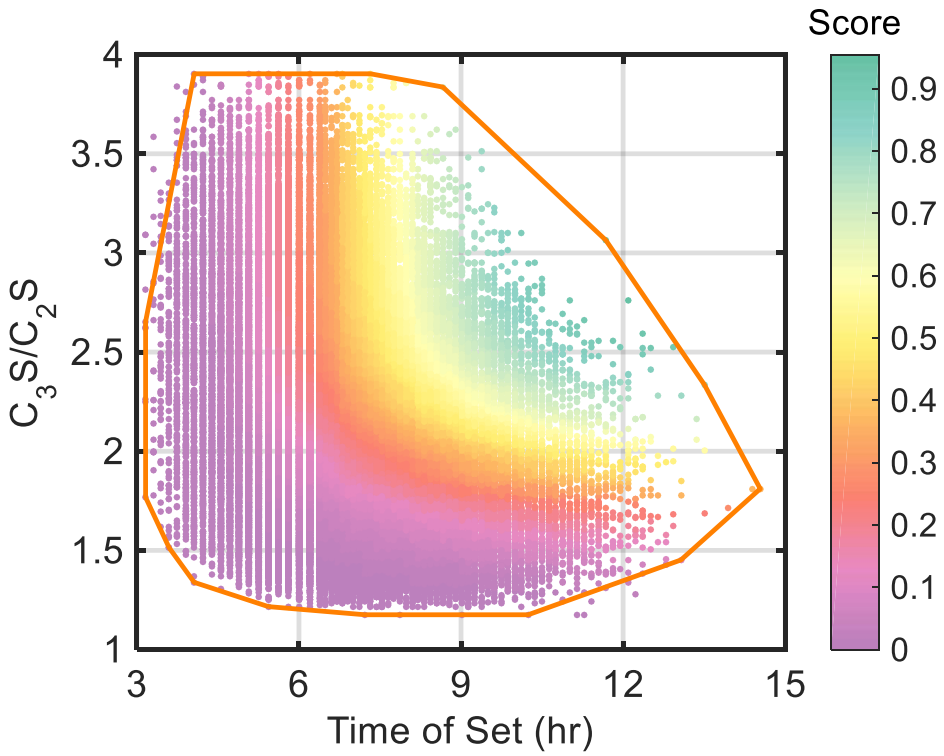

Figure 3-17. Joint score of cement

CHAPTER 4
PHYSICAL-CHEMICAL MODELING OF A ROTARY CEMENT KILN

As introduced in Chapter 2, numerical models (C. Csernyei & Straatman, 2016; Martins et al., 2002; Mastorakos et al., 1999; K. S. Mujumdar et al., 2006; Sadighi et al., 2011; Spang, 1972) exist to understand the behaviors of cement kilns, increase the cement production and decrease the energy consumption and greenhouse gas emissions. To simulate reactions of the rotary kiln and optimize the process and outputs, in this chapter, a physical-chemical one-dimensional kiln model is developed based on knowledge of thermodynamics and clinker chemistry from existing models. MATLAB R2016a™ solver ODE15s is used to solve an ordinary partial differential equation system of the kiln model. The temperature profiles and clinker species mass fractions are validated with the existing industrial kiln model and Bogue calculation.

Although measuring data from operation cement plants is available at times, it is subject to confidentiality and inherent limitations (C. M. Csernyei, 2016). The cement plant data such as clinker production, energy cost, CO_2 emissions is restricted to the precise operating parameters that occurred at that time. Also, the majority of these parameters can only be estimated within a certain degree of accuracy. Due to these reasons, research on the continued understanding of cement rotary kilns is slow and heavily focused on computational modeling.

4.1 Model Validation

4.1.1 Solution Methodology

According to previous kiln models developed during the last 50 years, knowledge inside the model is similar including the thermodynamics and clinker chemistry. However, the approaches researchers used to solve the model are quite different. Some people developed their own code with numerical methods (usually the fourth-order Runge-Kutta method) to solve for

the ODE/PDEs (C. Csernyei & Straatman, 2016; Martins et al., 2002; Spang, 1972), while others used commercial software or open source numerical solves for their models (Darabi, 2007; Guirao, Iglesias, Pistono, & Vázquez; Mastorakos et al., 1999; K. Mujumdar & Ranade, 2006; Nørskov, 2012; Sadighi et al., 2011; Wang, Lu, Li, Li, & Hu, 2006).

For the current study, the kiln model Equations (2-1) – (2-29) are implanted into Matlab2016a™ and the solver ODE15s is applied to solve the ODE system because of its high computational efficiency and convenience in coupling with the optimization tool developed in Chapter 3. By testing different ODE solvers including ODE45, ODE23, ODE15s, ODE23s, ODE23t, ODE23tb in Matlab2016, ODE15s is more stable and performs better than other solvers in solving stiff differential equations and dealing with singular matrix.

The procedure to solve for the computational kiln model is as follows:

1. An assumed temperature profile for the bed, gas, and shell was generated by assuming what the temperatures may be throughout the kiln based on results from other researchers (C. M. Csernyei, 2016; K. Mujumdar & Ranade, 2006). Based on Mujumdar and Csernyei's model, a linear profile for the gas temperature is generated in order to simplify the model. This profile was generated using the inlet and outlet gas temperature, as well as an assumption for the temperature and location of the peak gas temperature based on data received from the partner plant. The initial temperature profile was obtained by using a tool called "Plot Digitizer" to digitize the plots from papers. This tool allows users to pick the axis of a graph and choose the points on the plot, then it generates a table of the x and y values (shown in Figure 4-1)
2. Internal heat transfer components were solved from Equation (2-1) to (2-10) excluding the effects of clinker chemistry

3. ODE system (2-16) – (2-29) were solved for bed temperature and species mass fractions through the use of Matlab2016a ODE15s solver. The bed temperature requirement for each chemical reaction shown in Table 2-2 is taken into consideration

4. Shell temperature was solved using the heat balance Equation (2-29) by Newton-Raphson method (Chapra & Canale, 1998)

5. A check was performed to see if the new temperature profiles of shell and solid bed were within residual of 0.000001 of the previous profile

6. The new temperature profiles were passed back to the beginning of the model (step 2) and the process repeated again till convergence

4.1.2 Results and Discussion

From the solution methodology in Section 4.3, the 1D physical-chemical kiln model using Csernyei's input (C. M. Csernyei, 2016) is solved after the iterative processes converge to a solution for solid bed temperature and shell temperature. Mass fraction is plotted on the top of Csernyei's results. Bed height was taken as an adjustable factor for C_3S at the exit of the kiln. Red lines in Figure 4-2 show species mass fraction along the axial length of cement kiln without adjusting bed height, which generate 20% more C_3S compared with Csernyei's result, shown with black lines. Red lines in Figure 4-3 show the species mass fractions along the cement kiln after adjusting the bed height from 0.75m to 0.58m. The mass fraction for each species matches well with Csernyei's results. Figure 4-4 shows the temperature profiles of solid bed, shell, internal wall and freeboard gas along the kiln, which also matches well with Csernyei's results.

Table 4-1 shows the comparison of inlet and outlet mass fraction of material compared to the results of Bogue's calculation (Bogue, 1929) and Csernyei's prediction. From the clinker mass fraction at the outlet of the kiln, the present prediction is close to Csernyei's prediction (1.24% difference), while has 15.89% difference compared to Bogue's calculation. The reason

for the difference is Bogue's calculation assumes entire amount input constituent are converted into their species, which causes inherent error.

After comparison with Bogue's calculation and Csernyei's prediction, the present model is verified with more published industrial data as well as some other researchers' predictions (K. Mujumdar & Ranade, 2006). Table 4-2 shows the comparison between the prediction of present work with three cement plant data and Mujumdar's prediction. From the outlet mass fraction, the prediction of present work matches with published plant data very well.

4.2 Model Modification

4.2.1 CO_2 Mass Fraction

The virtual cement plant kiln model in Chapter 2 calculated the mass fraction of each solid component. Similarly, mass fraction of CO_2 emissions from limestone decomposition could be calculated with Equation (4-1).

$$v_g \frac{dY_{CO_2}}{dx} = \frac{A_s}{A_g}\frac{\rho_s}{\rho_g}\frac{M_{CO_2}}{M_{CaO}} k_1 Y_{CaCO_3} \tag{4-1}$$

The mass fraction of CO_2 emissions from limestone decomposition is shown in blue dash line in Figure 4-5.

4.2.2 Raw Meal and Fuel Costs

First, the cost of raw material for cement plant was estimated and is provided in Table 4-3, which lists the unit price for cement raw material in the current market (sand and gravel only). (https://www.statista.com/statistics/219381/sand-and-gravel-prices-in-the-us/).

By incorporating the unit price into VCP model based on the mass fraction of raw meal, the relationship between 7-day modulus and raw meal cost was calculated (see Figure 4-6). Modulus is observed to increase with the cost of raw meal, which is due to the increase of limestone used as raw meal. From the linear regression fit for the data, a positive correlation

between gas peak temperature and modulus is obtained. That is because higher peak temperature gives more alite, which plays an important role in cement strength development.

After the material cost is calculated, energy cost, or cost of fuel is considered. From (Chatziaras et al., 2016), the average energy required to produce one ton of cement is 3.3 GJ, which can be generated by 120 kg coal with a calorific value of 27.5 MJ/kg. Coal is the major fuel used for cement production (Worrell et al., 2013). The cost of coal is $2.07/GJ (https://www.statista.com/statistics/244479/us-consumer-price-estimates-for-coal-energy/). Figure 4-7 shows the relationship between modulus and cost of fuel. Because of the linear relation between energy and temperature, the cost of fuel has a linear relationship with temperature.

Figure 4-8 shows the relationship between modulus and total cost by combining material cost and fuel cost. Similar with Figure 4-6, modulus increases with total cost because of the positive correlation between modulus and both cost. From Figure 4-8, energy cost accounts about 30% of the total cost, which is verified by (Chatziaras et al., 2016).

Table 4-1. Species mass fractions model predictions compared with Bogue and Csernyei's prediction

Raw Meal at inlet	Mass Fraction from Csernyei's Work	Mass Fraction of Present Work
$CaCO_3$	0.3798	0.3798
CaO	0.3019	0.3019
SiO_2	0.1594	0.1594
Al_2O_3	0.0246	0.0246
Fe_2O_3	0.0396	0.0396
Inert + Other	0.0947	0.0947

Clinker at the Outlet	Mass Fraction from Bogue's Calculation	Mass Fraction from Csernyei's Work	Mass Fraction of present work
C_3S	0.582	0.546	0.546
C_2S	0.130	0.049	0.041
C_3A	0.063	0.027	0.027
C_4AF	0.075	0.068	0.068
CaO	0.000	0.034	0.033
Summation	0.85	0.724	0.715

Table 4-2. Model predictions compared with industrial data and Mujumdar's prediction

	Industrial kiln 1 (2006)			Industrial kiln 2 (2006)			Industrial kiln 3 (2006)		
	Plant Data	Mujumdar's Prediction	Present Work	Plant Data	Mujumdar's Prediction	Present Work	Plant Data	Mujumdar's Prediction	Present Work
Inlet Mass Fraction									
$CaCO_3$	0.340			0.398			0.305		
CaO	0.396			0.335			0.418		
SiO_2	0.179			0.185			0.190		
Al_2O_3	0.0425			0.041			0.043		
Fe_2O_3	0.0425			0.041			0.043		
Initial Temperature of Solid, K	1123			1250			1025		
Outlet Mass Fraction									
C_3S	0.483	0.508	0.489	0.508	0.502	0.503	0.500	0.504	0.506
C_2S	0.239	0.222	0.202	0.257	0.263	0.209	0.269	0.249	0.222
C_3A	0.051	0.051	0.048	0.048	0.051	0.048	0.042	0.052	0.048
C_4AF	0.143	0.149	0.116	0.151	0.148	0.109	0.142	0.147	0.118
Residual			1.82%			2.38%			2.08%

Table 4-3. Unit price for raw material of cement plant

Raw material	Chemical Composition	Unit Price($/Ton)
Limestone	$CaCO_3$+CaO	15
Sand and Gravel	SiO_2	4.4
Clay	Al_2O_3+Fe_2O_3	4

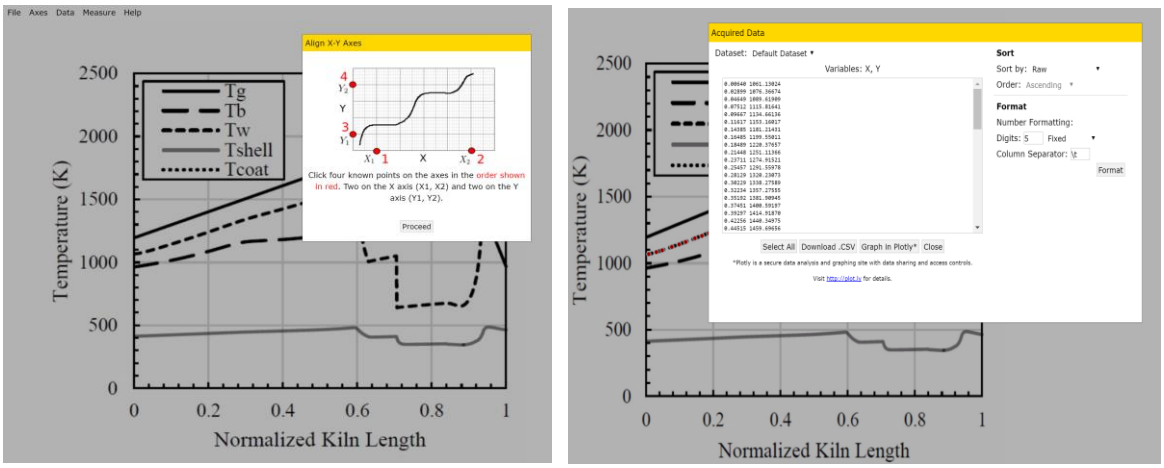

Figure 4-1. Digitization of the temperature plots from paper using “Plot Digitizer”

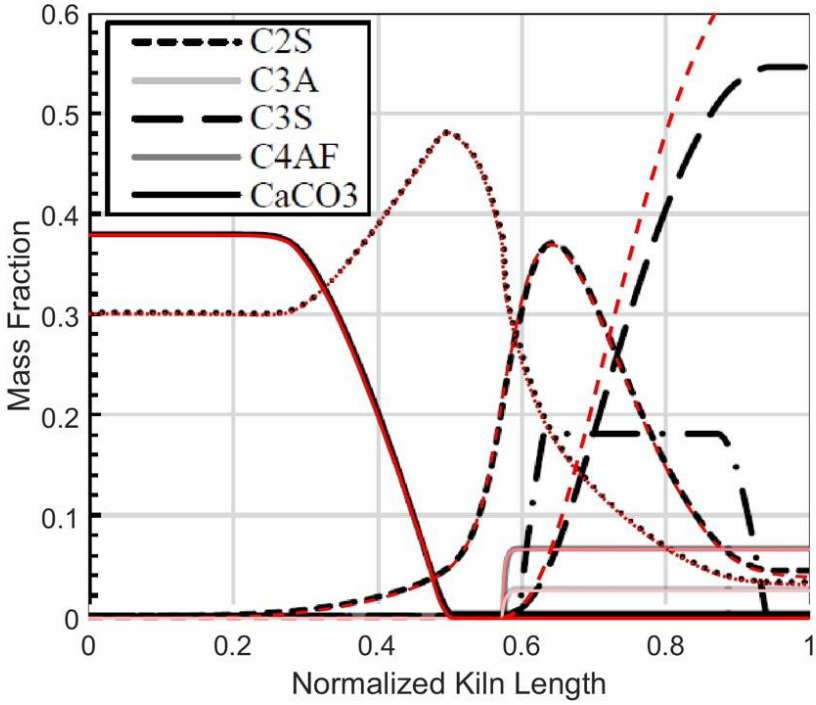

Figure 4-2. Species mass fractions along cement kiln without bed height adjustment compared with published data

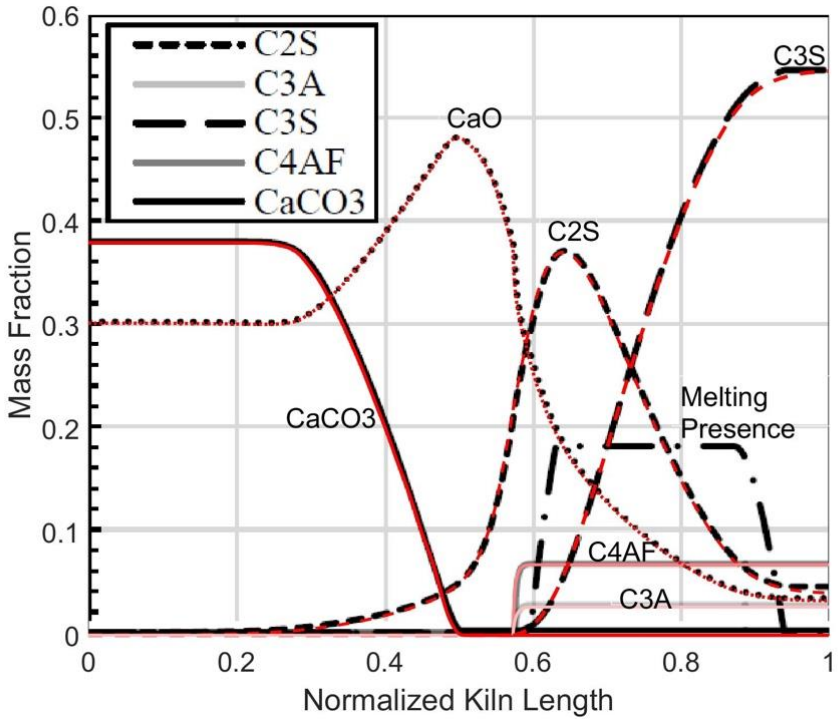

Figure 4-3. Species mass fractions along cement kiln with bed height adjustment compared with published data

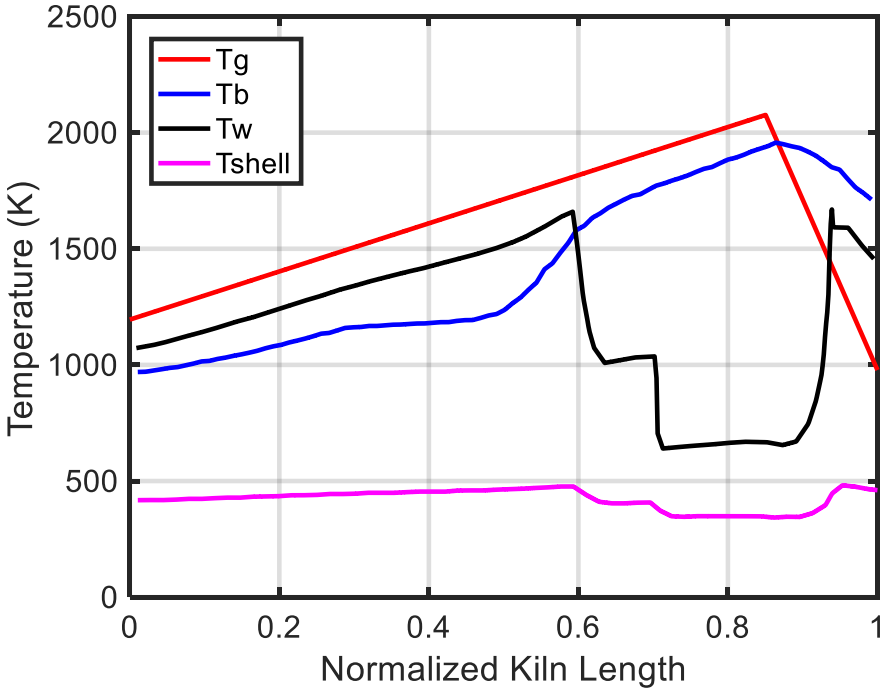

Figure 4-4. Temperature profiles in cement kiln from heat transfer.

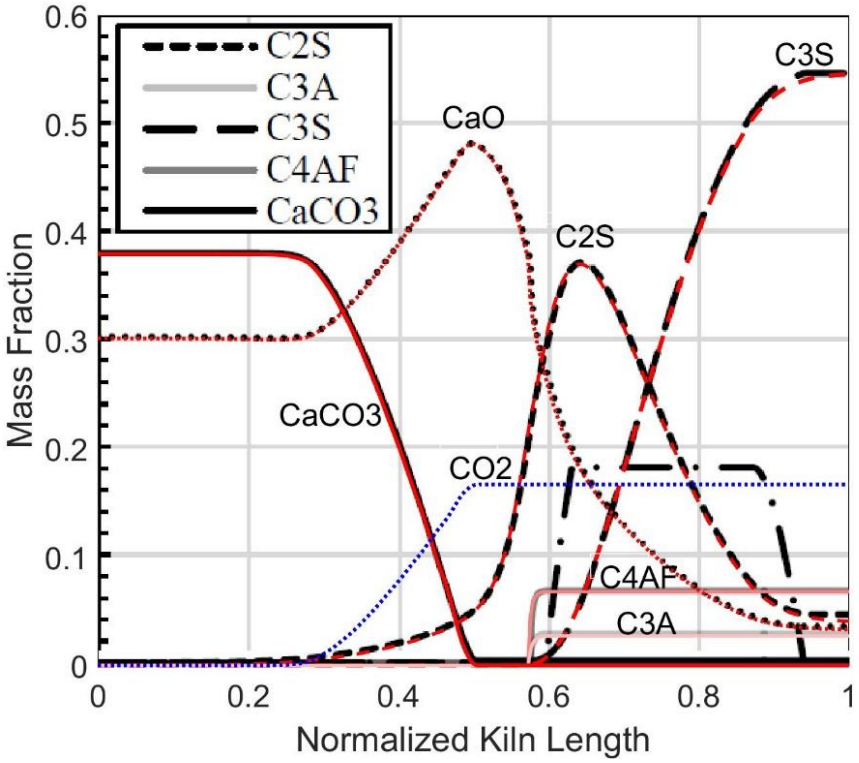

Figure 4-5. Mass fraction of CO_2 emissions from kiln model

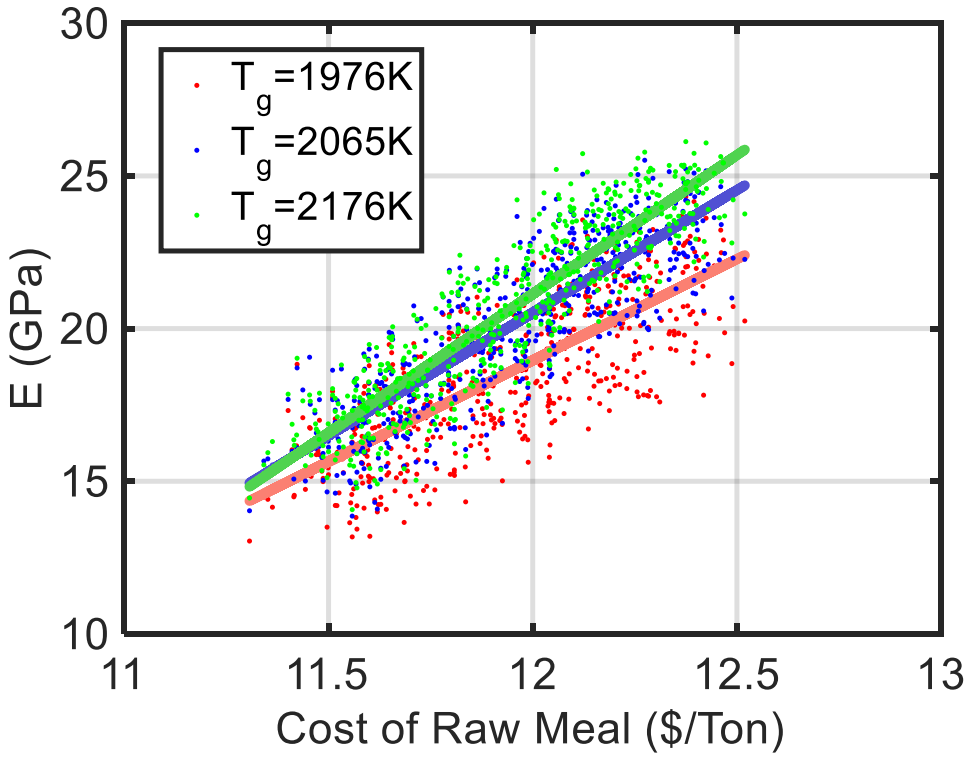

Figure 4-6. Relationship between 7-day modulus (GPa) and cost of raw meal ($/Ton) under different gas peak temperature

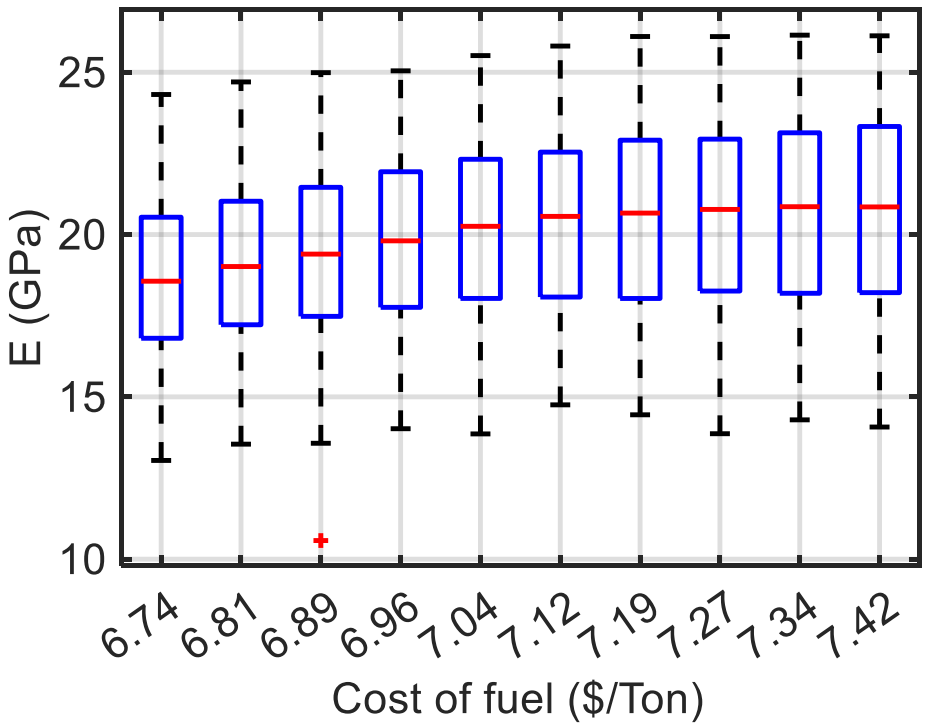

Figure 4-7. Relationship between 7-day modulus (GPa) and cost of fuel ($/Ton) under different gas peak temperature

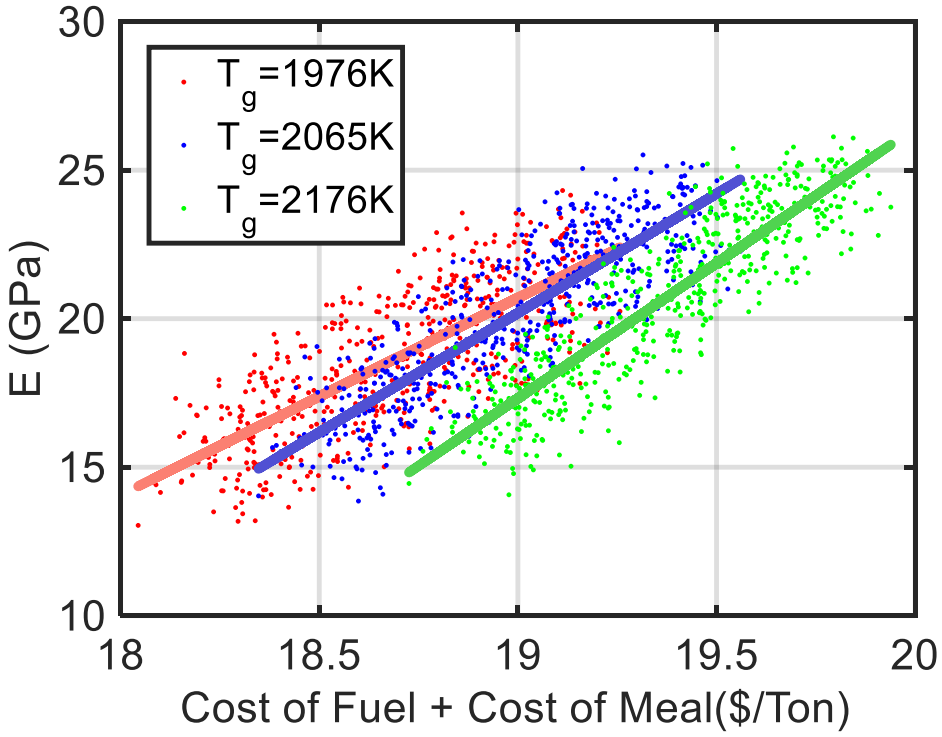

Figure 4-8. Relationship between 7-day modulus(GPa) and total cost under different gas peak temperature

CHAPTER 5
OPTIMIZATION OF COUPLED VCP/VCCTL MODEL

This chapter introduces a coupled model which utilizes the VCP in combination with the VCCTL to create a tool which models the production of Portland cement from the mine to the point of placement. The coupling of VCP and VCCTL was performed to provide a tool that couples cement production and hydration Portland cement. The model is a tool for the optimization of raw material input, fuel, energy, emissions and cost for manufacture of Portland cement in addition to the optimization of the physical properties of the resultant concrete.

5.1 Coupling VCP and VCCTL Modeling

5.1.1 Input Generation

Chapter 4 introduced 1D physical-chemical cement kiln model, which is considered as virtual cement plant (VCP). In order to simulate the VCP, input files including the mass fraction of raw meal, peak gas temperature and the location where peak gas temperature occurs within the kiln are required.

The chemical composition of the raw meal at the inlet of cement kiln includes $CaCO_3$, CaO, SiO_2, Al_2O_3, Fe_2O_3. It is common to use lime saturation factor (LSF), silica ratio (SR), and alumina ratio (AR) in chemical analysis for cements, clinkers and phases instead of using oxide components directly. The relationship between LSF, SR, AR and raw meal is as follows (Taylor, 1997):

$$\text{Lime saturation factor (LSF)} = CaO/(2.8SiO_2+1.2Al_2O_3+0.65Fe_2O_3) \quad (5\text{-}1)$$

$$\text{Silica ratio (SR)} = SiO_2/(Al_2O_3+Fe_2O_3) \quad (5\text{-}2)$$

$$\text{Alumina ratio (AR)} = Al_2O_3/Fe_2O_3 \quad (5\text{-}3)$$

LSF is a ratio of CaO to other three oxide components, which control the ratio of alite:belite produced within the cement kiln. The VCP model requires the mass fraction of raw

meal, calculated from Equations (5-1) – (5-3), where the LSR, SR, AR, Fe_2O_3, $CaCO_3$/CaO are considered as inputs which generate oxide components from the raw meal. According to Taylor, the typical range for each ratio for the production of portland cement is as follows:

LSF - [0.9, 1.05]

SR - [2.0, 3.0]

AR - [0.8, 2.0]

Furthermore, the typical range of Fe_2O_3 content [0.01,0.1]. The $CaCO_3$ to CaO ratio is typically within a range of [40%,60%] and is directly obtained from the decarbonation of the limestone through the kiln. Ultimately the mass fraction of the components, ($CaCO_3$, CaO, SiO_2, Al_2O_3, Fe_2O_3) should be equal to 1. The inputs are generated utilizing two methods: a) fixed intervals; b) uniformly distributed random numbers based on the ranges from each input.

Figure 5-1 and Figure 5-2 provide the distribution of 1956 inputs generated by fixed intervals, where distributions of raw meal derived from Equation (5-1) – (5-3). The input was generated from 100,000 individual samples, however, 1956 inputs or 1.96% satisfy the constraint (components equal to 1). Figure 5-3 and Figure 5-4 show the distribution of inputs generated by uniformly distributed random numbers from available sections and distribution of raw meal. The number 200,000 individual samples were generated and only 1732 (0.87%) inputs satisfy the constraint. The methodology used for the generation of different sample sizes (100,000 and 200,000) was done in an effort to acquire roughly the same number of inputs for each case (1956 and 1732). The fixed intervals (method a) did not provide a uniform distribution as shown in figure 5-1; method b, the uniformly distributed random numbers were used to generate the inputs for the coupled model.

Table 5-1 and Table 5-2 compare the VCP raw meal and clinker mass fraction with different input generation approaches. The results of the two approaches are slightly different, which is to be expected since different methods to generate inputs were used and provides differences within the raw meal as well as cement clinker.

Taylor reported that the maximum LSF for modern cements is 1.02 and the range for LSF (0.90 – 1.05) was borne from the use of a range slightly above the maximum reported. However, the results obtained in Table 5-2, provide a low range of alite (18-48%), but is typically 40-70% by mass (Stutzman, 2004). Subsequent to the production of the low values for alite, the model was reproduced using the raw meal mass fractions from published industrial kiln data (C. M. Csernyei, 2016; K. Mujumdar & Ranade, 2006) and are applied to determine the range of inputs. After calculating LSF, AR, SR, Fe_2O_3 and $CaCO_3$/CaO from Equation (5-1) – (5-3) using the mass fractions of raw meal at inlet of the four industrial kilns (shown in Table 4-1 and Table 4-2), the ranges for material inputs is as follows: LSF [1.18, 1.36], SR [2.1, 2.5], AR [0.6, 1.0], Fe_2O_3 [0.0396, 0.0430], $CaCO_3$/CaO [42%, 56%].

Table 5-3 lists the expanded VCP input ranges combing Taylor's work and information from industrial kilns.

As introduced in Chapter 4, gas temperature profile is considered as input for the VCP model, which contains the peak gas temperature and location of the peak gas temperature. Figure 5-5 gives an example of gas temperature as input profile for VCP. The peak gas temperature is about 2100K, which happened at the point 0.84 of normalized kiln length away from entry of the kiln. Based on other researchers' gas profiles (C. M. Csernyei, 2016; K. Mujumdar & Ranade, 2006), peak gas temperature range is chosen as [1976, 2176] K and the range of location of peak gas is chosen as [0.6, 0.9].

5.1.2 Input Range Testing

After the ranges for VCP inputs are established, cases with different range of material input are analyzed. Table 5-4 shows the VCP results with different material input ranges. The results are shown with regards to alite and belite mass fractions at different gas peak temperatures. From Table 5-4, clinker mass fraction using Taylor's material input range does not cover enough searching space for the optimization tool. After expanding the input range by using information from industrial kilns for VCP, alite space increases from [0.2, 0.45] to [0.2, 0.7] and belite space increase from [0.25, 0.38] to [0, 0.38].

5.1.3 Schematic of coupled VCP-VCCTL model

In the following sections, the expanded inputs including 537 different kinds of chemistry, 10 different peak gas temperatures and 10 different locations of peak gas temperature are considered for coupled VCP/VCCTL model. 53,700 inputs were ported to VCP, after 20 hours running with Matlab2016a, 53,700 clinkers containing the information of mass fractions of virtual clinker phases and related temperature profiles were created. The resultant "virtual clinkers" phase chemistry and fineness are passed to VCCTL and run on UF HPC for virtual cement initial microstructure reconstruction and hydration, as described in Chapter 2. Subsequent to 6 days of run-time on the HPC, a series of output indicators with respect to the performance for each virtual cement including time of set, 7-day mortar modulus, 7-day mortar strength, 3-day heat are calculated.

5.1.4 Case Studies

Table 5-5 shows the results of coupled VCP-VCCTL with 53,700 inputs. Based on the output of VCP, mass fractions of different cement clinker phases are plotted versus different peak gas temperature and peak gas locations (also known as flame locations). For example, the first plot in Table 5-5 shows alite mass fraction of virtual cements with 537 raw meal

combinations versus 10 peak gas temperatures. The results indicate that alite increases with the peak gas temperature (or the highest temperature of flame inside the kiln), belite decreases with the peak gas temperature, and CaO decreases with the peak gas temperature. The sensitivity of clinker phases to temperature is increased when the flame is close to the exit of the kiln. That means, if more alite is desired, one could move the flame position closer to the kiln exit, which provides more of an influence than just increasing the peak gas temperature. Similarly, based on the output of coupled VCP-VCCTL model, 7-day modulus and 3-day heat of hydration has a similar trend with peak gas temperature and flame position, which matches with the results from Figure 4-6. This case gives a meaningful guidance for the design of a cement kiln. Instead of increasing the maximum temperature of flame inside the kiln to create a cement with higher early strength, a simple position change of the flame is more energy efficient and sustainable.

5.2 Optimization of VCP-VCCTL Model

This section proposed an optimization tool for cement by applying PSO on coupled VCP-VCCTL model to save material cost, energy consumption, and decrease CO_2 emissions.

5.2.1 Cost vs. Modulus

The production of cement typically involves two major costs: energy and materials. The cost of energy is reported to represent a total of 20-40% of the total cost (Chatziaras et al., 2016; Worrell et al., 2013).

Multi-objective PSO was integrated into the coupled VCP-VCCTL model to create an integrated computational optimization VCP-VCCTL tool for energy saving, cost saving and greenhouse gas emissions reduction without sacrificing cement productivity and performance. Similar to Chapter 3, Pareto fronts of four different bi-objective scenarios are plotted in Figure 5-7 to show clear trade-off between modulus and material cost.

In Figure 5-7, the Min (cost of raw meal)-Max (E) Pareto front is what the cement industry wants. To preserve strength, the cost cannot be reduced too much from 24.7 to 24.1 $/Ton (2.43% savings). From the Min-Max Pareto front, some moduli have to be sacrificed if less cost is required. Most of the cement in Figure 5-7 is cheaper and weaker.

5.2.2 CO_2 Emissions vs. Modulus

As introduced in Chapter 2, 50% of the total emissions comes from calcination/ decomposition of limestone inside the cement kiln, which is a considerable amount of emissions. Reduction of CO_2 emissions from limestone is taken into consideration in this section.

In order to reduce CO_2 emissions without sacrificing cement strength, CO_2 emissions from limestone and 7-day modulus are considered as the objectives in PSO at the same time. Figure 5-8 shows the four Pareto fronts for different optimization scenarios on E vs. CO_2 emissions from limestone decomposition. In Figure 5-8, the Min(CO_2 emssion)-Max(E) Pareto front is what the cement industry wants. The point with 0.14 CO_2 emissions and 27.8 GPa is the optimal cement. When mass fraction of CO_2 emissions is more than 0.14, most of the cement give more emissions without sacrificing too much strength. More alite means more decomposition, which typically gives more strength. The results of this optimization suggest the coupled VCP/VCCTL model could be used as a tool to optimize for a design cement.

5.2.3 Cost vs. CO_2 Emissions vs. Modulus

Figure 5-9 shows the Pareto front for Min(cost)-Min(CO_2 emssions)-Max(E), which is what the cement industry wants. From the Pareto front, producing cements with high modulus cost more money and release more CO_2 emissions. If the cost of raw meal is reduced from 12.4 $/ton to 11.4 $/ton (9% reduction) and the mass fraction of CO_2 emissions is reduced from 0.16 to 0.14 (15% reduction), modulus would be reduced from 26GPa to 22GPa (18% reduction). This information could be used for make the decision based on the weight of strength, economy

and sustainability. For example, if it is acceptable to sacrifice 18% strength for a cement company, both the sustainability and economic value would improve a lot.

Table 5-1. Comparison of VCP raw meal mass fraction from different input generation approaches

	Lower Bound		Upper Bound		Mean Value	
	Fixed Interval	Uniformly Distributed	Fixed Interval	Uniformly Distributed	Fixed Interval	Uniformly Distributed
$CaCO_3$	0.2645	0.2666	0.4288	0.4258	0.3440	0.3424
CaO	0.2645	0.2665	0.4288	0.4250	0.3440	0.3457
SiO_2	0.1997	0.2014	0.2447	0.2433	0.2211	0.2216
Al_2O_3	0.0342	0.0337	0.0691	0.0740	0.0512	0.0512
Fe_2O_3	0.0264	0.0247	0.0591	0.0599	0.0398	0.0394

Table 5-2. Comparison of VCP clinker mass fraction from different input generation approaches

	From fixed interval inputs			From random inputs		
	Lower bound	Upper bound	Mean Value	Lower bound	Upper bound	Mean Value
C_3S	0.1890	0.4822	0.2998	0.1953	0.4574	0.3028
C_2S	0.2330	0.3972	0.3343	0.2445	0.3917	0.3360
C_3A	0.0406	0.1268	0.0797	0.0412	0.1149	0.0725
C_4AF	0.0691	0.1405	0.0989	0.0712	0.1360	0.1008

Table 5-3. Expanded VCP material input ranges combing Taylor's ranges and ranges of industrial kilns

VCP Material Input	Taylor's range	Range of Industrial Kilns	Gap Range between Taylor and Industrial Kilns	Expanded Range
LSF	[0.9, 1.05]	[1.18, 1.36]	[1.05,1.18]	[0.9,1.36]
SR	[2.0, 3.0]	[2.1, 2.5]	[2.1,2.5]	[2.0,3.0]
AR	[0.8, 2.0]	[0.6, 1.0]	[0.6,1.0]	[0.6,2.0]
Fe_2O_3	[0.01,0.1]	[0.0396, 0.0430]	[0.0396,0.0430]	[0.01,0.1]
$CaCO_3$/CaO	[40%, 60%]	[42%, 56%]	[42%,56%]	[40%,60%]

Table 5-4. Comparison of VCP cases with different material input range

	543 Chemistry (537 Taylor's Range + 4 Industrial Kiln Range)	561 Chemistry (Industrial Kiln Range)	366 Chemistry (Gap Range)	537 Chemistry (Expanded Range)
C_3S vs. T_{g_peak}	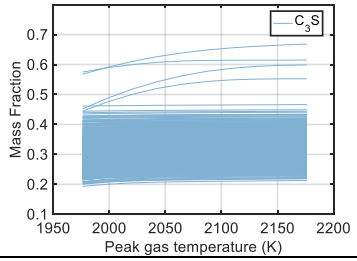	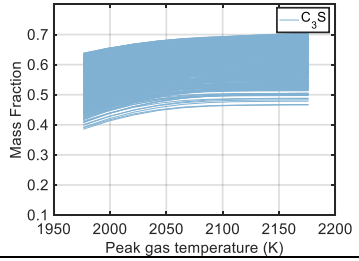	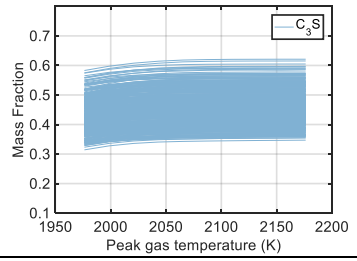	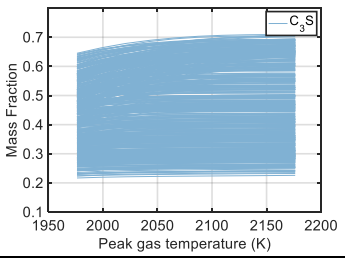
C_3S vs. T_{g_peak} (Box Plot)	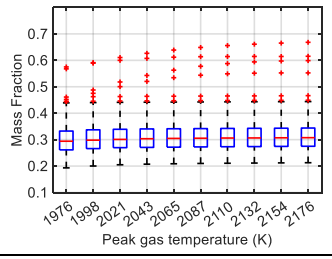	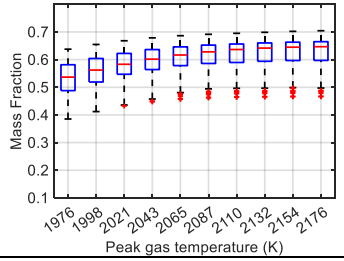	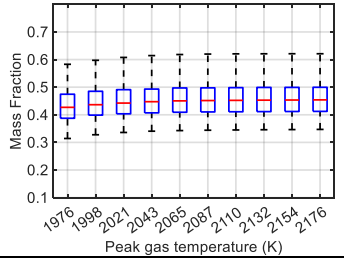	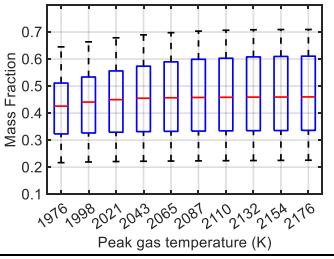
C_2S vs. T_{g_peak}	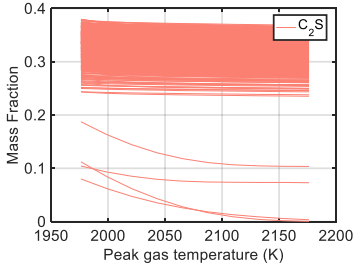	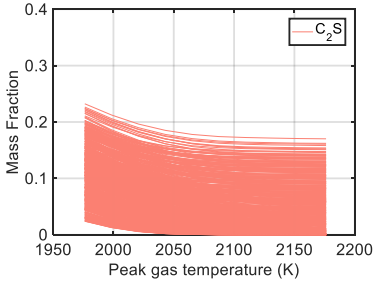	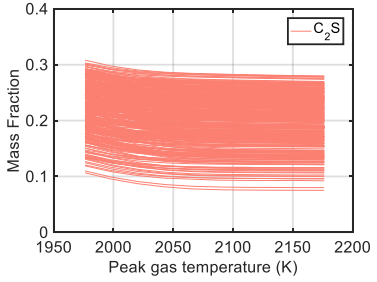	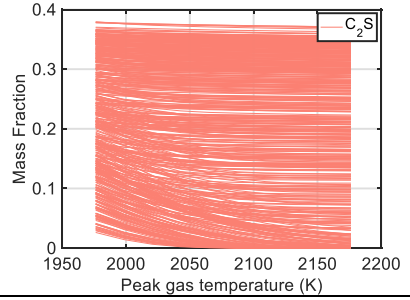

Table 5-4. Continued

	543 Chemistry (537 Taylor's Range + 4 Industrial Kiln Range)	561 Chemistry (Industrial Kiln Range)	366 Chemistry (Gap Range)	537 Chemistry (Expanded Range)
C_2S vs. T_{g_peak} (Box Plot)	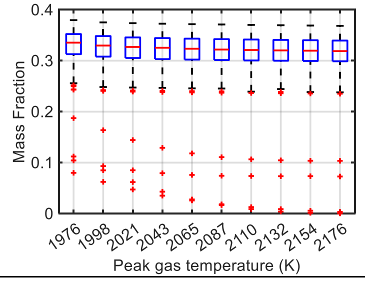	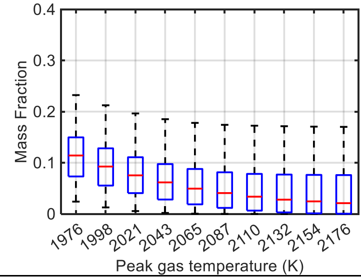	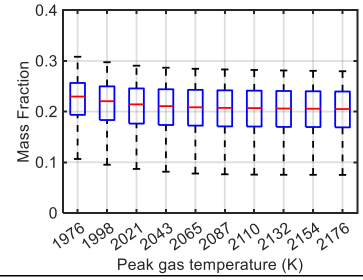	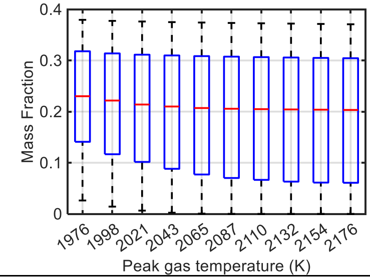

Table 5-5. Coupled VCP-VCCTL results with 53,700 inputs

	L_{g_peak}=0.6	L_{g_peak}=0.7	L_{g_peak}=0.8	L_{g_peak}=0.9
C_3S vs. T_{g_peak}	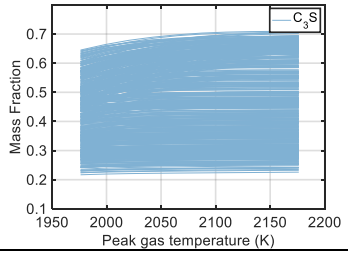	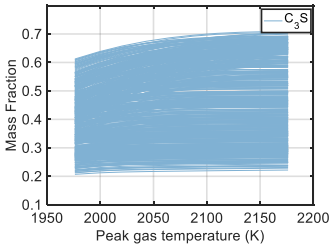	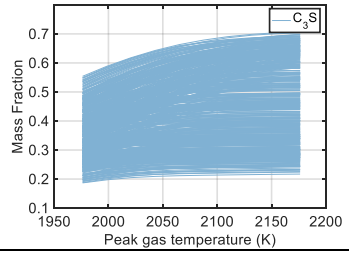	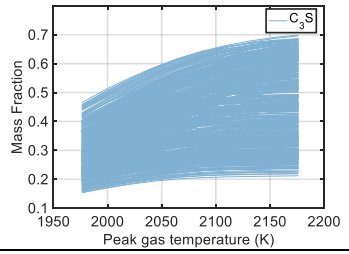
C_3S vs. T_{g_peak} (Box Plot)	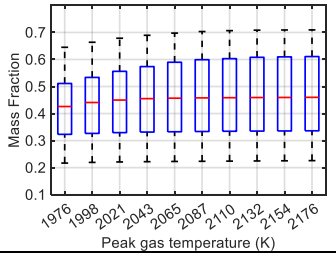	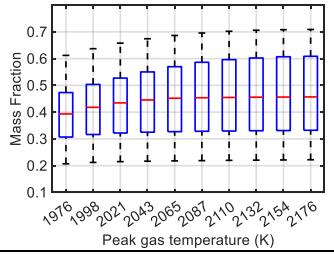	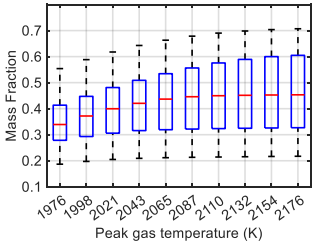	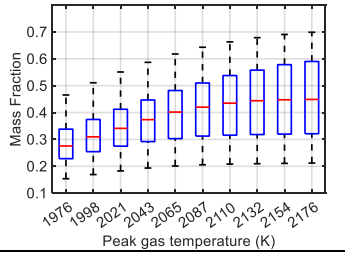
C_2S vs. T_{g_peak}	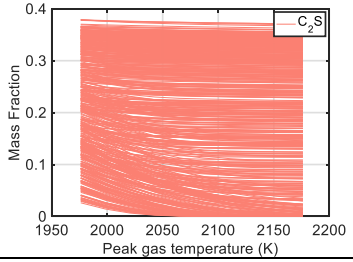	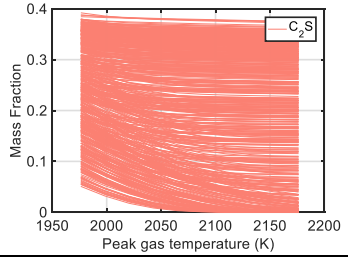	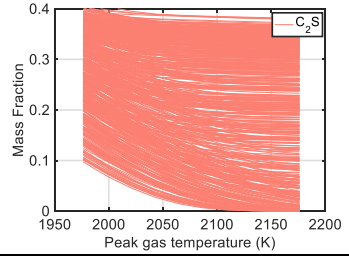	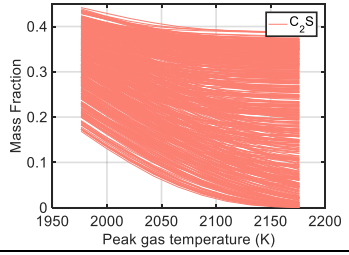
C_2S vs. T_{g_peak} (Box Plot)	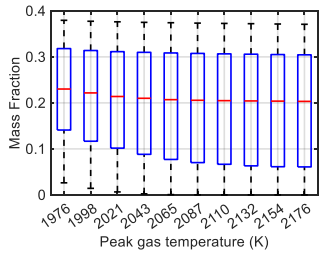	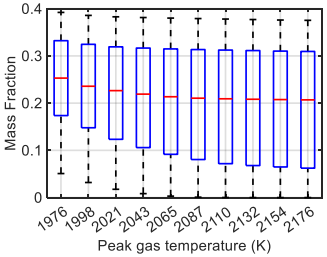	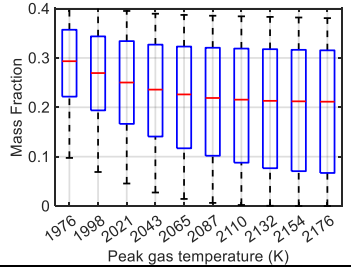	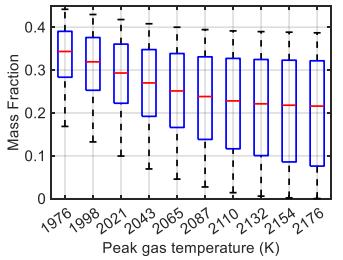

Table 5-5. Continued

	L_{g_peak}=0.6	L_{g_peak}=0.7	L_{g_peak}=0.8	L_{g_peak}=0.9
CaO vs. T_{g_peak}	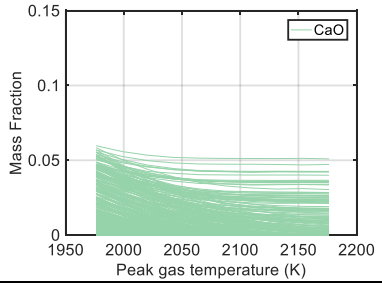	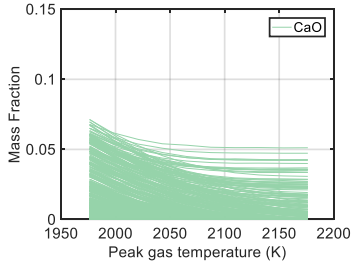	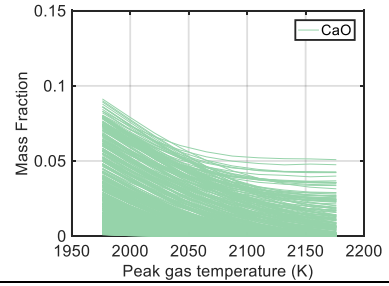	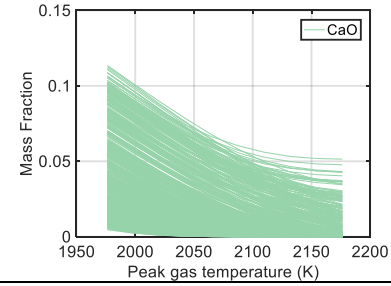
CaO vs. T_{g_peak} (Box Plot)	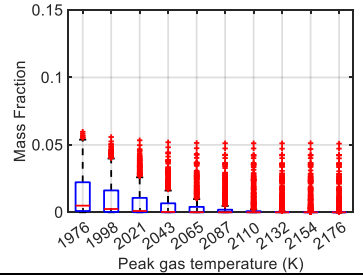	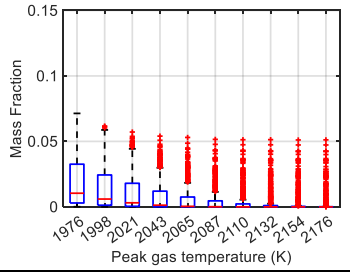	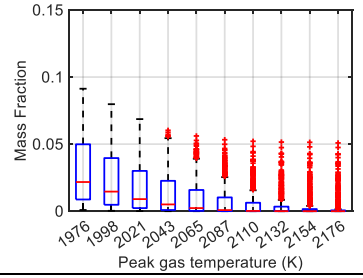	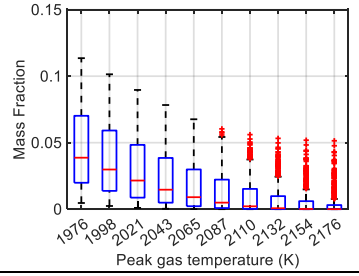
7-day modulus vs. T_{g_peak}	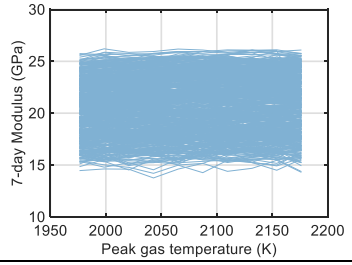	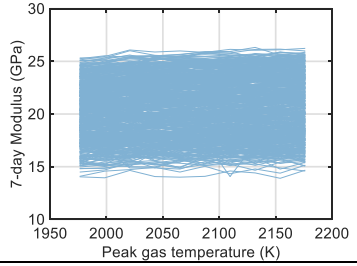	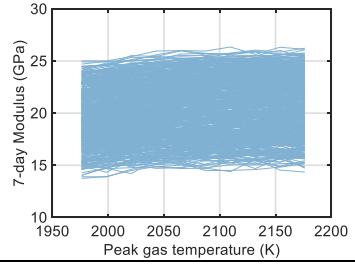	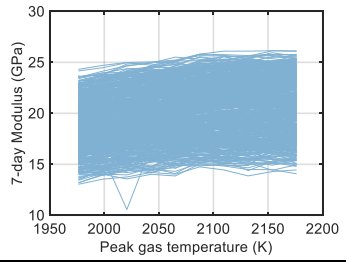
7-day modulus vs. T_{g_peak} (box plot)	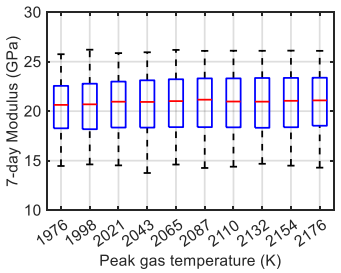	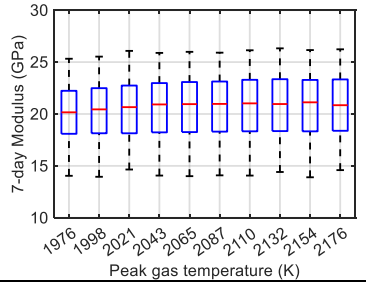	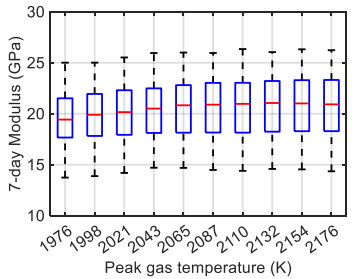	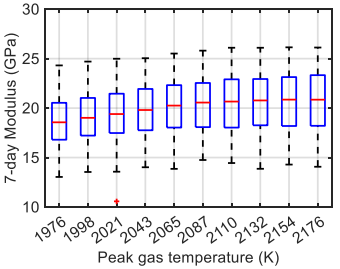

Table 5-5. Continued

	L_{g_peak}=0.6	L_{g_peak}=0.7	L_{g_peak}=0.8	L_{g_peak}=0.9
3-day heat vs. T_{g_peak}	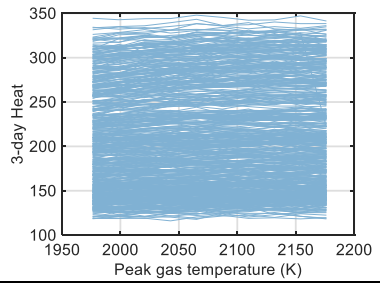	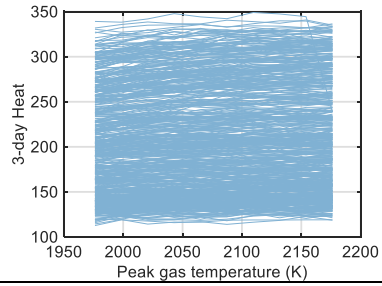	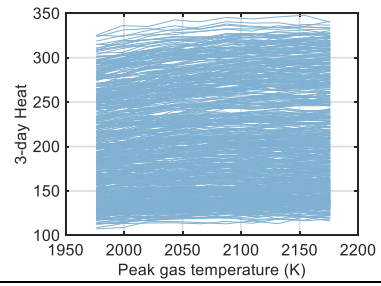	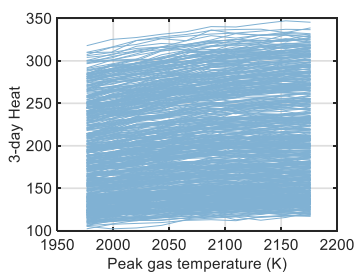
3-day heat vs. T_{g_peak} (box plot)	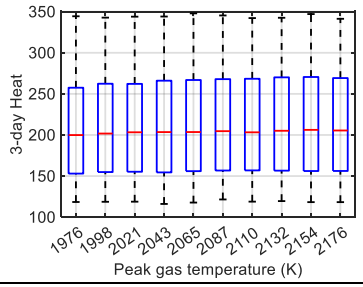	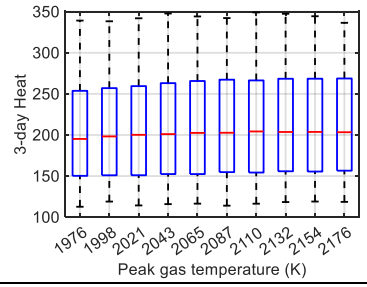	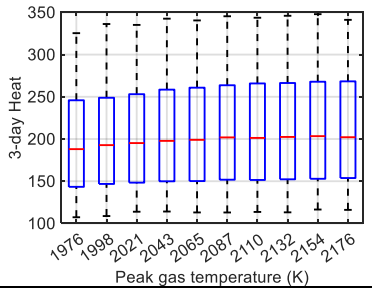	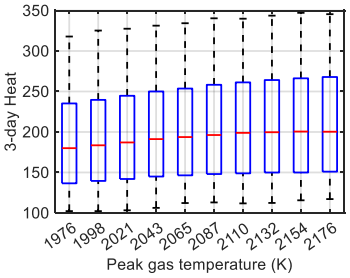

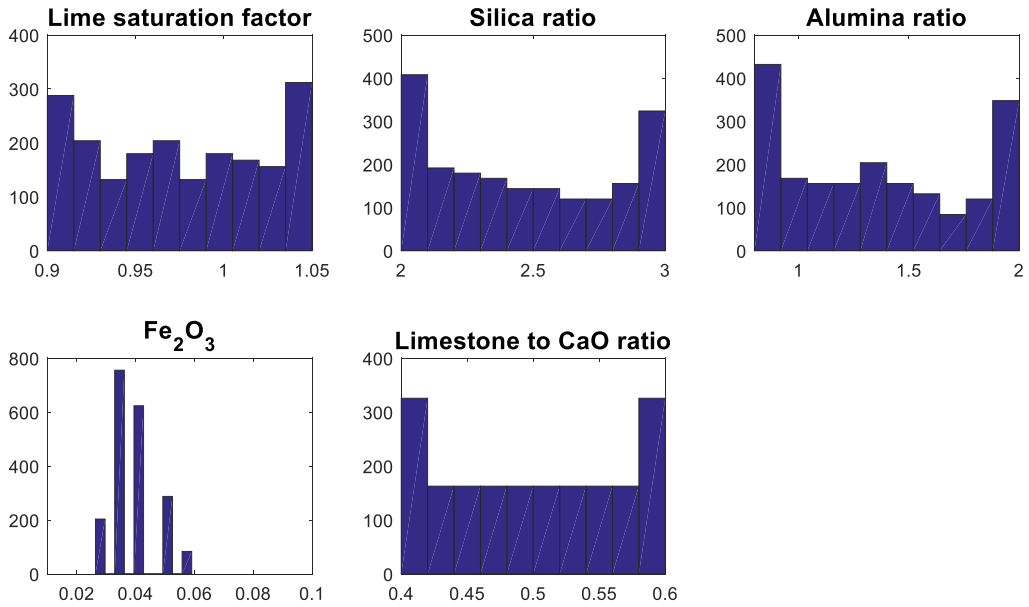

Figure 5-1. Distribution of inputs for VCP generated from fixed intervals

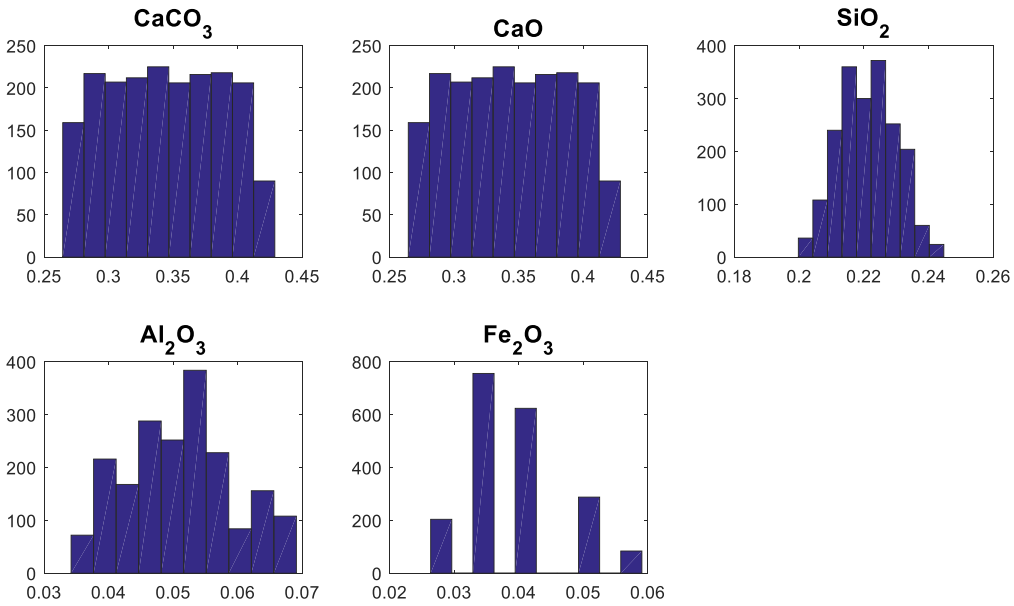

Figure 5-2. Distribution of raw meals derived from fixed interval inputs of VCP

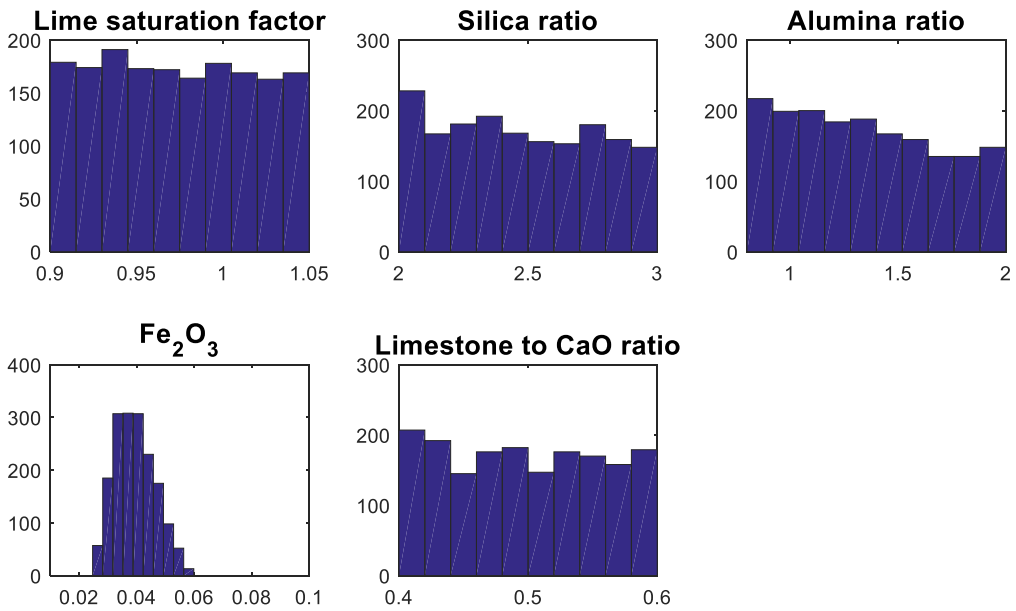

Figure 5-3. Distribution of input for VCP generated from uniformly distributed inputs

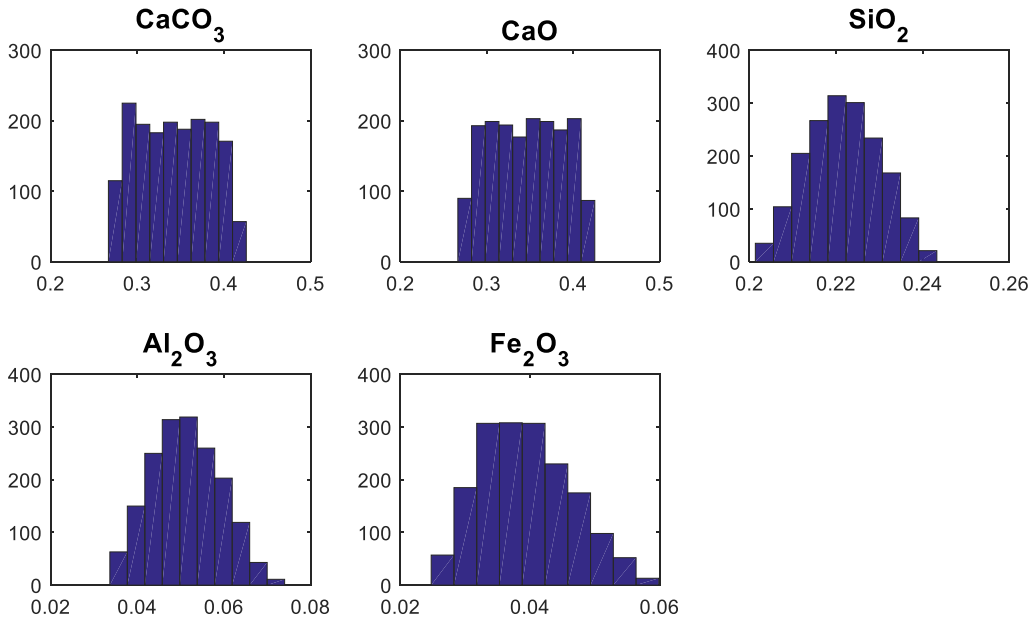

Figure 5-4. Distribution of raw meals derived from uniformly distributed inputs of VCP

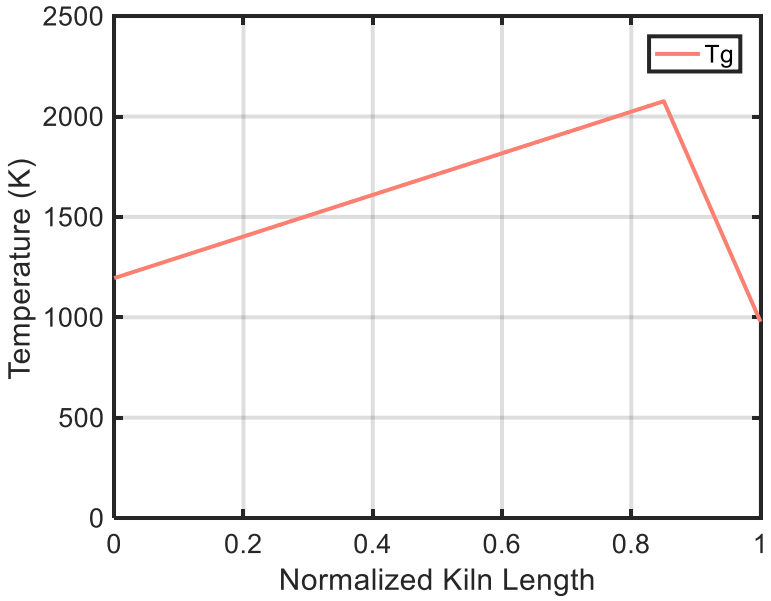

Figure 5-5. Example of gas temperature input profile for VCP

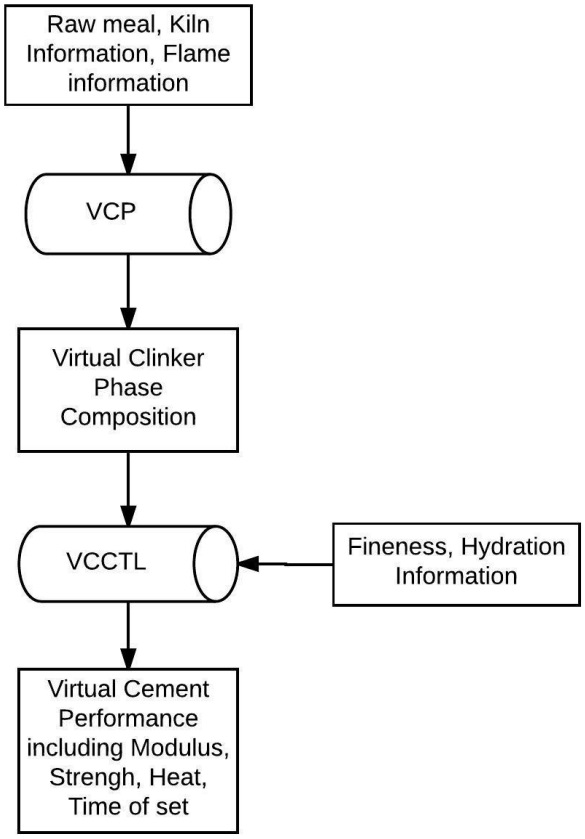

Figure 5-6. Flow of coupled VCP-VCCTL model

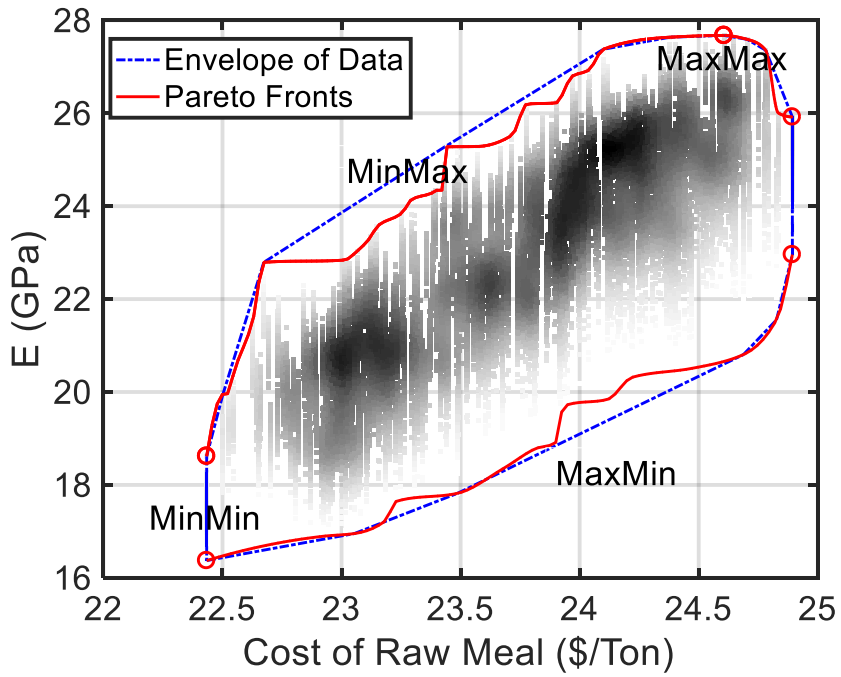

Figure 5-7. Pareto fronts of four different bi-objective optimization scenarios on E vs. cost of raw meal compared with the data envelope

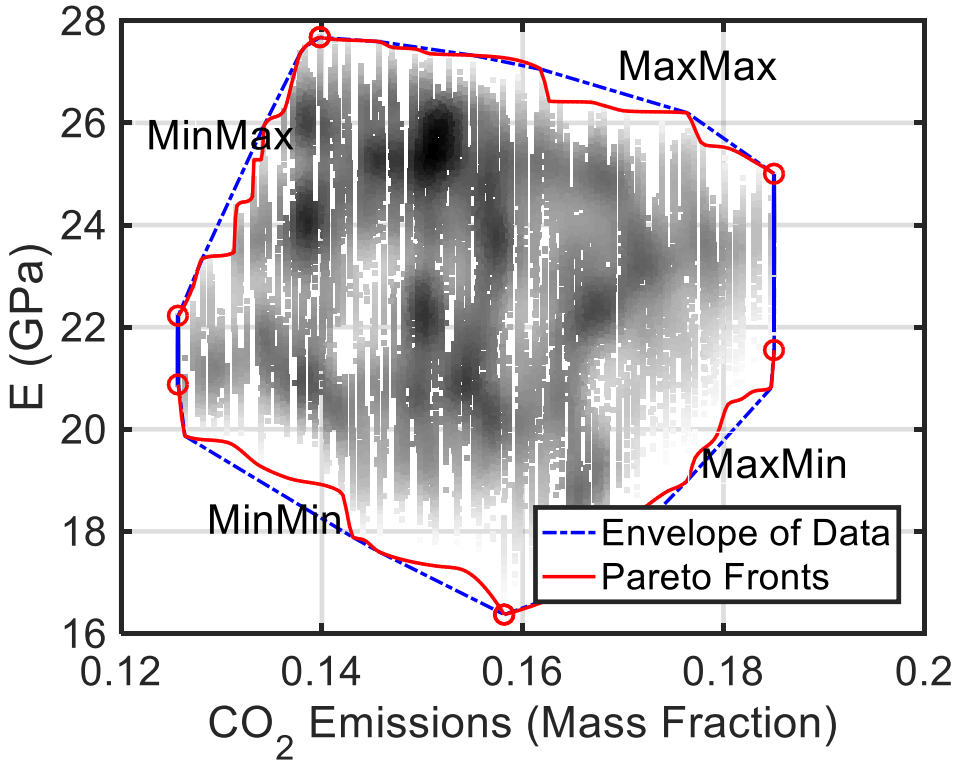

Figure 5-8. Pareto fronts of four different bi-objective optimization scenarios on E vs. CO_2 emissions from limestone compared with the data envelope

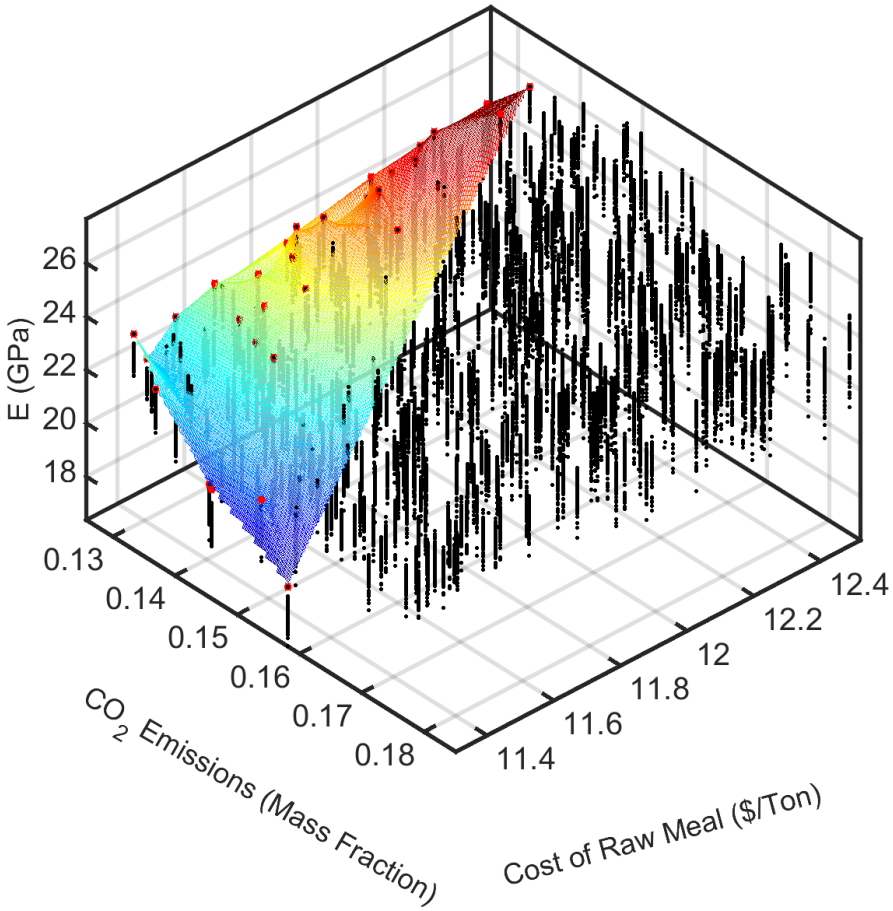

Figure 5-9. Pareto fronts of tri-objective optimization scenarios on E vs. CO2 emissions from limestone vs. cost

CHAPTER 6
CONCLUSIONS AND RECOMMENDATIONS

In summary, the completed research work to date focuses on the metaheuristic algorithms applied to virtual cement and cement plant modeling. Single-objective and multi-objective optimizations with PSO and GA are applied to a set of sample cement data from VCCTL. A scoring system is created to evaluate cement based on Pareto front optimization results. A 1D physical-chemical cement rotary kiln model is simulated with Matlab2016a solver and integrated with VCCTL and multi-objective metaheuristic algorithm on the HiperGator high performance computing cluster at University of Florida. A computational framework simulating cement and cement plant intelligently based on users' requirements and guiding the optimal designs is proposed.

The integrated model in this dissertation could provide a quantitative optimization tool for different energy efficiency measures addressed from cement plants and reduce energy, material consumption and greenhouse gas emissions without losing the performance of material.

However, there is some limitations of the computational framework including lack of criterion for detecting unrealistic virtual testing data. Currently, user-defined range of input is given to VCP-VCCTL model to conduct optimization. For the future work, threshold could be introduced into the model to detect unrealistic cases. Another challenge of this model is it needs more experiment data from cement plant to validate the accuracy of the model. Also, the model could be less computationally expensive with more efficient approaches within the coupling and the algorithm.

LIST OF REFERENCES

Aarts, E. H., & Korst, J. H. (1988). Simulated annealing. *ISSUES, 1*, 16.

Ahmad, S., & Alghamdi, S. A. (2014). A statistical approach to optimizing concrete mixture design. *The Scientific World Journal, 2014*.

Aïtcin, P.-C. (2000). Cements of yesterday and today: concrete of tomorrow. *Cement and Concrete research, 30*(9), 1349-1359.

Akhtar, S. S., Ervin, E., Raza, S., & Abbas, T. (2013). *From coal to natural gas: Its impact on kiln production, Clinker quality and emissions.* Paper presented at the Cement Industry Technical Conference (CIC), 2013 IEEE-IAS/PCA.

Arrhenius, S. (1889). Über die Reaktionsgeschwindigkeit bei der Inversion von Rohrzucker durch Säuren. *Zeitschrift für physikalische Chemie, 4*(1), 226-248.

Atmaca, A., & Yumrutaş, R. (2014). Analysis of the parameters affecting energy consumption of a rotary kiln in cement industry. *Applied Thermal Engineering, 66*(1), 435-444.

Babushkin, V. I., Matveev, G. M., & Mchedlov-Petrosiẫn, O. P. (1985). *Thermodynamics of silicates*: Springer.

Barr, P. V. (1986). *Heat transfer processes in rotary kilns.* University of British Columbia.

Benhelal, E., Zahedi, G., Shamsaei, E., & Bahadori, A. (2013). Global strategies and potentials to curb CO 2 emissions in cement industry. *Journal of cleaner production, 51*, 142-161.

Bentz, D. P. (1997). Three‐Dimensional Computer Simulation of Portland Cement Hydration and Microstructure Development. *Journal of the American Ceramic Society, 80*(1), 3-21.

Bentz, D. P., Feng, X., & Stutzman, P. E. (2000). *Analysis of CCRL proficiency cements 135 and 136 using CEMHYD3D*: National Institute of Standards and Technology, Technology Administration, US Department of Commerce.

Bickley, J. A., Hooton, R. D., & Hover, K. C. (2006). Performance specifications for durable concrete. *Concrete international, 28*(09), 51-57.

Bićanić, N., De Borst, R., Mang, H., & Meschke, G. (2003). *Computational modelling of concrete structures.* Paper presented at the Proc. of the EURO-C Conference.

Bogue, R. H. (1929). Calculation of the compounds in Portland cement. *Industrial & Engineering Chemistry Analytical Edition, 1*(4), 192-197.

Bonnans, J.-F., Gilbert, J. C., Lemaréchal, C., & Sagastizábal, C. A. (2006). *Numerical optimization: theoretical and practical aspects*: Springer Science & Business Media.

Bremermann, H. J. (1958). *The evolution of intelligence: The nervous system as a model of its environment*: University of Washington, Department of Mathematics.

Bullard, J. W. (2014). *Virtual Cement and Concrete Testing Laboratory: Version 9.5 User Guide*.

Bullard, J. W., Ferraris, C., Garboczi, E. J., Martys, N., & Stutzman, P. (2004). Virtual cement. *Chapt, 10*, 1311-1331.

Bullard, J. W., & Stutzman, P. E. (2006). Analysis of CCRL proficiency cements 151 and 152 using the virtual cement and concrete testing laboratory. *Cement and Concrete Research, 36*(8), 1548-1555.

Burke, E. K., & Kendall, G. (2005). *Search methodologies*: Springer.

Cement, A. ASTM C150, Type I-Normal Portland type. 1. *Acquire all cement for entire project from same source*.

Chapra, S. C., & Canale, R. P. (1998). *Numerical methods for engineers* (Vol. 2): McGraw-Hill New York.

Chatziaras, N., Psomopoulos, C. S., & Themelis, N. J. (2016). Use of waste derived fuels in cement industry: a review. *Management of Environmental Quality: An International Journal, 27*(2), 178-193.

Chen, Y., & Odler, I. (1992). On the origin of Portland cement setting. *Cement and Concrete Research, 22*(6), 1130-1140.

Collins, N., Eglese, R., & Golden, B. (1988). Simulated annealing–an annotated bibliography. *American Journal of Mathematical and Management Sciences, 8*(3-4), 209-307.

Csernyei, C., & Straatman, A. G. (2016). Numerical modeling of a rotary cement kiln with improvements to shell cooling. *International Journal of Heat and Mass Transfer, 102*, 610-621.

Csernyei, C. M. (2016). *Numerical Modelling of a Rotary Cement Kiln with External Shell Cooling Fans.* The University of Western Ontario.

Damtoft, J. S., Lukasik, J., Herfort, D., Sorrentino, D., & Gartner, E. M. (2008). Sustainable development and climate change initiatives. *Cement and concrete research, 38*(2), 115-127.

Darabi, P. (2007). *A mathematical model for cement kilns.* University of British Columbia.

Deb, K., Pratap, A., Agarwal, S., & Meyarivan, T. (2002). A fast and elitist multiobjective genetic algorithm: NSGA-II. *IEEE transactions on evolutionary computation, 6*(2), 182-197.

Eberhart, R., & Kennedy, J. (1995). *A new optimizer using particle swarm theory.* Paper presented at the Micro Machine and Human Science, 1995. MHS'95., Proceedings of the Sixth International Symposium on.

Fraser, A. S. (1957). Simulation of genetic systems by automatic digital computers ii. effects of linkage on rates of advance under selection. *Australian Journal of Biological Sciences, 10*(4), 492-500.

Garboczi, E. J., & Bentz, D. P. (1995). *Multi-scale picture of concrete and its transport properties: introduction for non-cement researchers*: National Institute of Standards and Technology.

Garboczi, E. J., & Bentz, D. P. (2001). The effect of statistical fluctuation, finite size error, and digital resolution on the phase percolation and transport properties of the NIST cement hydration model. *Cement and Concrete Research, 31*(10), 1501-1514.

Garboczi, E. J., & Berryman, J. G. (2001). Elastic moduli of a material containing composite inclusions: effective medium theory and finite element computations. *Mechanics of Materials, 33*(8), 455-470.

Garboczi, E. J., Bullard, J. W., & Bentz, D. P. (2004). Virtual testing of cement and concrete—USA 2004. *Concrete international, 26*(12), 33-37.

Geem, Z. W., Kim, J. H., & Loganathan, G. (2001). A new heuristic optimization algorithm: harmony search. *Simulation, 76*(2), 60-68.

Ghezal, A., & Khayat, K. H. (2002). Optimizing self-consolidating concrete with limestone filler by using statistical factorial design methods. *ACI Materials Journal, 99*(3), 264-272.

Glover, F., & Laguna, M. (2013). *Tabu Search∗*: Springer.

Goel, T., & Stander, N. (2010). *A Study of the Convergence Characteristics of Multiobjective Evolutionary Algorithms.* Paper presented at the 13th AIAA/ISSMO Multidisciplinary Analysis Optimization Conference.

Goldberg, D. E., & Samtani, M. P. (1986). *Engineering optimization via genetic algorithm.* Paper presented at the Electronic Computation:.

Grosan, C., Abraham, A., & Chis, M. (2006). Swarm intelligence in data mining. *Swarm Intelligence in Data Mining*, 1-20.

Guirao, J., Iglesias, S., Pistono, J., & Vázquez, R. Model of Mass and Energy Transfer in a Clinker Rotary Kiln.

Haecker, C., Bentz, D., Feng, X., & Stutzman, P. (2003). Prediction of cement physical properties by virtual testing. *Cement International, 1*(3), 86-92.

Haecker, C.-J., Garboczi, E., Bullard, J., Bohn, R., Sun, Z., Shah, S., et al. (2005). Modeling the linear elastic properties of Portland cement paste. *Cement and Concrete Research, 35*(10), 1948-1960.

Hain, M., & Wriggers, P. (2008). Numerical homogenization of hardened cement paste. *Computational Mechanics, 42*(2), 197-212.

Holland, J. H. (1975). Adaptation in natural and artificial systems. An introductory analysis with application to biology, control, and artificial intelligence. *Ann Arbor, MI: University of Michigan Press*.

Holland, J. H. (1992). *Adaptation in natural and artificial systems: an introductory analysis with applications to biology, control, and artificial intelligence*: MIT press.

Hottel, H., & Sarofim, A. (1965). Radiative transport. *McCravv Hill, New York*.

Hu, X., Eberhart, R. C., & Shi, Y. (2003). *Engineering optimization with particle swarm.* Paper presented at the Swarm Intelligence Symposium, 2003. SIS'03. Proceedings of the 2003 IEEE.

Jaumard, B., OW, P. S., & Simeone, B. (1988). A selected artificial intelligence bibliography for operations researchers. *Annals of Operations Research, 12*(1), 1-50.

Kabir, G., Abubakar, A., & El-Nafaty, U. (2010). Energy audit and conservation opportunities for pyroprocessing unit of a typical dry process cement plant. *Energy, 35*(3), 1237-1243.

Kaige, S., Murata, T., & Ishibuchi, H. (2003). *Performance evaluation of memetic EMO algorithms using dominance relation-based replacement rules on MOO test problems.* Paper presented at the Systems, Man and Cybernetics, 2003. IEEE International Conference on.

Kirkpatrick, S. (1984). Optimization by simulated annealing: Quantitative studies. *Journal of statistical physics, 34*(5), 975-986.

Lagergren, E. S., Snyder, K. A., & Simon, M. J. (1997). Concrete Mixture Optimization Using Statistical Mixture Design Methods.

Li, G., Goel, T., & Stander, N. (2008). *Assessing the convergence properties of NSGA-II for direct crashworthiness optimization.* Paper presented at the 10th International LS-DYNA® User's Conference, Detroit MI.

Li, L., Huang, Z., & Liu, F. (2009). A heuristic particle swarm optimization method for truss structures with discrete variables. *Computers & Structures, 87*(7), 435-443.

Li, L., Huang, Z., Liu, F., & Wu, Q. (2007). A heuristic particle swarm optimizer for optimization of pin connected structures. *Computers & Structures, 85*(7), 340-349.

Li, S. Q., Ma, L. B., Wan, W., & Yao, Q. (2005). A Mathematical Model of Heat Transfer in a Rotary Kiln Thermo‐Reactor. *Chemical engineering & technology*, *28*(12), 1480-1489.

Mamlouk, M. S., & Zaniewski, J. P. (1999). *Materials for civil and construction engineers*: Addison-Wesley Reading, Mass, USA.

Martins, M. A., Oliveira, L. S., & Franca, A. S. (2002). Modeling and simulation of limestone calcinations in rotary kilns. *ZKG International*, *55*(4), 76-87.

Martí, L., García, J., Berlanga, A., & Molina, J. M. (2007). *A cumulative evidential stopping criterion for multiobjective optimization evolutionary algorithms.* Paper presented at the Proceedings of the 9th annual conference companion on Genetic and evolutionary computation.

Mastorakos, E., Massias, A., Tsakiroglou, C., Goussis, D., Burganos, V., & Payatakes, A. (1999). CFD predictions for cement kilns including flame modelling, heat transfer and clinker chemistry. *Applied Mathematical Modelling*, *23*(1), 55-76.

Mindess, S., & Young, J. (1981). Concrete. Englewood: NJ, Prentice Hall.

Mujumdar, K., & Ranade, V. (2006). Simulation of rotary cement kilns using a one-dimensional model. *Chemical Engineering Research and Design*, *84*(3), 165-177.

Mujumdar, K. S., Arora, A., & Ranade, V. V. (2006). Modeling of rotary cement kilns: applications to reduction in energy consumption. *Industrial & engineering chemistry research*, *45*(7), 2315-2330.

Mujumdar, K. S., Ganesh, K., Kulkarni, S. B., & Ranade, V. V. (2007). Rotary Cement Kiln Simulator (RoCKS): Integrated modeling of pre-heater, calciner, kiln and clinker cooler. *Chemical Engineering Science*, *62*(9), 2590-2607.

Muthukumar, M., & Mohan, D. (2004). Optimization of mechanical properties of polymer concrete and mix design recommendation based on design of experiments. *Journal of applied polymer science*, *94*(3), 1107-1116.

Neville, A. M. (1995). *Properties of concrete*.

Nissen, V. (1993). *Evolutionary algorithms in management science: An overview and list of references*: European Study Group for Evolutionary Economics.

Noshirvani, G., Shirvani, M., Askari-Mamani, J., & Nourzadeh, H. (2013). Estimation of coating thickness in a rotary kiln by using shell temperature and kiln modeling. *ZKG international*(11), 58-71.

Nørskov, L. K. (2012). *Combustion of solid alternative fuels in the cement kiln burner*. Technical University of Denmark.

Odelson, J. B., Kerr, E. A., & Vichit-Vadakan, W. (2007). Young's modulus of cement paste at elevated temperatures. *Cement and Concrete Research, 37*(2), 258-263.

Odler, I. (1998). Hydration, setting and hardening of Portland cement. *LEA's Chemistry of Cement and Concrete, 4*, 241-297.

Osman, I. H. (1995). An introduction to meta-heuristics. *Operational Research Tutorial Papers*, 92-122.

Osman, I. H., & Laporte, G. (1996). Metaheuristics: A bibliography: Springer.

Parsopoulos, K. E., & Vrahatis, M. N. (2002). Recent approaches to global optimization problems through particle swarm optimization. *Natural computing, 1*(2-3), 235-306.

Patel, R., Hossain, K., Shehata, M., Bouzoubaa, N., & Lachemi, M. (2004). Development of statistical models for mixture design of high-volume fly ash self-consolidating concrete. *Materials Journal, 101*(4), 294-302.

Peray, K. E., & Waddell, J. J. (1986). *The rotary cement kiln*: Edward Arnold.

Pirlot, M. (1992). General local search heuristics in combinatorial optimization: a tutorial. *Belgian Journal of Operations Research, Statistics and Computer Science, 32*(1-2), 7-69.

Press, W. H., Teukolsky, S. A., Vetterling, W. T., & Flannery, B. P. (2007). Numerical recipes: the art of scientific computing: Cambridge University Press, New York.

Rajeev, S., & Krishnamoorthy, C. (1992). Discrete optimization of structures using genetic algorithms. *Journal of structural engineering, 118*(5), 1233-1250.

Rayward-Smith, V. J., Osman, C., Reeves, C. R., & Smith, G. D. (1996). *Modern heuristic search methods*: John Wiley.

Reddy, B. V., & Jagadish, K. (2003). Embodied energy of common and alternative building materials and technologies. *Energy and buildings, 35*(2), 129-137.

Reddy, B. V., Leuzinger, G., & Sreeram, V. (2014). Low embodied energy cement stabilised rammed earth building—A case study. *Energy and Buildings, 68*, 541-546.

Romeo, L. M., Catalina, D., Lisbona, P., Lara, Y., & Martínez, A. (2011). Reduction of greenhouse gas emissions by integration of cement plants, power plants, and CO2 capture systems. *Greenhouse Gases: Science and Technology, 1*(1), 72-82.

Roudenko, O., & Schoenauer, M. (2004). A steady performance stopping criterion for Pareto-based evolutionary algorithms.

Sadighi, S., Shirvani, M., & Ahmad, A. (2011). Rotary cement kiln coating estimator: Integrated modelling of kiln with shell temperature measurement. *The Canadian Journal of Chemical Engineering, 89*(1), 116-125.

Saidur, R., Hossain, M., Islam, M., Fayaz, H., & Mohammed, H. (2011). A review on kiln system modeling. *Renewable and Sustainable Energy Reviews, 15*(5), 2487-2500.

Sharda, R. (1994). Neural networks for the MS/OR analyst: An application bibliography. *Interfaces, 24*(2), 116-130.

Shetty, M. (2005). *Concrete technology*: publisher not identified.

Shi, Y. (2001). *Particle swarm optimization: developments, applications and resources.* Paper presented at the evolutionary computation, 2001. Proceedings of the 2001 Congress on.

Simon, M. (2003). *Concrete mixture optimization using statistical methods: final report*: US Department of Transportation, Federal Highway Administration, Research, Development and Technology, Turner-Fairbank Highway Research Center.

Simon, M., Snyder, K., & Frohnsdorff, G. (1999). *Advances in concrete mixture optimization.* Paper presented at the Proceedings of International Congress on Creating with Concrete University of Dundee,(ed. Dhir & McCarthy) pp.

Sonebi, M., & Bassuoni, M. (2013). Investigating the effect of mixture design parameters on pervious concrete by statistical modelling. *Construction and Building Materials, 38*, 147-154.

Soudki, K., El-Salakawy, E., & Elkum, N. (2001). Full factorial optimization of concrete mix design for hot climates. *Journal of materials in civil engineering, 13*(6), 427-433.

Spang, H. (1972). A dynamic model of a cement kiln. *Automatica, 8*(3), 309-323.

Stadler, K. S., Poland, J., & Gallestey, E. (2011). Model predictive control of a rotary cement kiln. *Control Engineering Practice, 19*(1), 1-9.

Standard, A. D245, 2006,"Standard Practice for Establishing Structural Grades and Related Allowable Properties for Visually Graded Lumber," ASTM International, West Conshohocken, PA. *ASTM D245, 6*.

Stewart, B. S., Liaw, C.-F., & White, C. C. (1994). A bibliography of heuristic search research through 1992. *IEEE transactions on Systems, Man, and Cybernetics, 24*(2), 268-293.

Stutzman, P. (2004). Scanning electron microscopy imaging of hydraulic cement microstructure. *Cement and Concrete Composites, 26*(8), 957-966.

Tan, O., Zaimoglu, A. S., Hinislioglu, S., & Altun, S. (2005). Taguchi approach for optimization of the bleeding on cement-based grouts. *Tunnelling and underground space technology, 20*(2), 167-173.

Taylor, H. F. (1997). *Cement chemistry*: Thomas Telford.

Thomas, J. J., Biernacki, J. J., Bullard, J. W., Bishnoi, S., Dolado, J. S., Scherer, G. W., et al. (2011). Modeling and simulation of cement hydration kinetics and microstructure development. *Cement and Concrete Research, 41*(12), 1257-1278.

Trautmann, H., Ligges, U., Mehnen, J., & Preuss, M. (2008). *A convergence criterion for multiobjective evolutionary algorithms based on systematic statistical testing.* Paper presented at the International Conference on Parallel Problem Solving from Nature.

Tscheng, S., & Watkinson, A. (1979). Convective heat transfer in a rotary kiln. *The Canadian Journal of Chemical Engineering, 57*(4), 433-443.

Vallgårda, A., & Redström, J. (2007). *Computational composites.* Paper presented at the Proceedings of the SIGCHI conference on Human factors in computing systems.

Voß, S., Martello, S., Osman, I. H., & Roucairol, C. (2012). *Meta-heuristics: Advances and trends in local search paradigms for optimization*: Springer Science & Business Media.

Wang, S., Lu, J., Li, W., Li, J., & Hu, Z. (2006). Modeling of pulverized coal combustion in cement rotary kiln. *Energy & Fuels, 20*(6), 2350-2356.

Watts, B. E. (2013). Analysis of the Sensitivity of a Concrete Virtual Model to Different Material Input Parameters.

Worrell, E., Kermeli, K., & Galitsky, C. (2013). Energy Efficiency Improvement and Cost Saving Opportunities for Cement Making An ENERGY STAR® Guide for Energy and Plant Managers: EPA-United States Environmental Protection Agency.

Wu, S.-J., & Chow, P.-T. (1995). Steady-state genetic algorithms for discrete optimization of trusses. *Computers & Structures, 56*(6), 979-991.

Xiaoyong, L., & Wendi, M. (2011). Optimization for mix design of high-performance concrete using orthogonal test. *Innovative Computing and Information*, 364-372.

Yang, L., Gurley, K. R., & Prevatt, D. O. (2013). Probabilistic modeling of wind pressure on low-rise buildings. *Journal of Wind Engineering and Industrial Aerodynamics, 114*, 18-26.

Zhang, Y., Cao, S.-X., Shao, S., Chen, Y., Liu, S.-L., & Zhang, S.-S. (2011). Aspen Plus-based simulation of a cement calciner and optimization analysis of air pollutants emission. *Clean Technologies and Environmental Policy, 13*(3), 459-468.

Zitzler, E., Thiele, L., Laumanns, M., Fonseca, C. M., & Da Fonseca, V. G. (2003). Performance assessment of multiobjective optimizers: An analysis and review. *IEEE Transactions on evolutionary computation, 7*(2), 117-132.

BIOGRAPHICAL SKETCH

Chengcheng Tao was born in Wuhu, Anhui Province, China. In June 2011, she received her bachelor's degree with highest honor in civil engineering from Shanghai Normal University, China. Then, she received her master's degree in civil engineering from Carnegie Mellon University in May, 2012 and master's degree in mechanical engineering from Johns Hopkins University in August, 2014. Her master's thesis topic was "Crystal plasticity based finite element modeling in polycrystalline ti-7al alloys". In August 2014, she was accepted into the Ph.D. program in the Department of Civil and Coastal Engineering at the University of Florida with a focus on optimization in cement and concrete and cement plant modeling under the guidance of Dr. Forrest Masters and Dr. Christopher Ferraro.